UNIVERSITAT POLITÈCNICA DE VALÈNCIA

DEPARTAMENTO DE TECNOLOGÍA DE ALIMENTOS
INSTITUTO INTERUNIVERSITARIO DE INVESTIGACIÓN DE RECONOCIMIENTO MOLECULAR Y DESARROLLO TECNOLÓGICO

Essential Oil Components Encapsulated in Mesoporous Silica Supports: A Bioactive Properties Evaluation and a Toxicological Approach

PhD Thesis

Submitted by
Carolina Acosta Romero

PhD Supervisors

Prof. José Manuel Barat Baviera
Dra. Andrea Bernardos Bau
Prof. Ramón Martínez Máñez

Valencia, September 2017

JOSÉ MANUEL BARAT BAVIERA, PhD in Food Technology and Professor at the *Universitat Politècnica de València*, ANDREA BERNARDOS BAU, PhD from the *Universitat Politècnica de València,* and RAMÓN MARTÍNEZ MÁÑEZ, PhD in Chemistry and Professor at the *Universitat Politècnica de València*

CERTIFY:

That the work *"***Essential Oil Components Encapsulated in Mesoporous Silica Supports: A Bioactive Properties Evaluation and a Toxicological Approach"** has been developed by Carolina Acosta Romero under their supervision in the Departamento de Tecnología de Alimentos and the Instituto Interuniversitario de Investigación de Reconocimiento Molecular y Desarrollo Tecnológico (IDM) of the *Universitat Politècnica de València*, as a Thesis Project in order to obtain the degree of PhD from the *Universitat Politècnica de València.*

Valencia, September 2017.

Prof. José Manuel Barat Baviera Dra. Andrea Bernardos Bau Prof. Ramón Martínez Máñez

“For a successful technology,

reality must take precedence over public relations,

for Nature cannot be fooled.”

“… And therefore when we go to investigate

we shouldn’t pre-decide what it is we are trying to do

except to find out more about it.”

Richard Feynman

Acknowledgements

Agradecimientos

En la vida, todo llega, y hoy, finalmente ha llegado el momento de transmitir lo agradecida que estoy con todos los que han estado durante estos últimos años.

En primer lugar, quiero agradecer a mis directores de tesis, por confiar en mí y ofrecerme la oportunidad de aprender tanto, y de tan diversas e interesantes líneas de investigación, **Ramón Martínez**, **José Barat**, gracias por vuestro apoyo profesional, y sobretodo personal. A mi directora, **Andrea Bernardos**, no encuentro las palabras para agradecer todo el cariño y apoyo que me has dado.

Agradezco también todo el tiempo y paciencia dedicada por **Loles Marcos, Félix Sancenón y Ana Fuentes**; desde el primer día, apoyando, corrigiendo y aconsejando, en el complicado camino de la investigación.

Gracias a quienes han confiado en mí, y abrieron las puertas de sus laboratorios. Personas que con tanta pasión por su trabajo hicieron mis estancias productivas, no solo a nivel profesional sino también a nivel personal.
Saverio Mannino, **Simona Bennedeti, Carlos Fuenmayor**, del DISTAM en la Universidad de Milan.
Mar Orzáez y todo el grupo del Centro de Investigación del Príncipe Felipe, CIPF.
Cristian Olguín, desde el grupo de electrónica de la Politècnica de València.
Marta e **Isabel Fernández** en la facultad de farmacia de la Universidad de València
Amadeu Griol, y su grupo, que me recibió en nanofotonica, y con paciencia enseño una ciencia totalmente desconocida para mi.
Finalmente, **Patricia Martorell, Salvador Genovés** y todo el equipo de Biología Celular en Biopolis, **Nuria, Silvia, Roberto**, gracias por acogerme con tanto cariño y literalmente, integrarme como una más de vosotros.

Gracias a todos y cada uno de los compañeros de laboratorio, que han estado durante estos años. Desde el Lab2.6 y los tiempos de *'Braulio'*, con Núria, María Moragues, Sameh, Luis Enrique, Lluis, Yoli, Elena. Pasando por el lab de diseño con Inma y Román, hasta los labs de la CPI y los "nuevos", que ya no son tan nuevos: Toni, Cris Marín, Irene, Monica, Alba, Amelia, Sara, Adrian, Luis, Santi, Xente, Borja. Todos, desde el primero hasta el último que he conocido. Vosotros habéis hecho de esto, que es cruzar un océano para hacer un doctorado, una experiencia completamente gratificante y enriquecedora. Graciès xiquets.

Gracias **Édgar**, gracias **María**, gracias por vuestra infinita paciencia y empatía, gracias por ser desde el primer momento, guía y compañía en este largo camino.

Sus, Cristi, Samu, Esteban, MªJesús, gracias por las xuxes, las catas. Marimar, Carmen, Tower, Eli, gracias, por alimentarme con cada almuerzo, y por dar alegría y sentido al día a día del laboratorio; vuestra compañía hace posible coger fuerzas cada mañana para seguir adelante.

Graciès sobretot per, "descobrir-nos a poc a poc les carències, per contar-nos les misèries amb formatge pa i vi", i cafè.

A los amigos heredados, gracias por estar en el coffee, por los amaneceres de SanJuan, por cerrar bares, por el rugby, por el futbol y el kalimotxo. **Jorge, Raquel, Santi, Xelo, Patri, Belén, David**, gracias por estar ahí, con o sin cerves. **Yannick**, gracias por compartir tu filosofía del 'melapelismo'. Gracias **Diego**, por dejarme esa valiosa herencia. Gracias **Javi**, otro amigo heredado.

Gracias a mis chicas del vermut, por alojarme en un rinconcito de su corazón, gracias por soportar mis debates que simpre buscan controversia, gracias por ser complices y amigas, **Diana**, **Ceci**, **Nataly**, gracias.

Gracias, mil y mil gracias a mi familia, que desde la distancia me ha apoyado sin entender muy bien el camino que he tomado. Gracias a la familia que aquí, a tantos kilómetros de donde nací, me ha recibido y me ha soportado tan pacientemente. Gracias a los inciertos caminos de la vida que me han cruzado con tres excelentes compañeros de viaje, gracias **Dante** y **Maitea**, gracias **Néstor**.

A mis amigos, gracias por todo, por escuchar pacientemente, por aguantar mis espontaneidades, que casi siempre rozan la imprudencia. **Lu, Alex, Alejo**, **Andrés**, **Jeff,** amigos de siempre, que sin importar distancias han estado cuando más los he necesitado. Gracias también a esos amigos que no sabes en que momento se hicieron irremplazables, **Claudia**, **Miguel**, **Alberto**, bellos. **Ivan**, tercero, último y primero, gracias, por tanto y por tan poco, gracias por estar ahí. Gracias por salvarme de mí misma.

Nina Simone, Cerati, "gracias totales"
Gracias por darle una banda sonora a este capítulo de mi vida.

Y a tí, Luz Alba, nada de esto sería posible sin ti,
Gracias Madre.

I believe in evidence. I believe in observation, measurement, and reasoning, confirmed by independent observers.
I'll believe anything, no matter how wild and ridiculous, if there is evidence for it. The wilder and more ridiculous something is, however, the firmer and more solid the evidence will have to be"

Isaac Asimov

Resumen

La presente tesis titulada: “Componentes de aceites esenciales encapsulados en soportes mesoporosos de sílice: una evaluación de sus propiedades bioactivas y un enfoque toxicológico” se centra en la evaluación de las propiedades funcionales y organolépticas de agentes naturales bioactivos, derivados de componentes de aceites esenciales, encapsulados en materiales mesoporosos de sílice; a la vez que evalua la toxicidad de los soportes utilizados, con el fin de proponer nuevos sistemas de liberación controlada por vía oral.

La primera sección de esta tesis muestra el efecto de la encapsulación de los compuestos de aceites esenciales (EOCs, por sus siglas en inglés) en soportes mesoporosos de sílice. Por un lado, se evalúa la eficiencia de los EOCs libres y encapsulados para reducir la viabilidad en líneas celulares de cáncer de colon. Además, se evalúa la selectividad de los EOCs frente a células de colon normales (líneas no tumorales). Por otro lado, se estudia la capacidad de enmascaramiento de olor de los soportes. Los resultados obtenidos, evidencian en primer lugar, que los EOCs encapsulados mejoran su actividad frente a células de cáncer, en comparación con la respuesta de los compuestos sin encapsular. La encapsulación hace que el efecto de los EOCs sea sostenido en el tiempo, y muestra índices de especificidad prometedores, cuando se evalua el efecto toxico de los EOCs frente a células de cáncer de colon y células normales. Los resultados de esta primera

sección, indican que los soportes basados en partículas de sílice mesoporosa (MSPs, por sus siglas en inglés) protegen y liberan eficientemente los compuestos, sino que, a la vez que la funcionalización de la superficie de las MSPs permite enmascarar el olor de los compuestos de mayor volatilidad, y con mayores inconvenientes a nivel sensorial (p.e. compuestos derivados del ajo). Por lo tanto, el sistema de encapsulación se plantea como una excelente alternativa para (i) promover la liberación controlada de EOCs, (ii) aprovechar y mejorar el efecto de sus propiedades bioactivas en células de cáncer de colón y (iii) controlar las desventajas técnicas relacionadas con la volatilidad y limitaciones organolepticas. Por último, se ha comprobado que los soportes empleados en la encapsulación de los compuestos derivados de ajo, mantienen su funcionalidad luego der ser inmovilizados en nanofibras de nylon. Con esto, se busca desarrollar un material híbrido y homogéneo, fácil de manejar, que libera controladamente los compuestos encapsulados desde soportes tipo fibras (composites). Esto expande el abanico de aplicaciones de los EOCs en la industria alimentaria y farmacológica.

La segunda sección de esta tesis, evalúa la toxicidad de los soportes de sílice mesoporosa (MSPs) mediante ensayos *in vitro* e *in vivo.* En primer lugar, la viabilidad celular permite identificar el impacto citotóxico de los MSPs sobre líneas celulares de colón. En particular, se evalúa los soportes mesoporosos de sílice, tipo MCM41, en función de (i) las dosis empleadas, (ii) la diferencia de

tamaño (micro y nanopartículas) y (iii) el efecto que la funcionalización de la superficie genera en la viabilidad celular. Por otro lado, empleando el modelo *in vivo* de los nematodos, *Caednorhabditis elegans*, y administrando por vía oral las MSPs, se evalua la influencia de las características de las partículas (MSPs) en función de la esperanza de vida (lifespan) y la calidad con la que viven y envejecen (healthspan) los nematodos. Los resultados de este estudio, muestran que el tamaño y la estructura de la superficie de las partículas, son parámetros determinantes al momento de diseñar soportes de bajo riesgo toxicológico.

En resumen, la presente tesis ha evaluado las características de la sílice mesoporosa, micro y nanoparticulada, como soporte de encapsulación para mejorar la actividad y las aplicaciones de los compuestos de aceites esenciales, al mismo tiempo que evalua su riesgo toxicológico. Los resultados obtenidos muestran la posibilidad de desarrollar soportes de sílice mesoporosa de bajo impacto toxicológico, de modo que puedan administrarse vía oral para la liberación controlada de compuestos de interés alimentario o farmacológico.

Resum

La present tesi titulada: "Components d'olis essencials encapsulats en suports mesoporosos de sílica: una avaluació de les seves propietats bioactives i un enfocament toxicològic" se centra en estudis de protecció i alliberament controlat d'agents naturals bioactius, derivats de components d'olis essencials, encapsulats en materials mesoporosos de sílica. Els components d'olis essencials encapsulats milloren les seves propietats funcionals i redueixen els problemes sensorials per aplicacions futures, garantint, al mateix temps, la baixa toxicitat dels suports desenvolupats.

La primera secció de la tesi mostra l'efecte d'encapsulació dels components d'olis essencials (EOCs, per les seves sigles en anglès) en suports mesoporosos de sílica sobre la millora de les seues propietats bioactives i el camuflament de problemes sensorials. Este estudi avalua l'eficiència dels EOCs lliures i encapsulats per a reduir la viabilitat en línies cel·lulars de càncer còlon. A més, la selectivitat dels EOCs es va provar enfront de cèl·lules de còlon normals (no canceroses). Els resultats han demostrat que l'efecte dels EOCs pot ser millorat i sostingut en el temps quan els EOCs estan encapsulats. Encara més, l'encapsulació dels EOCs mostra índexs d'especificitat prometedors, arribant a duplicar la toxicitat en les cèl·lules de càncer de còlon amb comparacio en les cèl·lules normals. Els resultats també mostren que els suports basats en partícules de sílice mesoporoses (MSPs,

per les seves sigles en anglès) no sols protegixen i alliberen EOCs eficientment, sinó que, a més, la funcionlització en superfície de les MSPs permet emmascarar l'olor dels EOCs d'alta volatilitat, que té una aplicació limitada a causa dels seus problemes sensorials (p.e. compostos derivats de l'all). Per tant, el sistema de subministrament proposat resulta una excel·lent alternativa per a (i) promoure l'alliberament controlat de EOCs, (ii) avançant en les seues propietats bioactives en cel·lulas de càncer còlon i (iii) controlant els desavantatges tècnics relacionats amb la volatilitat i la disseminació desagradable de les olors. Finalmet, les mostres utilitzades per encapsulació de compostos d'all es van immobilitzar en nanofibres per a proporcionar un sistema híbrid homogeni i fàcil de manejar amb administració controlada i característiques bioactives, per aplicacions potencials en l'àrea d'alimentació, farmacologia, medicina o enginyeria.

La segona secció avalua la toxicitat del suports de sílice mesoporosa per mitjà d'avaluacions *in vitro* e *in vivo.* La viabilitat cel·lular permet identificar l'impacte citotòxic basat en el tipus de suport base de sílice i les seues característiques (rang de dosi, grandària i canvis en l'estructura superficial). A més, utilitzant el model *in vivo* de nematodes, *Caednorhabditis elegants*, s'ha estudiat la influència de les característiques de la sílice mesoporosa, administrant micro i nanopartícules de base sílice, no sols en l'esperança de vida, sinó també en el comportament dels nematodes durant el seu envelliment. Aquest estudi ha

demostrat que la grandària i l'estructura superficial, són decisius per a reduir el risc de toxicitat dels suports de sílice mesoporosa i obrir la possibilitat d'utilitzar estos materials en aplicacions d'ingesta oral.

En resum, la present tesi ha avaluat les característiques de les partícules de sílice mesoporosa, com a suports d'encapsulació per a millorar l'activitat i les aplicacions dels EOCs, alhora que es va avaluar el seu principal risc tòxicologic. En conseqüència, els resultats obrin una opció adequada i de seguretat per als dispositius d'administració oral.

Abstract

The present PhD thesis, entitled: “Essential oil components encapsulated in mesoporous silica supports: a bioactive properties evaluation and a toxicological approach” focuses on the study of protection and controlled release of natural bioactive agents, derived from essential oil components (EOCs), encapsulated in mesoporous silica particles (MSPs). In addition, this thesis evaluates the silica-based supports to reduce the EOCs’ undesirable sensorial properties and for ensuring a low-health risk.

The first section of the thesis shows the effect of encapsulation of EOCs in mesoporous silica supports. This study evaluates the efficiency of free and encapsulated EOCs to reduce the viability of cancer colon cell lines. This section also shows the selectivity of encapsulated EOCs against cancer lines and their effect on normal (non-cancer) colon cells. Results indicate that EOCs effect can be enhanced and sustained in time when EOCs are encapsulated. Moreover, EOCs’ encapsulation shows promising specificity indices, reaching to double effect on colon cancer cells above normal cells. On the other hand, the encapsulation supports and their surface functionalization allows the odour masking of high volatility EOCs. Therefore, the delivery system based on MSPs represents an excellent alternative to promote controlled EOCs release, taking advance of their bioactive properties and solving the technical disadvantages related to volatility

and unpleasant odours. Finally, samples used for garlic components encapsulation were immobilised in nanofibers to provide homogeneous and easy-to-handle hybrid system for controlling delivery. The developed 'composite' has potential applications on food, pharmacology, medical or engineering fields.

The second section of the thesis evaluates the toxicity of the mesoporous silica supports through *in vitro* and *in vivo* assessments. Cell viability allows to identify the cytotoxic impact based on the kind of silica-based support, and their features (doses range, size and surface structure changes). Furthermore, the use of *Caednorhabditis elegans* model, shows the *in vivo* effects after MSPs ingestion. The toxicological study confirms that size and surface structure, are decisive MSPs' features for reducing the toxicity risks for health.

In summary, the present thesis evaluates the mesoporous silica-based particles as supports for EOCs encapsulation and identifies the main MSPs' features for reducing the health-toxicity impact. Results of this thesis show that MSPs improve the EOCs activity and help to solve technical problems related to sensorial features of EOCs. Moreover, these results open up a suitable and safety option for oral delivery devices.

TABLE OF CONTENTS

1 PREAMBLE

PREAMBLE

This PhD thesis forms part of the projects "***Improvement of the stability and control release of biomolecules by using microcapsules functionalized with molecular gates*** (AGL2012-39597-C02-01)" and "***Use of biocompatible supports for the development of new antimicrobials and controlled release systems*** (AGL2015-70235-C2-1-R)", funded by the 2013-2016 and 2016-2019 National Research Plan of the Spanish Ministry of Economy and Competitiveness, respectively.

In order to evaluate and enhance the functional properties of bioactive components from essential oils, the use of encapsulation supports to protect and controll the components' delivery is an interesting research area. In particular, design of oral release devices opens a wide range of food and pharmaceutical uses. However, some bioactive molecules are not compatible with real industrial application due to their physicochemical and organoleptic features. In addition, is needed to confirm the non-toxicity of encapsulation supports once they are administered by oral intake.

In this context, mesoporous silica particles (MSPs) are interesting supports for the bioactive components. In addition, a switchable "gate-like" ensemble, functionalised on the MSPs' surface, is capable of being "open" or "closed" when

certain external stimuli are applied. Thus, the surface functionalisation allows the controlled release while protect the encapsulated components.

Based on that, through the project, "***Use of biocompatible supports for the development of new antimicrobials and controlled release systems***", the research focuses to evaluate the mesoporous silica-based particles as encapsulation supports of bioactive components derived from essential oils. The developed system applies the concepts for controlling release which also help to mask some unpleasant sensorial features of essential oil components (EOCs).

Therefore, to confirm the possibilities of silica-based supports as oral devices geared towards the delivery on digestive tract, the project:"***Improvement of the stability and control release of biomolecules by using microcapsules functionalized with molecular gates***" focuses the research on the *in vitro* and *in vivo* toxicity of the developed supports.

The doctoral thesis entitled "Essential oil components encapsulated in mesoporous silica supports: an evaluation of their bioactive properties and a toxicological approach" is the third doctoral thesis undertaken within this framework.

2 OBJECTIVES

OBJECTIVES

The main objective of this PhD thesis was to encapsulated and evaluate the bioactive properties of components from essential oils and evaluate the toxic effect of mesoporous silica supports used for encapsulation.

To meet the main objective, the present thesis was divided into two different approaches with the following specific objectives:

I. ***Bioactive properties of essential oils components encapsulated in mesoporous silica supports.*** This was addressed to create functional supports by encapsulation, to take advance of the anticancer properties of components from essential oils in digestive tract, while reduce the drawbacks from their unpleasant sensorial features.

   i. To evaluate the anticancer properties of selected bioactive components on colon cells.

   ii. To assess the masking odour properties of the gated materials.

   iii. To combine technologies for widening the range of industrial applications of bioactive components using hybrid materials.

II. ***Nanotoxicological evaluation of mesoporous silica supports.*** This was addressed to evaluate the toxic effect of mesoporous silica particles of different sizes and different surface structure.

   i. To evaluate the cell viability of colon cell lines after incubation with different features of mesoporous silica supports.

   ii. To assess the effects on life expectancy and healthy aging of *in vivo* model fed with mesoprous silica supports.

3 GENERAL CONSIDERATIONS

3.1 Amorphous and mesoporous silica-based materials, a background

To understand the amorphous concept on silica materials, it is need to know about crystalline structures. In mineralogy and crystallography, an ordered arrangement of atoms, ions or molecules shape a crystalline material. The smallest set of atoms arranged and periodically repeated along the three-dimensional space is named the unit cell (Yanchitsky & Timoshevskii 2001). Which, can be associate to a specific pattern evaluated through X-ray powder diffraction (Toraya 1986).

In particular, silicon is a fourfold coordinate atom, normally tetrahedrally bonded to four neighbouring silicon atoms. Silicon crystallizes in a diamond cubic crystal structure; a face-centred diamond-cubic (Figure 3-1A). But rarely occurs as the pure element; instead, silicon has great chemical affinity for oxygen, making silicon dioxide, SiO_2 (silica). In silica, the silicon atom shows tetrahedral coordination, with four oxygen atoms surrounding a central silicon atom as shows Figure 3-1B (Bergna & Colloid 1994). Silicon–oxygen bond lengths vary between the different crystal forms (polymorphs), and deviations from these parameters constitute the amorphous structure (Lippincott et al. 1958). Thus, amorphous silica has silicon-oxygen bonds but exhibit only a short-range ordering of their atoms, with non-repeating pattern and no predictable order (Figure 3-1C). In this

manner, the amount of crystalline structure in amorphous silica is negligible (between 0.01 and 0.3 %) (Fruijtier-Pölloth 2012).

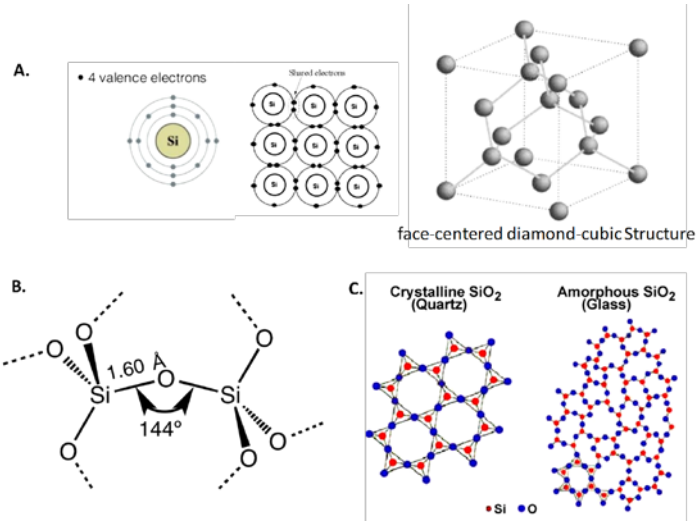

Figure 3-1. Silicon and silica chemical structures. A. Silicon atom and its crystal structure B. Coordination of silicon and oxygen atoms in silica C. Order of atoms on crystalline and amorphous silica

Amorphous silica can be synthesised as silica gel, precipitated, colloidal and pyrogenic (fumed) silica (Bergna & Colloid 1994). In general, synthetic amorphous silica (SAS) consists of nano-sized primary particles, which agglomerate on nano- and micrometer-size range. Due to the empty spaces left by the agglomeration a narrow pore distribution could appear. However, those pores are very unevenly distributed and do not associate to porous structure, hence SAS is defined as a non-porous structure (EOCD 2004; ECETOC 2006).

In contrast, mesoporous silica particles (MSPs) have well-ordered pore arrangements, which can give diffraction patterns on powder X-ray diffraction

(PXRD). MSPs structures do not have long-range order in the direction of a crystalline material (Figure 3-2A); but diffraction is due to periodically repletion of the homogeneous and ordered pore arrangement. Figure 3-2B shows the PXRD of a widely used MSPs; the unidirectional channels (hexagonal, cubic, or lamellar) produce a diffraction pattern (Figure 3-2A), which is nothing compared to crystalline structures. Thus, silica frameworks on MSPs are characterised by PXRD, but their structure is amorphous (Perez-Pariente, 2006).

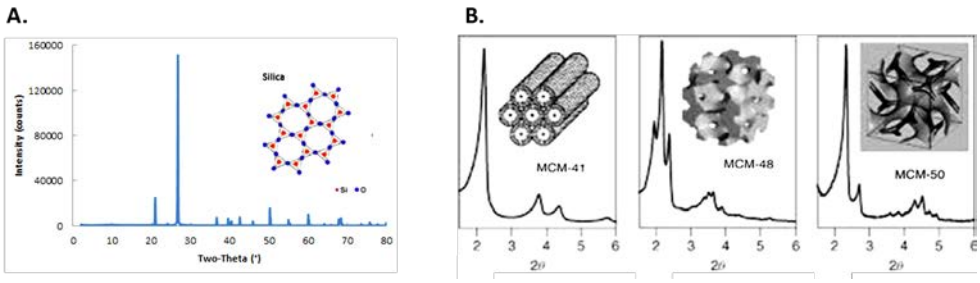

Figure 3-2. Diffraction X-ray patterns A. Repeating pattern of ordered atoms from crystalline silica structure B. Silica structures from uniform porous structure of MSPs with unidirectional chanels ordered as: hexagonal (MCM41), cubic (MCM-48) and lamellar (MCM50).

3.2 Mesoporous silica particles (MSPs)

The need of supports with pores of larger dimensions than the ones found in microporous zeolites (pore sizes less than 2 nm), motivated the research on mesoporous materials (pore sizes between 2-50 nm). In the 90's porous silica materials with uniform pore size were described; Mobil company divulged the synthesis and characterisation of a type of silica-based mesoporous materials, a

family of uniform pore materials named M41S. These materials present a large number of mesopores that confers high specific surface areas (700-1000 $m^2 \cdot g^{-1}$), a great loading capacity, a large specific pore volume (0.6-1 $cm^3 \cdot g^{-1}$) and an elevated total surface (1000 $cm^2 \cdot g^{-1}$) (Schmidt et al. 1995; Cong-Yan et al. 1993; Beck et al. 1992).

3.2.1 Synthesis of the MSPs

Ordered mesoporous silica relies on a bottom-up synthesis, via supramolecular self-assembly (also called soft-templating). Basically, two main components are used: (i) a surfactant template, able to form micelles in water solution which acts as a structure-directing agent, and (ii) an inorganic silica polymeric precursor, which self-organizes around the template to condensate and polymerize. It builds up the final mesostructured with regular arrays of uniformly organized mesochannel pores (Pal & Bhaumik 2013). Mechanisms involved on the fabrication of these materials are mainly based on the liquid crystal templating (Kresge, Leonowicz, Roth, Vartuli, & Beck, 1992). First a formation of surfactant micelles in solution (e.g. *N*-cetyltrimethylammonium bromide (CTABr)) occurs, then, surfactant micelles shape cylindrical micelles, and their stacking conform a regular array of micelle liquid crystals. Finally, as Figure 3-3 shows, the inorganic siliceous precursor (e.g. tetraethyl orthosilicate, sodium metasilicate) hydrolyses and condensates onto the positively charged surfaces of the micelle liquid

crystals. The final material is obtained after removing the surfactant template using either solvent extraction or calcination (500 - 600 °C) (Yang et al. 2004).

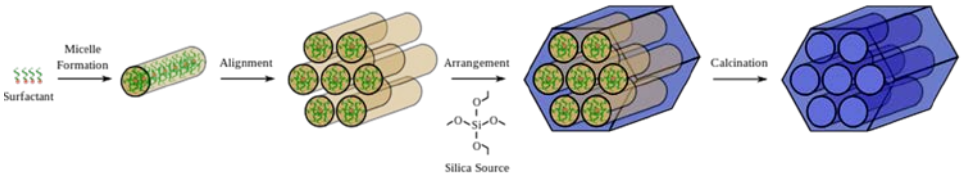

Figure 3-3. Synthesis of mesoporous silica-based materials from surfactant micelles to an ordered hexagonal porous structure (MCM-41 type material).

The mesoporous inorganic scaffold obtained in these conditions has cylindrical unidirectional empty channels of approximately 3 nm of diameter (when CTABr is used as surfactant) arranged in a uniform two-dimensional (2D) distribution. Depending on surfactant to silica ratio the hexagonal (MCM41), cubic (MCM48) o lamellar (MCM50) structure is obtained (Wang et al. 2003; Chan et al. 2001). Pore arrangement evaluation was shown in previous section, *vide supra*. Typically, the obtained material is spherical, rod or oval shaped among the nanometre size (under 100 nm).

The original approach of M41S family has been extended and silica-based mesoporous materials can be synthesised by alternative pathways. Variables such as time, concentration, temperature, pH, ionic strength, type of surfactant and type of silica precursor (fumed silica, sodium silicate, or a tetra-alkyl oxide of silane) can be modified to get MSPs with different features (Trewyn et al. 2007).

The synthetic protocol can include chelators agents, such as triethanolamine (TEAH), to control the hydrolysis and condensation process through 'atrane route', which modify the final size of materials (Telalović et al. 2010; Cabrera et al. 2000; C. T. Kresge et al. 1992).

In recent years, other MSPs' types have been synthesised, such as, folding sheet materials (FSM) (Yanagisawa et al. 1990), hexagonal mesoporous silica (HMS) (Tanev & Pinnavaia 1995), Santa Barbara amorphous silica (SBA-15) (Zhao et al. 1998; Kruk et al. 2000), Technische Universiteit Delft material (TUD-1) (Telalović et al. 2010; Jansen et al. 2001) Universidad Valencia material (UVM-7) (Cabrera et al. 2000; el Haskouri et al. 2002), anionic-templated mesoporous silica material (AMS-6) (Garcia-Bennett et al. 2004), Korea Advanced Institute of Science and Technology material (KIT-6) (Wang et al. 2014) and an extensive diversity of porous silica-based materials.

3.2.2 Modification of MSPs surface

Apart from homogeneous pore size distribution and high specific surface area and volume, MSPs highlights for exhibiting a high concentration of structural defects on their surface in the form of silanol (Si-OH) groups that can easily react with trialkoxysilane derivatives ($(R'O)_3$-Si-R), allowing the possibility of generating organic–inorganic hybrid materials (Vinu et al. 2005). These hybrid materials offer a wide range of new perspectives in the development of delivery systems through

the gated supports (Aznar et al., 2009; Coti et al., 2009; Giri et al., 2005). These supports contain switchable molecular-based entities which control the on-command delivery of cargo encapsulated. Gated materials are based on the combination of two components: (i) a suitable inorganic support acting as a carrier and (ii) a switchable supramolecular-based ensemble, that is attached to supports' surface. The "gate-like" system is able to be "opened" upon the application or the presence of a predefined stimulus (Coll et al. 2013), and thus cargo release can be controlled at will (Aznar et al., 2009).

In line with this concept, examples of MSPs functionalised with a number of different molecules and biomolecules, able to deliver the cargo upon the applications of physical (light, temperature, magnetic fields, ultrasounds) (Aznar et al., 2011; Johansson, Choi, Angelos, Liong, & Zinck, 2008; Saha & Stoddart, 2007), chemical (anions, cations, neutral molecules, redox-active species and pH) (Pérez-Esteve, Fuentes, et al. 2015; Casasús et al. 2008) and biochemical (such as enzymes, DNA and antibodies) (Oroval et al. 2013; Mamaeva et al. 2011) stimuli have been reported.

In particular, capped MSPs offer an interesting strategy for encapsulation, protecting, transporting and later administration of bioactive molecules (basic nutrients, bioactive components, sensory appeal compounds, and pre- and probiotics, and even drugs) under specific stimuli in the gastrointestinal tract

which opens up a wide range of possibilities to oral delivery devices (Pérez-Esteve, Ruiz-Rico, et al. 2015).

Among the gastrointestinal stimuli for on-command delivery applications, enzymes specific activities and pH variations are the most extended systems evaluated to date. Amylases presence for starch digestion motivates the use of polysaccharides as gates (Bernardos et al. 2010; Bernardos et al. 2009). Similarly, proteases, lipases and other digestive enzymes such as ribonucleases and deoxyribonucleases, in conjunction to salts from pancreatic juices complete the digestion between stomach and small intestine. Thus, molecules based on amino acids (peptides, proteins) or fats result interesting for capping MSPs supports (Coll et al. 2011; Coll et al. 2013; Shi et al. 2012). Additionally the pH variation along the mouth activity to stomach and intestine also have motivated the design of molecular gates based on polyamines and molecules that can be able to adopt different conformations in function of pH changes (Casasús et al. 2008; Bernardos et al. 2008). Applications for these capped supports can be motivating for new functional food or medical and pharmaceutical applications.

References

Aznar, E. et al., 2011. Finely tuned temperature-controlled cargo release using paraffin-capped mesoporous silica nanoparticles. *Angew Chem Int Ed Engl.*, 50(47), pp.11172–11175.

Aznar, E., Martínez-Máñez, R. & Sancenón, F., 2009. Controlled release using mesoporous materials containing gate-like scaffoldings. *Expert Opin Drug Deliv*, 6(6), pp.643–655.

Beck, J.S. et al., 1992. A New Family of Mesoporous Molecular Sieves Prepared with Liquid Crystal Templates. *J. Am. Chem. Soc.*, (114), pp.10834–10843.

Bergna, H.E. & Colloid, T., 1994. The Colloid Chemistry of Silica. *Advances*, 234(2), p.695. Available at: http://pubs.acs.org/doi/book/10.1021/ba-1994-0234.

Bernardos, A. et al., 2008. Controlled release of vitamin B2 using mesoporous materials functionalized with amine-bearing gate-like scaffoldings. *J Control Release*, 131(3), pp.181–189.

Bernardos, A. et al., 2009. Enzyme-responsive controlled release using mesoporous silica supports capped with lactose. *Angew Chem Int Ed Engl.t Ed.*, 48(32), pp.5854–7.

Bernardos, A. et al., 2010. Enzyme-responsive intracellular controlled release using nanometric silica mesoporous supports capped with "saccharides." *ACS Nano*, 4(11), pp.6353–6368.

Cabrera, S. et al., 2000. Generalised syntheses of ordered mesoporous oxides: the atrane route. *Solid State Sci.*, 2(4), pp.405–420.

Casasús, R. et al., 2008. Dual aperture control on pH- and anion-driven supramolecular nanoscopic gate-like ensambles. *J Am Chem Soc*, 130, pp.1903–1917.

Chan, H.B.S., Budd, P.M. & Naylor, T.D., 2001. Control of mesostructured silica particle morphology. *J. Mater. Chem.*, 11(3), pp.951–957.

Coll, C. et al., 2011. Enzyme-mediated controlled release systems by anchoring peptide sequeces on mesoporous silica supports. *Angew Chem Int Ed.*, 50, p.2138.

Coll, C. et al., 2013. Gated silica mesoporous supports for controlled release and signaling applications. *Acc Chem Res*, 46(2), pp.339–349.

Cong-Yan, C., Hong-Xin, L. & Davis, M.E., 1993. Studies on mesoporous materials I. Synthesis and characterization of MCM 41. *Microporous Materials*, (2), pp.17–26.

Coti, K.K. et al., 2009. Mechanised nanoparticles for drug delivery. *Nanoscale*, 1(1),16–39.

ECETOC, 2006. *Synthetic Amorphous Silica* , Bruselas: European Food Safety Authority .

EOCD, 2004. *Dossier on synthetic Amorphous Silica and Silicates*,

Fruijtier-Pölloth, C., 2012. The toxicological mode of action and the safety of synthetic amorphous silica-a nanostructured material. *Toxicology*, 294(2–3), pp.61–79.

Garcia-Bennett, A.E. et al., 2004. Structural Investigations of AMS-n Mesoporous Materials by Transmission Electron Microscopy. *Chemistry of Materials*, 16(5), pp.813–821.

Giri, S. et al., 2005. Stimuli-responsive controlled-release delivery system based on mesoporous silica nanorods capped with magnetic nanoparticles. *Angew Chem Int Ed.*, 44, pp.5038–5044.

el Haskouri, J. et al., 2002. Silica-based powders and monoliths with bimodal pore systems. *Chemical communications (Cambridge, England)*, (4), pp.330–331.

Jansen, J.C. et al., 2001. A new templating method for three-dimensional mesopore networks. *Chemical Communications*, (8), pp.713–714.

Johansson, E. et al., 2008. Light-activated functional mesostructured silica . *Sol-gel Sci. Technol*, 46, pp.313–322.

Kresge, C.T. et al., 1992. Ordered mesoporous molecular sieves synthesized by a liquid-cristal template mechanism. *Nature*, 359, pp.710–712.

Kruk, M. et al., 2000. Characterization of the porous structure of SBA-15. *Chemistry of Materials*, 12(7), pp.1961–1968.

Lippincott, E.R. et al., 1958. Infrared studies on polymorphs of silicon dioxide and germanium dioxide. *Journal of Research of the National Bureau of Standards*, 61(1), p.61.

Mamaeva, V. et al., 2011. Mesoporous silica nanoparticles as drug delivery systems for targeted inhibition of Notch signaling in cancer. *Molecular therapy : the journal of the American Society of Gene Therapy*, 19(8), pp.1538–1546.

Oroval, M. et al., 2013. An aptamer-gated silica mesoporous material for thrombin detection. *Chem commun.*, 49, pp.5480–5482.

Pal, N. & Bhaumik, A., 2013. Soft templating strategies for the synthesis of mesoporous materials: Inorganic, organic-inorganic hybrid and purely organic solids. *Advances in Colloid and Interface Science*, 189–190, pp.21–41.

Pérez-Esteve, É., Ruiz-Rico, M., et al., 2015. Mesoporous Silica-Based Supports for the Controlled and Targeted Release of Bioactive Molecules in the Gastrointestinal Tract. *Journal of Food Science*, 80(11), pp.E2504–E2516.

Pérez-Esteve, É., Fuentes, A., et al., 2015. Modulation of folic acid bioaccessibility by encapsulation in pH-responsive gated mesoporous silica particles. *Microporous and Mesoporous Materials*, 202, pp.124–132.

Perez-Pariente, J., 2006. Materiales mesoporosos de óxido de silicio. *Liberación de fármacos en matrices biocerámicas: avances y perspectivas*, pp.39–64.

Saha, S. & Stoddart, J.F., 2007. Photo-driven molecular devices. *Chem Soc Rev*, 36(1), pp.77–92.

Schmidt, R. et al., 1995. MCM-41: a model system for adsorption studies on mesoporous materials. *Microporous Materials*, 3(4–5), pp.443–448.

Shi, F. et al., 2012. Preparation and characterization of solid lipid nanoparticles loaded with frankincense and myrrh oil. *International journal of nanomedicine*, 7, pp.2033–43.

Tanev, P.T. & Pinnavaia, T.J., 1995. A neutral templating route to mesoporous molecular sieves. *Science*, 267(5), pp.865–867

Telalović, S. et al., 2010. TUD-1: synthesis and application of a versatile catalyst, carrier, material…. *Journal of Materials Chemistry*, 20(4), p.642.

Toraya, H., 1986. Whole-powder-pattern fitting without reference to a structural model: application to X-ray powder diffraction data. *Journal of Applied Crystallography*, 19(6), pp.440–447.

Trewyn, B.G. et al., 2007. Synthesis and functionalization of a mesoporous silica nanoparticle based on the sol-gel process and applications in controlled release. *Acc Chem Res*, 40(9), pp.846–853.

Vinu, A., Hossain, K.Z. & Ariga, K., 2005. Recent advances in functionalization of mesoporous silica. *Journal of nanoscience and nanotechnology*, 5(3), pp.347–371.

Wang, J. et al., 2003. Structure-selective synthesis of mesostructured/mesoporous silica nanofibers. *J Am Chem Soc*, 125(46), pp.13966–13967.

Wang, W. et al., 2014. Synthesis of KIT-6 type mesoporous silicas with tunable pore sizes, wall thickness and particle sizes via the partitioned cooperative self-assembly process. *Microporous and Mesoporous Materials*, 194, pp.167–173.

Yanagisawa, T. et al., 1990. The preparation of alkyltrimethylammonium-kanemite complexes and their conversion to microporous materials. *Bulletin of the Chemical Society of Japan*, 63(4), pp.988–992.

Yanchitsky, B.Z. & Timoshevskii, A.N., 2001. Determination of the space group and unit cell for a periodic solid. *Computer Physics Communications*, 139(2), pp.235–242.

Yang, C.M. et al., 2004. Stepwise removal of the copolymer template from mesopores and micropores in SBA-15. *Chemistry of Materials*, 16(15), pp.2918–2925.

Zhao, D. et al., 1998. Triblock copolymer syntheses of mesoporous silica with periodic 50 to 300 angstrom pores. *Science*, 279(5350), pp.548–52.

4 SECTION I

Bioactive properties from essential oils components encapsulated in mesoporous silica supports.

4.1 Introduction: Bioactive components derived from essential oils

Essential oils derived from plants are one of the more important agricultural products used in the industry. Essential oils are complex natural mixtures which can contain about 20-100 components at different concentrations. In particular, essential oils are primarily composed by two or three major components at high concentrations (20-70 %). Terpenoids and phenylpropanoids constitute the major constituents of the essential oils. Aromatic and aliphatic constituents are also present, as well as, monoterpenes, sesquiterpenes and oxygenated derivatives (Raut & Karuppavil 2014). For instance, carvacrol (30 %) and thymol (27 %) are the major components of the *Origanum compactum essential oil*, a-phellandrene (36 %) and limonene (31 %) of leaf and carvone (58 %) and limonene (37 %) of seed *Anethum graveolens essential oil*, menthol (59 %) and menthone (19 %) of *Mentha piperita essential oil*. Commonly, these major components determine the bioctive properties of the essential oils (Adorjan & Buchbauer 2010). A wide variety of bioactive properties are interesting for health, pharmaceutical, cosmetic and food applications. Among the properties associated to EOCs, antimicrobial, antioxidant, anti-inflammatory, antimutagenic and anticancer effect draw the attention of latest studies.

4.1.1 Antimicrobial and antifungal activity

Metabolites from herbs and spices are involved in plant chemical defence system. Among plant extracts components, aldehydes, phenolic and mainly, oxygenated terpenoids have been related to antimicrobial and antifungal activity. EOCs from *Curcuma*, *Thymus*, *Origanum, Allium*, and *Cinnamomum* species have been mainly tested against *Staphylococcus aureus*, *Bacillus cereus*, *Escherichia coli*, *Pseudomonas aeruginosa, Clostridium perfringens*, *Listeria monocytogenes* and *Vibrio parahaemolyticus,* and most of EOCs have shown high selectivity against those food pathogens (Ruiz-Rico et al. 2017; Burt 2004; Hammer & Carson 2011; Bassolé & Juliani 2012). Moreover, EOCs such as carvacrol, eugenol, thymol, cinnamaldehyde, limonene, eucalyptol, and other terpenoids, have been tested against *Aspergillus flavus, Aspergillus niger*, *Penicillium expansum, Zygosaccharomyces rouxii* and *Zygosaccharomyces bailii* displaying remarkable antifungal properties (Ribes et al. 2016; Janatova et al. 2015).

Efficiencies of EOCs are determined in function of concentrations required to inhibit the growth of target organisms. Usually, minimum growth inhibitory concentrations (MICs), minimum lethal concentrations (MLCs), as well as concentration where viability decrease fewer than half of the population, EC50, MIC50 and LD50 are values used for compared the components' bioactivity (Hammer & Carson 2011).

4.1.2 Antioxidant and Anti-inflammation activity

The high amount of oxygenated monoterpenes and phenolic components of EOCs, give them a high antioxidant capacity. Colorimetric tests of free-radical scavenging have shown the antioxidant activity of essential oils due to thymol, carvacrol, eugenol, terpineol, menthol, limonene, and citronellol components. Although mono and sesquiterpenes are related to antioxidant properties, studies have shown that phenols and flavonoids components are major responsibles of EOCs' antioxidant capacity (Adorjan & Buchbauer 2010; Miguel 2010).

On the other hand, inflammation, as the initial response of protective reaction to harmful stimuli, is currently treated with anti-inflammatory drugs. But, recently, EOCs' components have been shown anti-inflammatory effects. Thymoquinone, a component of the volatile oil of *Nigella sativa L.*, suppressed adjuvant-induced arthritis in rats, as well as decrease the expression of pro-inflammatory cytokines of induced colitis in mice. Thyme, as major component from oregano oil, also showed decrease of inflammatory cytokines of colitis (Botsaris 2007). Other promising inhibition of inflammation have been evidenced by components such as citronellol, limonene, camphene, curcumene, rosmarininc acid and carvacrol (Adorjan & Buchbauer 2010).

4.1.3 Anticancer evidences

Findings suggest that bioactive properties of EOCs are associated to mitochondrial dysfunction and changes in intracellular redox potential. It opens interesting applications beyond the well-known antimicrobial and antibacterial properties, and focuses the attention on anti-cancer studies (Adorjan & Buchbauer 2010). Tumour cell lines of melanomas breast, prostate and cervical adenocarcinomas, as well as glioblastoma, and lung fibroblasts have been evaluated with wide variety of EOCs. Results suggest that EOCs are suitable for treat cancer cells (Llana-Ruiz-Cabello et al. 2014; Oliveira et al. 2015). Phytochemicals from essential oils not only have shown a significant potential as chemo-preventive agents, but also, some studies have shown the EOCs effect on multi-drug resistant cancer cells (Bakkali et al. 2008). In contrast to cytotoxic agents such as doxorubicin, camptothecin, and other synthetic products used currently in chemotherapy (Heikkilä et al. 2010; Lai et al. 2012), the use of EOCs offers a suitable alternative in the field of anti-cancer natural products (Raut & Karuppavil 2014; Kris-Etherton et al. 2002). Latest studies suggest that depending on type and doses, EOCs exhibit cytotoxic effects due to pro-oxidant effects at cellular level but few results are associated to DNA damage (Bakkali et al. 2008).

In particular, EOCs *in vitro* assays have shown chain reactions from the cell wall or the outer cell membrane, through organelles like mitochondria and

peroxisomes. These effects suggest a phenolic-like prooxidant activity. Hence, studies point apoptosis as the main route of EOCs' cytotoxic effect with a small number of genotoxic effects (Jaganathan & Supriyanto 2012).

4.1.4 Gastrointestinal studies with EOCs

Alternative products based on plants-derived metabolites motivate their use and evaluation to deal with current drugs limitations. In life science the use of EOCs have shown interesting application for treat gastrointestinal tract. In cases of diarrheal control, carminative and digestive effects, as well as hepato-protective effects and other gastrointestinal disorders. Natural-derived products from EOCs are traditionally used (Botsaris 2007). Among gastrointestinal approaches, the focus on anticancer therapies using EOCs has drawn the interest of food and medical science. *In vitro* studies have shown interesting results of EOCs effect on liver and colon carcinoma cell lines (Oliveira et al. 2015).

Currently, the third most common malignancy that affect people worldwide and one of the major causes of cancer-related to death is colon cancer. Latest studies have pointed six-main components from essential oils: allyl-isothiocyanate, cinnamaldehyde, eugenol, diallyl disulphide, carvacrol and thymol (see Figure 4-1); which displayed a remarkable *in vitro* activity against colon cancer (Coussens & Werb 2002).

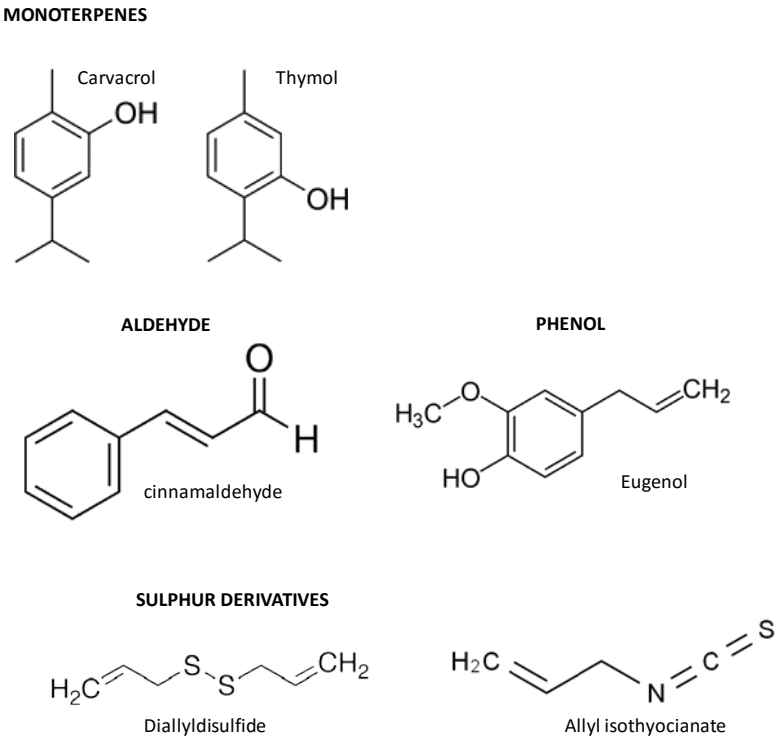

Figure 4-1. Chemical structures of mainly EOCs used on colon cancer studies.

Allyl isothiocyanate (AI)

A volatile organic compound, found in horseradish (*Armoracia rusticana, syn. Cochlearia armoracia*) of the *Brassicaceae* family, which also includes mustard, wasabi, and cruciferous vegetables such as broccoli, and cabbage. The 3-isothiocyanato-1-propene, has strong antibacterial properties and some studies have shown the cytotoxic effect on colon cells (Geng et al. 2011; Musk & Johnson 1993; Zhang 2010).

Cinnamaldehyde (CN)

From the stem bark of *Cinnamomum cassia,* the (2E)-3-phenylprop-2-enal, is known to possess several biological activities, including antifungal, cytotoxic and anti-mutagenic properties with a noticeable antitumor effects *in vivo* and *in vitro*, on colon cancer.(Li et al. 2016; Jeong et al. 2003; Yu et al. 2014; Ribes et al. 2016)

Eugenol (EU)

Component of *Syzigium aromaticum* (cloves), the 4-allyl-2-methoxyphenol, has been used as analgesic and antibacterial agent and it has been reported to possess anticancer and antigenotoxic activity (Jaganathan et al. 2011; Hussain et al. 2011; Jaganathan & Supriyanto 2012).

Diallyl disulphide (DA)

A sulphur-containing component found in the *Alliaceae* family such as garlic and onion, the 4,5-dithia-1,7-octadiene is responsible for health-benefit effects related to antimicrobial, antithrombotic and antitumor activity (Rattanachaikunsopon & Phumkhachorn 2008; Casella et al. 2013; Sundaram & Milner 1996; Song et al. 2009; Jo et al. 2008).

Carvacrol (CV)

Carvacrol, 5-isopropyl-2-methylphenol, one of the major phenolic constituents of many of the essential oils of *Origanum* species. **CV** have antibacterial, antifungal, insecticidal, and antioxidant effects as well as general

antiseptic properties. The *in vitro* evaluations of **CV** on colon cancer cells have shown a pro-oxidant activity, which induce cellular apoptosis (Llana-Ruiz-Cabello et al. 2014; Llana-Ruiz-Cabello et al. 2015; Fan et al. 2015; Arunasree 2010).

Thymol (TY)

A natural monoterpene phenol derivative, 2-isopropyl-5-methylphenol, isomeric with carvacrol; mainly found in oil of thyme and extracted from *Thymus vulgaris* (common thyme). Thymol has been used as fungicide and antibacterial, studies show that sinergical effect of **CV** and **TY** reduces bacterial resistance to antibiotics. On the other hand, some evidences suggest thymol for the treatment of gastrointestinal disseases. In particular, **CV** and **TY** have shown antimutagenic and antitumor properties (Llana-Ruiz-Cabello et al. 2014; Llana-Ruiz-Cabello et al. 2015).

4.1.5 Legal aspects

Most of EOCs are registered by the European Commission for use as flavourings in food industry. Registered additives such as flavourings, do not present risk to the health of the consumer. Among others carvacrol, cinnamaldehyde, eugenol, limonene, menthol and thymol are registered. However, components such as estragole and methyl eugenol were deleted from the list in 2001 due to their being genotoxic (Commission Decision of 23 January, 2002).

In order to considering a safety additive, need to be evaluated by toxicological and metabolic studies, according to Commission Decision of 23 February, 1999; Commission Regulation (EC) No 1565/2000; Commission Regulation (EC) No. 622/2002; and regulation (EC) No 2232/96. When components are added to food preparations for purpose other than flavouring, the components may be treated as new food additives. However, approval as a food additive would involve toxic and metabolic studies to confirm their safety use.

4.1.6 Safety data

In spite of the fact that a considerable number of EOCs are registered as food flavourings, some studies indicate irritation and toxicity. For instance, eugenol, menthol and thymol, when applied in root canal treatments, have been known to cause irritation of mouth tissues. Results suggest that gum irritation may be related to membrane lysis and surface activity and that tissue penetration may be related at least partly to membrane affinity and lipid solubility (Manabe et al., 1987). Cinnamaldehyde, carvacrol and thymol appear to have no significant or marginal effects *in vivo* whilst *in vitro* they exhibit mild to moderate toxic effects at the cellular level. Genotoxicity data appear not to raise concern in view of the present levels of use (Stammati et al. 1999).

On the other hand, some EOCs have been known to cause allergic contact dermatitis in people who use them frequently (Carson and Riley, 2001; Bleasel et al., 2002). It is recommended that more safety studies be carried out before EOCs are more widely used or at greater concentrations in foods or pharmaceutical applications.

4.1.7 Organoleptic aspects

Among the technical disadvantages for industrial use of EOCs, the easy volatility and the spread of unpleasant or intense odours, reduce the applicability in food or pharmaceutical devices. For instance, although carvacrol produces a 'warmly pungent' aroma (Kim et al., 1995b), it has been tested without causing adverse organoleptic changes (Roller and Seedhar, 2002). However, the use of sulphur derivatives; mainly found in garlic and onion components, involves a complete damage in the final products (Maldonado et al. 2005).

References

Adorjan, B., Buchbauer, G., 2010. Biological properties of essential oils: An updated review. Flavour Fragr. J. doi:10.1002/ffj.2024

Arunasree, K., 2010. Anti-proliferative effects of carvacrol on human metastatic breast cancer cell line, MDA-MB 231. Phytomedicine 17, 581–588.

Bakkali, F., Averbeck, S., Averbeck, D., Idaomar, M., 2008. Biological effects of essential oils--a review. Food Chem Toxicol 46, 446–475. doi:10.1016/j.fct.2007.09.106

Bassolé, I.H.N., Juliani, H.R., 2012. Essential oils in combination and their antimicrobial properties. Molecules. 17(4), 3989-4006. doi:10.3390/molecules17043989

Bleasel, N., Tate, B., Rademaker, M. 2002. Allergic contact dermatitis following exposure to essential oils. Australas J. Dermatol. 43(3), 211-3.

Botsaris, A.S., 2007. Plants used traditionally to treat malaria in Brazil: the archives of Flora Medicinal. J. Ethnobiol. Ethnomed. 3, 18. doi:10.1186/1746-4269-3-18

Burt, S., 2004. Essential oils: their antibacterial properties and potential applications in foods—a review. Int. J. Food Microbiol. 94, 223–253. doi:10.1016/j.ijfoodmicro.2004.03.022

Carson, CF., Riley, TV. 2001. Safety, efficacy and provenance of tea tree (*Melaleuca alternifolia*) oil. Contact. Dermatitis. 45(2), 65-7

Casella, S., Leonardi, M., Melai, B., Fratini, F., Pistelli, L., 2013. The role of diallyl sulfides and dipropyl sulfides in the *in vitro* antimicrobial activity of the essential oil of garlic, *Allium sativum L.*, and leek, *Allium porrum L.* Phyther. Res. 27, 380–383. doi:10.1002/ptr.4725

Coussens, LM., Werb, Z. 2002. Inflammation and cancer. Nature. 420(6917), 860-7.

Fan, K., Li, X., Cao, Y., Qi, H., Li, L., 2015. Carvacrol inhibits proliferation and induces apoptosis in human colon cancer cells. Anticancer. Drugs 26, 813–823. doi:10.1097/CAD.0000000000000263

Geng, F., Tang, L., Li, Y., Yang, L., Choi, K.S., Kazim, A.L., Zhang, Y., 2011. Allyl isothiocyanate arrests cancer cells in mitosis, and mitotic arrest in turn leads to apoptosis via Bcl-2 protein phosphorylation. J. Biol. Chem. 286, 32259–32267. doi:10.1074/jbc.M111.278127

Hammer, K.A., Carson, C.F., 2011. Antibacterial and Antifungal Activities of Essential Oils, in: Lipids and Essential Oils as Antimicrobial Agents. pp. 256–293. doi:10.1055/s-0031-1282081

Heikkilä, T., Santos, H. a H.A., Kumar, N., Murzin, D.Y., Salonen, J., Laaksonen, T., Peltonen, L., Hirvonen, J., Lehto, V.-P., Heikkila, T., Santos, H. a H.A., Kunar, N., Murzin, D.Y., Salonen, J., Laaksonen, T., Peltonen, L., Hirvonen, J., Lehto, V.-P., 2010. Citotoxicity study of ordered mesoporous silica MCM-41 and SBA-15 microparticles on Caco-2 cells. Eur. J. Pharm. Biopharm. 74, 483–494. doi:10.1016/j.ejpb.2009.12.006

Hussain, A., Brahmbhatt, K., Priyani, A., Ahmed, M., Rizvi, T. a., Sharma, C., 2011. Eugenol Enhances the Chemotherapeutic Potential of Gemcitabine and Induces Anticarcinogenic and Anti-inflammatory Activity in Human Cervical Cancer Cells. Cancer Biother. Radiopharm. 26, 519–527. doi:10.1089/cbr.2010.0925

Jaganathan, S.K., Mazumdar, A., Mondhe, D., Mandal, M., 2011. Apoptotic effect of eugenol in human colon cancer cell lines. Cell Biol. Int. 35, 607–15. doi:10.1042/CBI20100118

Jaganathan, S.K., Supriyanto, E., 2012. Antiproliferative and molecular mechanism of eugenol-induced apoptosis in cancer cells. Molecules. 17(6), 6290-304. doi:10.3390/molecules17066290

Janatova, A., Bernardos, A., Smid, J., Frankova, A., Lhotka, M., Kourimsk??, L., Pulkrabek, J., Kloucek, P., 2015. Long-term antifungal activity of volatile essential oil components released from mesoporous silica materials. Ind. Crops Prod. 67, 216–220. doi:10.1016/j.indcrop.2015.01.019

Jeong, H.-W., Han, D.C., Son, K.-H., Han, M.Y., Lim, J.-S., Ha, J.-H., Lee, C.W., Kim, H.M., Kim, H.-C., Kwon, B.-M., 2003. Antitumor effect of the cinnamaldehyde derivative CB403 through the arrest of cell cycle progression in the G2/M phase. Biochem. Pharmacol. 65, 1343–1350. doi:10.1016/S0006-2952(03)00038-8

Jo, H.J., Song, J.D., Kim, K.M., Cho, Y.H., Kim, K.H., Park, Y.C., 2008. Diallyl disulfide induces reversible G2/M phase arrest on a p53-independent mechanism in human colon cancer HCT-116 cells. Oncol. Rep. 19, 275–280.

Kim, J., Marshall, MR., Wei, C. 1995. Antibacterial activity of some essential oil components against five food borne pathogens. J. Agric. Food Chem. 43, 5839-2845.

Kris-Etherton, P.M., Hecker, K.D., Bonanome, A., Coval, S.M., Binkoski, A.E., Hilpert, K.F., Griel, A.E., Etherton, T.D., 2002. Bioactive compounds in foods: their role in the prevention of cardiovascular disease and cancer. Am. J. Med. 113 Suppl, 71S–88S. doi:10.1016/S0002-9343(01)00995-0

Lai, K.C., Kuo, C.L., Ho, H.C., Yang, J.S., Ma, C.Y., Lu, H.F., Huang, H.Y., Chueh, F.S., Yu, C.C., Chung, J.G., 2012. Diallyl sulfide, diallyl disulfide and diallyl trisulfide affect drug resistant gene expression in colo 205 human colon cancer cells *in vitro* and *in vivo*. Phytomedicine 19, 625–630.

Li, J., Teng, Y., Liu, S., Chen, Y., Zhang, Y., Xi, S., Xu, S., Wang, R., Zou, X., 2016. Cinnamaldehyde affects the biological behavior of human colorectal cancer cells and induces apoptosis via inhibition of the PI3K/Akt signaling pathway. Oncol. Rep. 35, 1501–1510. doi:10.3892/or.2015.4493

Llana-Ruiz-Cabello, M., Gutiérrez-Praena, D., Pichardo, S., Moreno, F.J., Bermúdez, J.M., Aucejo, S., Cameán, A.M., 2014. Cytotoxicity and morphological effects induced by carvacrol and thymol on the human cell line Caco-2. Food Chem. Toxicol. 64, 281–290. doi:10.1016/j.fct.2013.12.005

Llana-Ruiz-Cabello, M., Gutiérrez-Praena, D., Puerto, M., Pichardo, S., Jos, Á., Cameán, A.M., 2015. *In vitro* pro-oxidant/antioxidant role of carvacrol, thymol and their mixture in the intestinal Caco-2 cell line. Toxicol. Vitr. 29, 647–656. doi:10.1016/j.tiv.2015.02.006

Maldonado, P.D., Chánez-Cárdenas, M.E., Pedraza-Chaverrí, J., 2005. Aged garlic extract, garlic powder extract, S-allylcysteine, diallyl sulfide and diallyl disulfide do not interfere with the antibiotic activity of gentamicin. Phyther. Res. 19, 252–254. doi:10.1002/ptr.1674

Manabe, A., Nakayama, S., Sakamoto, K. 1987. Effects of essential oils on erythrocytes and hepatocytes from rats and dipalmitoyl phoshphatidylchholine-liposomes. Jpn. J. Pharmacol. 44(1), 77-84.

Miguel, M.G., 2010. Antioxidant and anti-inflammatory activities of essential oils: A short review. Molecules. doi:10.3390/molecules15129252

Musk, S.R.R., Johnson, I.T., 1993. Allyl isothiocyanate is selectively toxic to transformed cells of the human colorectal tumour line ht29. Carcinogenesis 14, 2079–2083. doi:10.1093/carcin/14.10.2079

Oliveira, P.F. de, Alves, J.M., Damasceno, J.L., Oliveira, R.A.M., Dias, H.J., Crotti, A.E.M., Tavares, D.C., 2015. Cytotoxicity screening of essential oils in cancer cell lines. Rev. Bras. Farmacogn. 25, 183–188. doi:10.1016/j.bjp.2015.02.009

Rattanachaikunsopon, P., Phumkhachorn, P., 2008. Diallyl sulfide content and antimicrobial activity against food-borne pathogenic bacteria of chives (Allium schoenoprasum). Biosci. Biotechnol. Biochem. 72, 2987–2991. doi:10.1271/bbb.80482

Raut, J.S., Karuppavil, S.M., 2014. A status review on the medicinal properties of essential oils. Ind. Crop. Prod. 62, 250–264.

Ribes, S., Fuentes, A., Talens, P., Barat, J.M., 2016. Use of oil-in-water emulsions to control fungal deterioration of strawberry jams. Food Chem. 211, 92–99. doi:10.1016/j.foodchem.2016.05.040

Roller, S., Seedhar, P. 2002. Carvacrol and cinnamic acid inhibit microbial growth in fres-cut melon and kiwifruit at 4 °C and 8 °C. Letter in Applied Microbiology. 35, 390-394.

Ruiz-Rico, M., Pérez-Esteve, E., Barat, J.M., 2017. Use of nanotechnology as an antimicrobial tool in the food sector, in: Nanobiotechnology: Human Heatlh and the Environment. CRC Press.

Song, J.-D., Lee, S.K., Kim, K.M., Park, S.E., Park, S.-J., Kim, K.H., Ahn, S.C., Park, Y.C., 2009. Molecular mechanism of diallyl disulfide in cell cycle arrest and apoptosis in HCT-116 colon cancer cells. J. Biochem. Mol. Toxicol. 23, 71–9. doi:10.1002/jbt.20266

Stammati, A., Bonsi, P., Zucci, F., Moezelaar, R., Alakomi, HL., Von Wright, A. 1999. Toxicity of selected plant volatiles in microbial and mammalian short-term assays. Food Che. Toxicol. 37, 813-823.

Sundaram, S.G., Milner, J.A., 1996. Diallyl disulfide induces apoptosis of human colon tumor cells. Carcinogenesis 17, 669–673.

Yu, C., Liu, S.L., Qi, M.H., Zou, X., 2014. Cinnamaldehyde/ chemotherapeutic agents interaction and drug-metabolizing genes in colorectal cancer. Mol. Med. Rep. 9, 669–676. doi:10.3892/mmr.2013.1830

Zhang, Y., 2010. Allyl isothiocyanate as a cancer chemopreventive phytochemical. Mol. Nutr. Food Res. doi:10.1002/mnfr.200900323

4.2 Evaluation of essential oil components encapsulated into mesoporous silica particles as natural-derived agents against colon cancer cells

Evaluation of essential oil components encapsulated into mesoporous silica particles as natural-derived agents against colon cancer cells

Carolina Acosta,[a] Andrea Bernardos,[*b,c] Pavel Kloucek,[d] Matej Bozik,[d] Ramon Martinez-Manez, [b,c] Jose Manuel Barat [a]

Grupo de Investigación e Innovación Alimentaria (CUINA),
Universitat Politècnica de València. Camino de Vera s/n, E-46022 Valencia, Spain.
[b] Instituto Interuniversitario de Investigación de Reconocimiento Molecular y Desarrollo Tecnológico
Universitat Politècnica de València, Universitat de València. Camino de Vera s/n, E-46022 Valencia, Spain
[c] CIBER de Bioingeniería, Biomateriales y Nanomedicina (CIBER-BBN), Spain.
[d] Department of Quality of Agricultural Products, Faculty of Agrobiology, Food and Natural Resources
Czech University of Life Sciences Prague, Kamycka 129, Prague 6-Suchdol, 165 21, Czech Republic.

Submitted 2017

The synthesis of micro- and nano-sized mesoporous silica particles (MSPs) for encapsulating essential oil components (EOCs) and their use against colon cancer cells is described. Allyl-isothiocyanate, cinnamaldehyde, eugenol, diallyl disulphide, carvacrol and thymol, free and encapsulated in MSPs were evaluated against the colon carcinoma HCT116 cell line. It was found that encapsulated EOCs displayed remarkable enhanced anticancer activity than when free. In addition, EOCs and encapsulated EOCs in MSPs were also tested against the human colon normal (non-tumour) cell line CCD112-CoN, and was found that some encapsulated EOCs displayed an enhanced toxicity to colon cancer cells when compared to non-malignant cells. As far as the authors know, this is the first example of the use of EOCs encapsulated in MSPs as natural-derived agents showing selectivity against colon cancer cells in comparison with non-tumour colon cells.

Keywords: essential oil components; encapsulation; mesoporous silica particles; controlled release; cancer colon cells.

INTRODUCTION

Secondary metabolites found in plant extracts, such as essential oil components (EOCs), have been widely studied for their insecticidal, antifungal and antibacterial activity (Maldonado et al. 2005; Ribes et al. 2016; Adorjan & Buchbauer 2010; Flesar et al. 2010; Jing et al. 2014; Shaffer et al. 2016). Moreover, numerous bioactive components from plant-derived EOCs have been studied as anti-cancer agents with promising results (de Mesquita et al. 2009). Recent studies have evaluated the cytotoxic potential of EOCs against tumour cell lines and it was found a substantial anti-proliferative effect due to EOCs (Jeong et al. 2003; Geng et al. 2011; Jaganathan & Supriyanto 2012; Bianchini & Vainio 2001). Moreover, direct exposure of cancer cells to EOCs have demonstrated to be dose-dependent, and some values of EC50 (absolute concentration, whereby cell viability decrease fewer than 50 % of population) have been established above 10 $\mu g \cdot mL^{-1}$ (Oliveira et al. 2015; Jaganathan & Supriyanto 2012). In contrast to common anticancer drugs, which achieve EC50 values at concentrations lower than 30 $\mu g \cdot mL^{-1}$ (Suffness & Pezzuto 1990), natural-derived components, such as EOCs, have a potential anticancer activity and are suitable candidates to be used in prevention and therapeutic strategies. In particular, combined therapies of EOCs and current synthetic cytotoxic agents have shown promising results (Yu et al. 2014; Adorjan & Buchbauer 2010). The synergistic interaction not only enhance

the therapy efficacy, but also reduce the chemotherapeutic-associated gene expressions, which are related to collateral health troubles (Li et al. 2016; Yu et al. 2014; Hussain et al. 2011). In contrast to common cytotoxic agents such as doxorubicin, camptothecin, and others currently used in chemotherapy (Heikkilä et al. 2010), EOCs do not promote the expression of drugs-resistance, neither *in vitro* nor *in vivo* studies (Ravizza et al. 2008; Lai et al. 2012). Hence, the use of EOCs as cytotoxic is a timely field of research (Raut & Karuppavil 2014; Kris-Etherton et al. 2002; Oliveira et al. 2015). In fact, recent studies have demonstrated the therapeutic potential of EOCs for prevention and treatment of colon cancer (Liao et al. 2009; Ogasawara et al. 2001; Li et al. 2016). In particular, among EOCs, allyl-isothiocyanate, cinnamaldehyde, eugenol, diallyl disulphide, carvacrol and thymol have displayed a remarkable *in vitro* activity against colon cancer cells. Allyl isothiocyanate (**AI**), 3-isothiocyanato-1-propene, is a volatile organic compound, found in horseradish (*Armoracia rusticana,* syn. *Cochlearia armoracia*) of the *Brassicaceae* family, and in mustard, wasabi and cruciferous vegetables such as broccoli and cabbage. **AI**, has strong antibacterial properties and some studies have shown its cytotoxic and anti-tumorigenic activity on colon cells (Geng et al. 2011; Musk & Johnson 1993; Zhang 2010). Cinnamaldehyde (**CN**), (2E)-3-phenylprop-2-enal, is obtained from the stem bark of *Cinnamomum verum* or *C. casia*. **CN** is known to possess several biological activities, including

antifungal, cytotoxic and anti-mutagenic with a noticeable *in vivo* and *in vitro* antitumor effects on colon cancer (Li et al. 2016; Jeong et al. 2003; Yu et al. 2014; Ribes et al., 2016; Hussain et al. 2011). Eugenol (**EU**), 4-allyl-2-methoxyphenol, is a component of *Syzigium aromaticum* (cloves). **EU** has been used as analgesic and antibacterial agent and it has been reported to possess anticancer and antigenotoxic activity (Jaganathan et al. 2011; Hussain et al. 2011; Jaganathan & Supriyanto 2012). Diallyl disulphide (**DA**), 4,5-dithia-1,7-octadiene, is a sulphur-containing component found in the *Alliaceae* family such as in garlic and onion. **DA** is responsible for health-benefit effects related to antimicrobial, antithrombotic and antitumor activity (Rattanachaikunsopon & Phumkhachorn 2008; Casella et al. 2013; Sundaram & Milner 1996; Song et al. 2009; Jo et al. 2008). Carvacrol (**CV**), 5-isopropyl-2-methylphenol, is one of the major phenolic constituents of essential oils from *Origanum* species, whereas thymol (**TY**), 2-isopropyl-5-methylphenol, is a natural monoterpene phenol derivative (isomeric with carvacrol) mainly found in oil from *Thymus vulgaris* (common thyme). **CV** and **TY** have antibacterial, antifungal, insecticidal, and antioxidant effects as well as general antiseptic properties. The *in vitro* evaluations of **CV** and **TY** on colon cancer cells have shown a pro-oxidant activity, which induce cellular apoptosis (Llana-Ruiz-Cabello et al. 2014; Llana-Ruiz-Cabello et al. 2015; Fan et al. 2015; Arunasree 2010).

However, the employment of EOCs shows technical disadvantages, such as easy volatility, low water solubility and instability in presence of oxygen, light and temperature (Guimarães et al. 2015). In this scenario, encapsulation has been used recently for controlling these drawbacks (Marques 2010). Among potential encapsulation systems organic structures based on polysaccharides, proteins, polymers, emulsions or liposomes have been widely studied (Sherry et al. 2013). These traditional delivery systems, usually release their cargo via diffusion-controlled processes, or through the simple degradation of the polymeric matrix (Johnson et al. 2008). As an alternative, recent studies have also suggested that silica supports can be used for the encapsulation of different cargoes to prevent degradation and increase bioavailability (Pérez-Esteve et al., 2015; Wong et al. 2011). Among silica-based supports, mesoporous silica particles (MSPs) have been used as inorganic scaffolds for the storage and release of drugs and (bio)organic molecules (C. Kresge et al. 1992; Dirk 2006; Vallet-Regi F. et al. 2007; Muñoz et al. 2003), for applications in diagnosis and cancer therapy (Xie et al. 2016). MSPs can be prepared in sizes from micrometres to nanometres, with pores in the 2-10 nm range. MSPs have a very large specific surface area (up to 1200 $m^2 \cdot g^{-1}$) and volume, rendering them a large loading capacity. In addition, the good biocompatibility of MSPs, their high inertness, ease of functionalization and chemical stability, make MSPs an ideal support for encapsulation (Salonen et al.

2008; Muñoz et al. 2003). Recent studies have shown that encapsulation of EOCs into MSPs are a suitable approach for the development of antifungal and antibacterial systems, able to release EOCs along the time and improve their antimicrobial activity (Bernardos et al. 2015; Janatova et al. 2015; Park & Pendleton 2012). However, as far as we known, there are not evidences on the use of encapsulated EOCs into MSPs as potential materials for cancer therapy.

Bearing in mind that supports based on silica nanomaterials will be an interesting oral administration system, gastrointestinal diseases could be treated with natural-derived agents such as EOCs encapsulated into silica nanomaterials. Furthermore, the use of bioactive components from essential oil against colon cancer cells has drawn much attention nowadays, showing the therapeutic potential of EOCs for prevention and treatment of colon cancer (Liao et al. 2009; Ogasawara et al. 2001; Li et al. 2016).

Taking into account the above mentioned facts, we report herein the effect of EOCs free and encapsulated against colon cells. Six-EOCs: allyl-isothiocyanate, cinnamaldehyde, eugenol, diallyl disulphide, carvacrol and thymol, were incubated on human colon carcinoma and normal (non-tumour) colon cell lines. Mesoporous silica microparticles and mesoporous silica nanoparticles (**MSMs** and **MSNs**, respectively), were selected as supports for EOCs encapsulation. As far as we know, examples related with the use of EOCs encapsulated in MSPs against

colon cancer cells have not yet been reported. Our results pointed to the potential use of EOCs encapsulated in MSPs as potential materials for decrease the viability of colon cancer cells.

EXPERIMENTAL SECTION

Chemicals

All the chemicals were purchased at the highest possible grade available and were directly used with no further purification. Tetraethylorthosilicate (TEOS), N-cetyltrimethylammonium bromide (CTABr), sodium hydroxide (NaOH), triethanolamine (TEAH) and 3-aminopropyltriethoxysilane (APTES) were provided by Sigma Aldrich. Essential oil components (EOCs): allyl-isothiocyanate, cinnamaldehyde, eugenol, diallyl disulphide, carvacrol and thymol were purchased from Sigma-Aldrich-UK. Fetal bovine serum (FBS), trypan blue solution (0.4 %) cell culture grade, trypsin, penicillin, streptomycin and DMEM-low glucose, and McCoy's 5A culture media were provided by Gibco-Invitrogen. The cell proliferation reagent WST-1 was obtained from Roche Applied Science.

Synthesis of mesoporous silica microparticles

Mesoporous silica micro-sized particles (**MSMs**) were synthesized following reported procedures (Cabrera et al., 2000), in which 4.68 g of CTABr were added at 118 °C to a TEAH solution (25.79 g) that contained 0.045 mol of a silatrane derivative (TEOS, 11 mL). Next 80 mL of water were slowly added with vigorous stirring at 70 °C. After a few minutes, a white suspension was formed. This

mixture was aged at room temperature overnight. The resulting powder (MSMs as-synthesised) was collected by filtration, washed and dried at 70 °C. In order to remove the template phase, the powder was calcined at 550 °C for 5 h in an oxidant atmosphere to obtain the micro-sized particles.

Synthesis of mesoporous silica nanoparticles

Mesoporous silica nano-sized particles (**MSNs**) were synthesized using the procedure previously reported by Bernardos et al. (2010): n-cetyltrimethylammoniumbromide (CTABr, 2.0 g, 5.48 mmol) was first dissolved in 960 mL of deionised water. NaOH (aq) (2.0 M, 7.0 mL) was then added and the temperature was adjusted to 95 °C. TEOS (10.0 mL, 44.8 mmol) was added dropwise to the surfactant solution. The mixture was allowed to stir for 3 h to give a white precipitate. The product was centrifuged, and washed with deionised water and ethanol. Finally, the resulting powder (MSNs as-synthesised) was dried at 60 °C (Bernardos et al., 2010). To prepare the final porous support, as-synthesised material was calcined at 550 °C using an oxidant atmosphere for 5 h in order to remove the template phase and obtain the nano-sized particles.

Methods of characterization

Powder X-ray diffraction (PRXD), transmission electron microscope (TEM), N_2 adsorption-desorption isotherms, thermogravimetric analyses (TGA) and elemental analysis (EA) were employed to characterize the mesoporous silica particles. PXRD measurements were taken on a Seifert 3000TT diffractometer

using CuKα radiation. The TEM images were obtained with a 100 kV Philips CM10 microscope. N_2 adsorption-desorption isotherms were recorded with a Micromeritics ASAP2010 automated sorption analyzer. The samples were degassed at 120 °C in vacuum overnight. The specific surface areas were calculated from the adsorption data in the low pressure range using the BET model, and pore size was determined following the BJH method (Brunauer et al., 1938). TGA were carried out on a TGA/SDTA 851e Mettler Toledo balance in an oxidant atmosphere (air, 80 $mL \cdot min^{-1}$) with a heating program that consisted of a heating ramp of 10 °C per minute from 120 to 1000 °C, and an isothermal heating step at this temperature for 30 min. The elemental analysis was performed in a EA-1110 CHN Elemental Analyser. Finally, the EOCs detection was determined through gas chromatography mass spectrometry, GC-MS, Agilent Technologies 6890N Network Gas Chromatography System equipped with an Agilent Technologies 5973 inert mass selective detector, fitted with an HS-5MS column (30 m × 0.25 mm × 0.25 μm film thickness, (5% phenil)-methyl silox Agilent Technologies).

Encapsulation of EOCs in MSPs (EOCs-MSPs)

According to previous procedures, micro and nano-sized particles, **MSMs** and **MSNs** respectively, loading with EOCs was achieved via vapor adsorption by mixing EOCs (50 mg) with the MSPs (50 mg) in a tightly closed vial (Bernardos et

al., 2015; Janatova et al., 2015; Park et al., 2011). The mixture was incubated in an oven at 40 °C for 24 h while being continuously shaken. After 24 h, vials remained overnight (10-12 h) uncapped at room temperature, to evaporate the excess of EOCs. Using this approach, the final EOCs encapsulated were prepared in **MSMs**. EOCs-MSMs: AI-MSM, CN-MSM, EU-MSM, DA-MSM, CV-MSM and TY-MSM loaded with allyl-isothiocyanate (**AI**), cinnamaldehyde (**CN**), eugenol (**EU**), diallyl disulphide (**DA**), carvacrol (**CV**) and thymol (**TY**) respectively. Similarly, EOCs encapsulated in **MSNs,** EOCs-MSNs: AI-MSN, CN-MSN, EU-MSN, DA-MSN, CV-MSN and TY-MSN were prepared.

Release studies

In a typical experiment, 1 mg of encapsulated particles (EOCs-MSMs or EOCs-MSNs) was suspended in 2 mL of culture media, and at a certain time, suspensions were centrifuged. The supernatant liquid was separated and extracted with hexane (2 mL of hexane at a time, three extractions).

Gas chromatography mass spectrometry (GC-MS) was used and an aliquot of 1 µL was injected with a pulsed split ratio of 10:1. Injection temperature was 240 °C, the interface set to 250 °C and the ion source adjusted to 200 °C. The carrier gas used was helium set at a constant flow rate of 1 $mL \cdot min^{-1}$. The temperature program was 3 min isothermal heating at 60 °C, followed by a 10 $°C \cdot min^{-1}$ oven temperature ramp to 120 °C, 8 $°C \cdot min^{-1}$ ramp to 180 °C and a final 6

°C·min^{-1} oven temperature ramp to 230 °C with 2 min heating at 230 °C. Mass spectra were recorded at two scans per sec with an m/z 50-600 scanning range. A retention time and mass spectral library for peak identification was implemented.

Cell culture

The human colon cell lines were obtained from ATCC–LGC Standards. HCT116 cells were grown in McCoy's 5A culture medium, and CCD112-CoN cells were grown in DMEM-low glucose. Culture medium were supplemented with FBS at 10 % and antibiotics (100 U·mL^{-1} of penicillin, 100 µg·mL^{-1} of streptomycin). Cells were maintained at 37 °C in an atmosphere of 5 % CO_2 and 95 % air, cells undergone passage twice a week.

Samples preparation for viability assay

Samples of free EOCs, EOCs-MSMs and EOCs-MSNs were weighed and sterilised by UV irradiation for 20 min. Then were dispersed in culture medium (McCoys' 5A and DMEM for HCT116 and CCD112-CoN, respectively) and disposed in an ultrasound bath for 10 min to reduce particle aggregates. The required amount of the corresponding suspension was used to prepare dispersions in range from 2.0 to 200 µg·mL^{-1} of equivalent concentration of EOCs (based on release evaluation the equivalent EOCs encapsulated concentration was determined).

WST-1 Cell Viability Assay

Cells were cultured in sterile 96-well plates at a seeding density of 2.5×10^3 cells per well, and they were allowed to settle for 24 h. Then, previously prepared EOCs dispersions (free and encapsulated) were added to cells and after 24 h and 48 h, WST-1 (10 µL) was added to each well. After WST-1 was added, cells were further incubated for 2 h and absorbance was measured at 450 and 620 nm.

Statistical analyses

Cell viability was evaluated through sigmoidal fit of dose-response curves, and the Origin software package was used. Statistical analyses were determined by One-Way and factorial ANOVA through SPSS software.

RESULTS AND DISCUSSION

Synthesis and characterisation of the EOCs-encapsulated systems

MSMs and **MSNs** were synthesised using well-known procedures (see experimental section), and selected EOCs (i.e. allyl isothiocyanate, cinnamaldehyde, eugenol, diallyl disulphide, carvacrol and thymol) were encapsulated through vapour adsorption procedures inside the mesopores (Scheme 4.2-1).

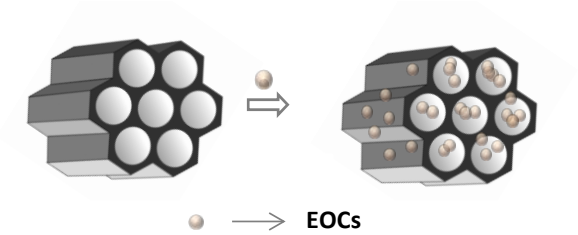

Scheme 4.2-1. Encapsulation of EOCs into mesoporous silica supports.

The materials were characterised by powder X-ray diffraction (PXRD), TEM and N_2 adsorption-desorption studies (see Figure 4.2-1 and 4.2-2 for **MSMs** and **MSNs**, respectively). The X-ray patterns of the as-synthesised particles show four low-angle reflections, typical of a hexagonal array, which can be indexed as (100), (110), (200) and (210) Bragg reflections (see Figures 4.2-1A and 4.2-2A). A significant shift of the (100) reflection in the PXRD patterns for the calcined samples was clearly observed which corresponds to an approximate cell contraction of ca. 4.8 and 4.5 Å (see Figures 4.2-1B and 4.2-2B for **MSMs** and **MSNs**, respectively). This displacement and the also observed broadening of the (110) and (200) peaks, were more likely related to the condensation of silanols in the calcination step when the template was removed. For the loaded solids EOCs-MSMs and EOCs-MSNs, the PXRD pattern showed the characteristic (100) reflection (Figures 4.2-1C and 4.2-2C, respectively); which indicated that mesoporous structure was preserved after the loading process (see Figures 4.2-1C and 4.2-2C, data shown for cinnamaldehyde encapsulation).

TEM images of the calcined **MSMs** and **MSNs** solids showed the typical channels of the mesoporous matrix, visualised as alternate black and white stripes (see Figure 4.2-1D and Figure 4.2-2D). As TEM images show, **MSMs** were obtained as irregular micrometric particles with a size in the 1000 – 3000 nm range, whereas **MSNs** were obtained as spherical particles with diameters ranging from 80 to 100 nm. After EOCs encapsulation, TEM images showed that the mesoporous structure remained in all cases (Figures 4.2-1E and 4.2-2E).

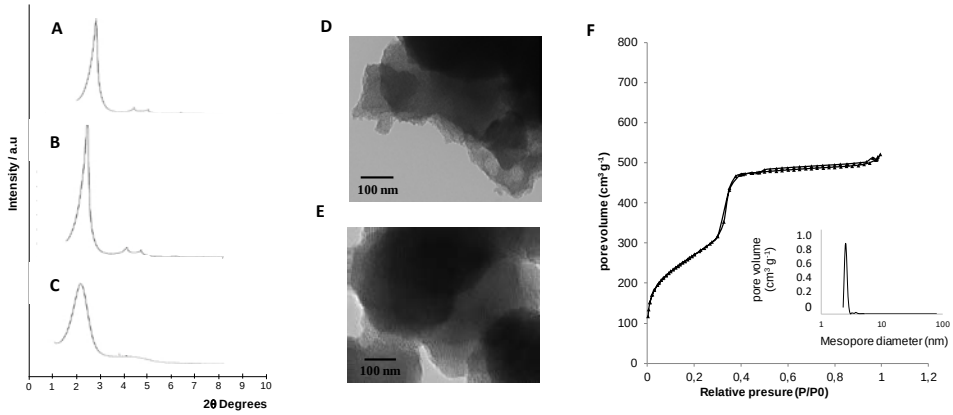

Figure 4.2-1. Characterisation of micro-sized particles MSMs, data for cinnamaldehyde encapsulation. First the PRXD pattern shows: A. MSMs As-synthesised material, B. calcined MSMs and C. EOCs (cinnamaldehyde) loaded in MSMs. Then the TEM images show: D. the MSMs support and E. the loaded particles (CN-MSM) shows the preservation of the mesopore structure. F. The nitrogen adsorption-desorption isotherm of calcined material (MSMs) and inset shows pore size distribution of material before the EOCs loading.

N_2 adsorption–desorption isotherms of calcined **MSMs** and **MSNs** particles show typical curves consisting of one single adsorption step at the intermediate

P/P_0 value (0.1 – 0.4) which can be related to the nitrogen condensation inside the mesopores by capillarity (see Figure 4.2-1F and Figure 4.2-2F for **MSMs** and **MSNs**, respectively). The absence of a hysteresis loop in this interval and the narrow pore distribution (insets in Figures 4.2-1F and 4.2-2F) suggests the existence of uniform cylindrical mesopores. Through the BJH model on the adsorption branch of the isotherms, pore diameters and pore volumes were calculated. Micro and nanp-sized particles has similar pore diameters (2.5 and 2.2 nm, respectively), but pore volumes are slightly different, 0.78 and 0.68 $cm^3 \cdot g^{-1}$, for **MSMs** and **MSNs**, respectively (Brunauer P.H. Teller, E., 1938).

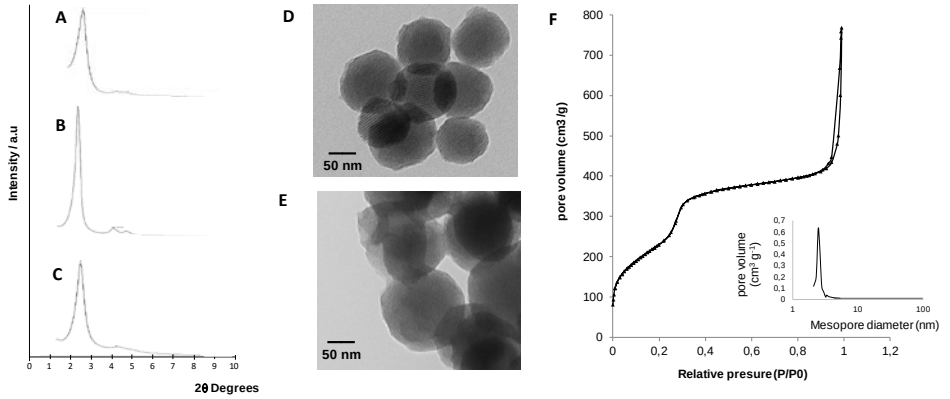

Figure 4.2-2. Characterisation of nano-sized particles, MSNs, data shown for cinnamaldehyde encapsulation. PRXD pattern of: A. MSNs as-synthesised, B. Calcined MSNs, C. Nano-sized particles loaded with cinnamaldehyde, D.TEM images of MSNs, E. TEM images of loaded particles (CN-MSN) and F. Nitrogen adsorption-desorption isotherms of MSNs and inset shows the pore size distribution.

The application of BET model resulted in values of 989.8 and 875.4 $m^2 \cdot g^{-1}$ for the total specific surface for micro (**MSMs**) and nano-sized (**MSNs**) particles, respectively. The N_2 adsorption–desorption isotherm of **EOCs-MSMs** and **EOCs-**

MSNs are typical of mesoporous systems with filled mesopores (data shown for encapsulation of cinnamaldehyde). Consequently, relatively low N_2 adsorbed volume and surface area values were registered.

The quantification of EOCs in the loaded materials was assessed through elemental (EA) and thermogravimetry analyses (TGA) (data in Table 4.2-1). Typical cargo contents of ca. 0.5 mg of EOCs per mg of SiO_2 were found.

Table 4.2-1. Content (α) in grams of EOCs per gram of SiO_2.

Sample (**EOCs-MSMs**)	α_{cargo} (g/g SiO_2)	Sample (**EOCs-MSNs**)	α_{cargo} (g/g SiO_2)
AI–MSM	0.19 ± 0.01	AI–MSN	0.36 ± 0.09
CN–MSM	0.52 ± 0.04	CN–MSN	0.53 ± 0.01
EU–MSM	0.45 ± 0.05	EU–MSN	0.48 ± 0.04
DA–MSM	0.40 ± 0.08	DA–MSN	0.41 ± 0.06
CV–MSM	0.44 ± 0.05	CV–MSN	0.45 ± 0.04
TY–MSM	0.49 ± 0.03	TY–MSN	0.32 ± 0.03

Release studies

Release experiments of EOCs from EOCs-MSMs and EOCs-MSNs were carried out. In a typical experiment 1 mg of the EOCs-loaded particles were suspended in 2 mL of culture media and aliquots taken at certain times were extracted with hexane. The hexane-extracts were analysed through GC-MS and release responses were obtained (Figure 4.2-3). First result shows that any of EOCs-loaded particle was able to deliver a 100 % of the encapsulated EOCs. The limitations to reach the 100 % release is tentatively ascribed to the interactions of

the EOCs' structures with the surface of the silica support. This evidence is in line with previous studies, where silica pore networks have been reported to bound strongly the cargo (Park et al. 2011). On the other hand, except for AI-MSM the cargo of EOCs loaded was similar for micro and nanoparticles. Hence, we can assume that the proposed method for loading EOCs into MSPs, is able to reach a similar range of EOCs per grams of particles (SiO_2), no matter MSPs' size. However, the same can not be said for EOCs type. As Table 4.2-1 shows, AI-MSM has the minimum content of encapsulated component (significantly lower than the range observed). So, it is worth recalling the Figure 4-1, and the **AI** differences from other EOCs' structure, where, the nitrogen presence can to influence the encapsulation yield. Although the main goal of this project is not to optimize the loaded cargo or go further to the chemical structures. It should be noted that the EOCs' structure need to be taking into account, because EOCs'structure is related not only with encapsulation but also with release mechanisms.

As Figure 4.2-2 shows, there are no significant differences on delivery profile of EOCs released from micro or nano-sized particles. However, the released percentage varies depending on the component evaluated. Once again, **AI** has the minimum data, reaching just a 40 % of release, which is significantly lower than the 80 % of 90 % of release of **DA** and **CV**, respectively.

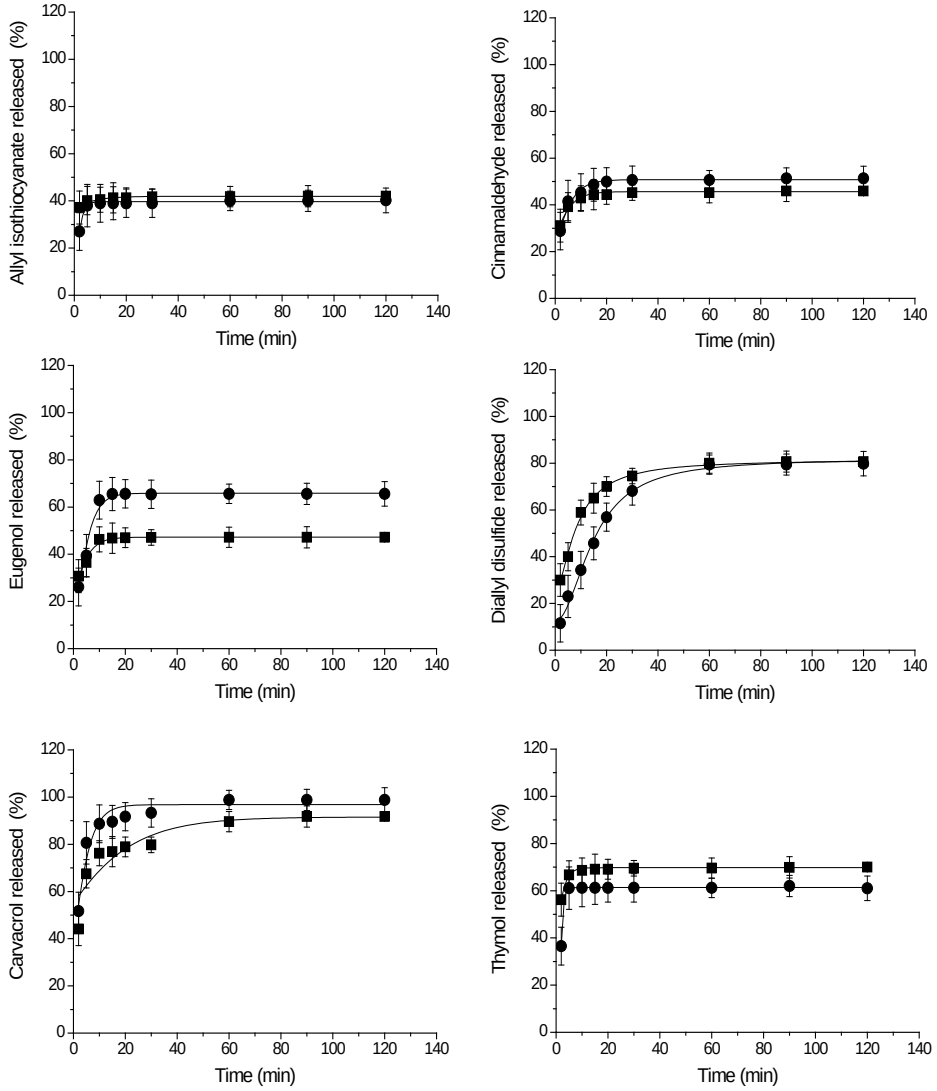

Figure 4.2-3. Release profile of EOCs encapsulated from micro particles EOCs-MSMs [■] and nano particles EOCs-MSNs [●] A. Allyl isothiocyanate, B. Cinnamaldehyde C. Eugenol D. Diallyl disulphide E. Carvacrol and F. Thymol.

Evaluation of EOCs and encapsulated EOCs against cancer colon cells

The effect that EOCs encapsulated in mesoporous silica particles have on cancer cells is an appealing research field. Herein, different amounts of EOCs free and encapsulated (at equivalent EOCs' concentrations) were incubated with the colon cancer cell line HCT116 and cell viability was measured after 24 and 48 h. In parallel, both **MSMs** and **MSNs** (without any cargo loaded inside the pores), were also incubated with cells at concentrations from 10 to 100 μg of particles per mL of culture medium. Results indicated that unloaded MSPs induced no significant cell viability reduction. This is in line with previous reports, which indicated that mesoporous silica-based particles have no significant toxicity in cells below 100 $\mu g \cdot mL^{-1}$ (Heikkilä et al. 2010).

Figure 4.2-4 shows the equivalent concentration of EOCs (free and encapsulated) to reduce cell viability by 50 percent (EC50) at 24 and 48 h. Results suggest that free EOCs required higher concentrations than encapsulated EOCs (EOCs-MSPs) to reduce viability in colon cancer cells. In most cases, EOCs free require more than 100 $\mu g \cdot mL^{-1}$ to reduce cell viability. However, once EOCs are encapsulated, EC50 is significantly reduced.

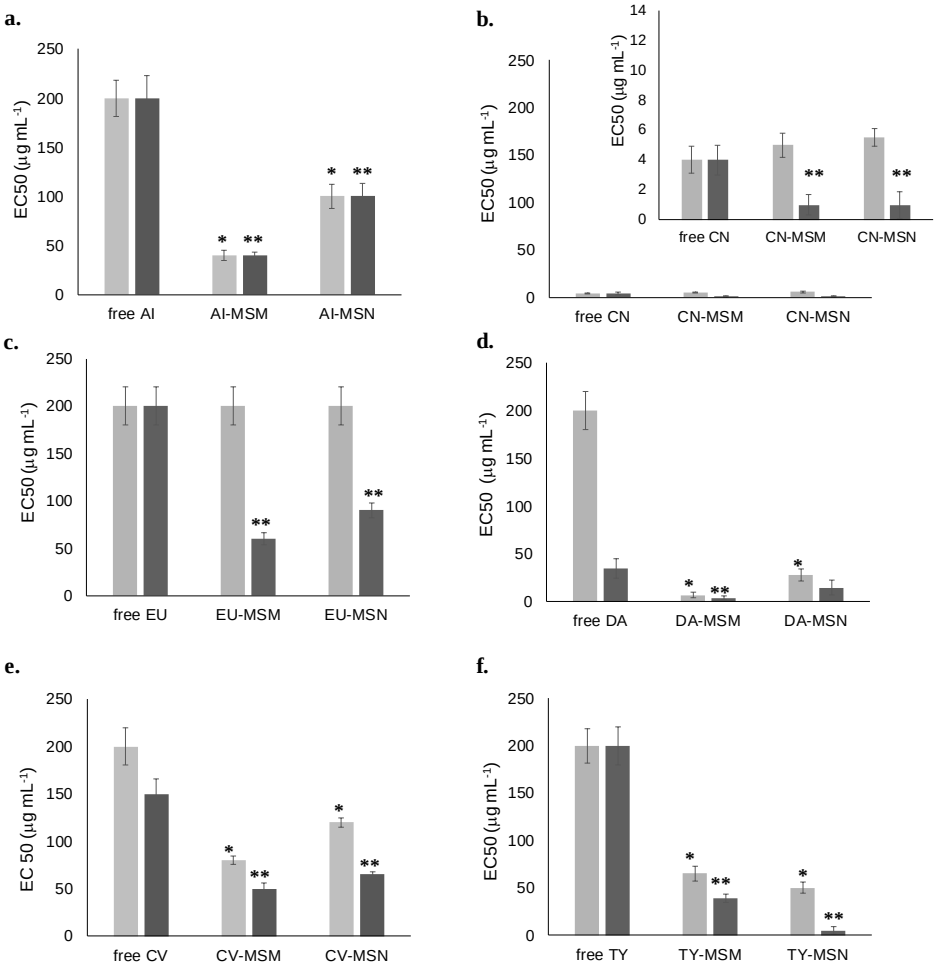

Figure 4.2-4. Concentration of EOCs needed to reduce the cell viability of HCT116 to 50 % (EC50), comparing 6-EOCs free and encapsulated into micro-sized (EOCs-MSMs) and nano-sized particles (EOCs-MSNs) after 24 h, grey bars and 48 h, dark bars. a. Allyl isothyocianate (AI) b. Cinnamaldehyde (CN) c. Eugenol (EU) d. Diallyl disulfide (DA) e. Carvacrol (CV) and f. Thymol (TY).

Significant differences for EOCs-MSPs compared to the free EOCs, at *24 h and **48 h. (means and standard deviations, n = 3).

Previous studies of the six selected EOCs on colon cancer cell lines such as Caco-2, LoVo, HT29, SW480 and Colo205, indicated that EC50 were obtained only

when concentrations above 100 $\mu g \cdot mL^{-1}$ (Llana-Ruiz-Cabello et al. 2014; Jaganathan et al. 2011; Li et al. 2016; Sundaram & Milner 1996)**.** In particular, *in vitro* studies with HCT116, with free cinnamaldehyde and carvacrol indicated that concentrations up to 80 $\mu g \cdot mL^{-1}$ reduce cell viability to 50 % (Li et al. 2016; Fan et al. 2015), which is a significantly higher concentration than that we need when using CN-MSPs and CV-MSPs. Hence, it is possible to enhance the EOCs activity through encapsulation into MSPs.

Viability studies for 24 h and 48 h, allowed us to find that viability reduction was sustained in time when EOCs are encapsulated in MSPs, which is in line with previous antifungal studies of encapsulated EOCs (Bernardos et al. 2015). We may assume that encapsulation inhibit the losses due to volatilisation of EOCs and enhance their distribution in cell medium, reducing EOCs doses to achieve the same cell viability decrease in comparison with free-EOCs.

Few studies have evaluated the effect on cancer cells of encapsulated EOCs. Specifically, on colon cancer, Majeet et al (2014) performed an *in vitro* evaluation of eugenol encapsulated in nanoemulsions. The authors found a major level of apoptosis via reactive oxygen species (ROS) generation after 24 h. In particular, nanoemulsions of eugenol increased its bioactivity (Majeed et al. 2014). Nevertheless, the nanoemulsion showed a EC50 at concentrations of eugenol close to 100 $\mu g \cdot mL^{-1}$, which is higher than equivalent concentration of eugenol

encapsulated (EU-MSPs). It suggests that MSPs offer suitable alternative option to traditional encapsulation systems, which opens a range of industrial and pharmaceutical applications. In addition, encapsulated EOCs decrease colon cancer cells viability, while the amount of MSPs used is low and did not display any toxicity.

Evaluation of EOCs on normal colon cells

During last years, the molecular cytotoxic mechanisms of our six selected EOCs have been widely studied on cancer cell lines. Proliferation inhibition and cell death due to pro-apoptotic signals are the main ways described which affect in a dose and time-dependent manner (Bottone et al. 2002; Yang et al. 2009; Llana-Ruiz-Cabello et al. 2014; Li et al. 2016; Jaganathan et al. 2011). However, there are few evaluations of the effect that EOCs have on non-tumour cell lines. So far, essential oil components from garlic has been tested on human prostate cancer and normal cells. According to authors, an induction of cell cycle arrest in G(2)-M phase was observed, and it was related to reactive oxygen species (ROS) generation, which mainly affected prostate cancer cells than normal cells (Xiao et al. 2005).

In addition, a recent study evaluated a combination of eugenol and gemcitabine (a common chemotherapeutic agent) against cervical cells, which results in an interesting synergistic interaction, eugenol enhances the efficacy of

gemcitabine while minimize the toxicity on normal cells. The study showed a dose-dependent and selective cytotoxicity toward cervical cancer cells compared to non-tumour cells (Hussain et al. 2011). In the context of our study, there are not, as far as we are aware, any evaluation which compares free and encapsulated EOCs on non-tumour colon cells.

In this section, cell viability of colon normal cell, CCD112-CoN, was evaluated after incubation with free-EOCs and EOCs-MSPs, and the results are compared with those obtained for colon cancer cells. We first confirmed that unloaded supports **MSMs** and **MSNs** were not toxic for CCD112-CoN cells.

Figure 4.2-5 shows that the viability of normal colon cells incubated with free EOCs was reduced at same level as cancer cells. However, higher dose of equivalent EOCs amount from EOCs-MSPs was required to reduce the cell viability of normal cells (data at 24 h in Figure 4.2-5 is not shown, because, significant results on viability decrease were achieved after 48 h). In particular, EC50 for encapsulated thymol and cinnamaldehyde in **MSMs** and **MSNs**, was reached using a significantly larger concentration for normal cells than for cancer cells (Figures 4.3-5F and 5B, respectively). Besides, carvacrol and allyl isothiocyanate have a selective effect, when they are encapsulated in nano-sized particles CV-MSN and AI-MSN, respectively (Figures 4.2-5E and 5A). Although supports' size did not

affect the behaviour release, the way in which particles interact with cells may change in function of other factors.

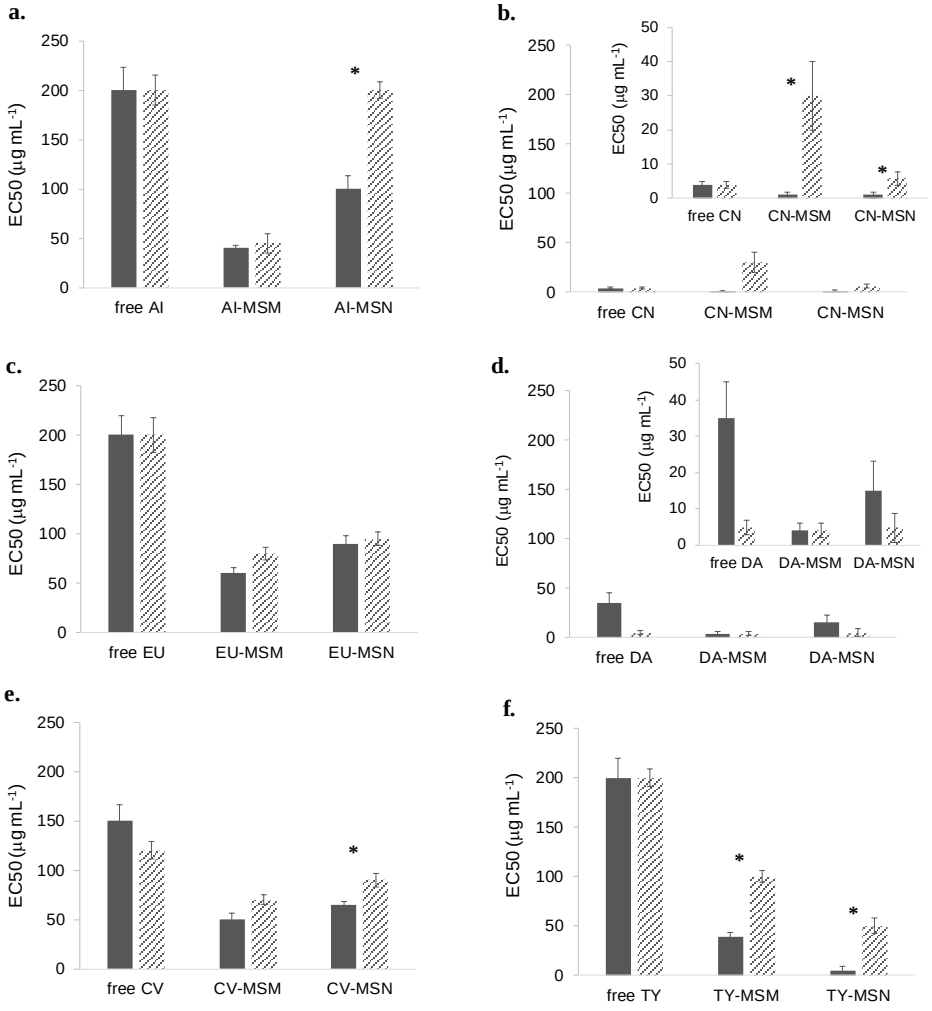

Figure 4.2-5. Concentration needed to reduce the cell viability to 50 % (EC50), comparing free compound and encapsulated into microparticles (EOCs-MSMs) and nanoparticles (EOCs-MSNs) after 48 h. Evaluation on HCT116 cells and CCD112-CoN cells, dark and striped bars, respectively. a. Allyl isothiocyanate (AI) b. Cinnamaldehyde (CN) c. Eugenol (EU) d. Diallyl disulphide (DA) e. Carvacrol (CV) and f. Thymol (TY). *Significant differences of the EC50 compared EOCs-MSPs effect between normal and cancer cells (means and standard deviations, n = 3).

For instance, depends on the EOCs structures, the interactions between the membrane's cells and particles can be altered, which will impact directly on cell viability. Although the toxic mechanisms of EOCs-MSPs would need further investigation, we demonstrate here the possibility to use low doses of EOCs-MSPs to reduce cancer cells viability without affecting normal cells. To the best of our knowledge, this is the first study to show that colon cancer cells are more sensitive to EOCs-MSPs than normal colon cells.

In this scenario, and in order to compare the obtained results, a selectivity index (SI) for the EOCs tested against the tumour cell line versus the non-tumour cell line at 48 h, was calculated (see Table 4.2-2). SI values for EOCs encapsulated were higher than those for free-EOCs. SI value greater than 2.0, means that the component tested is at least twice more cytotoxic on cancer cells than normal ones, and SI values equal to zero, means that component is toxic for normal cells as well as the tumour one (Suffness & Pezzuto 1990; Oliveira et al. 2015).

Table 4.2-2. Toxicity selectivity (SI) at 48 h of EOCs incubated into cancer cells compared with normal cells.

Sample (**Free EOCs**)	SI	Sample (**EOCs-MSMs**)	SI	Sample (**EOCs-MSNs**)	SI
AI	1.0	**AI–MSM**	1.0	**AI–MSN**	2.1
CN	1.0	**CN–MSM**	4.8	**CN–MSN**	2.0
EU	1.0	**EU–MSM**	1.7	**EU–MSN**	0.9
DA	0.2	**DA–MSM**	0.5	**DA–MSN**	0.0
CV	0.8	**CV–MSM**	1.2	**CV–MSN**	2.1
TY	1.0	**TY–MSM**	2.7	**TY–MSN**	3.5

In particular, thymol and cinnamaldehyde encapsulated into **MSMs** and **MSNs** had SI values above 2.0. It can be concluded that EOCs might be suitable natural-derived molecules for alternative therapies and MSPs are interesting supports for encapsulate bioactive components.

CONCLUSIONS

We have reported herein a study of the *in vitro* toxicity of EOCs free and encapsulated in silica mesoporous particles (both micro and nanometric) to colon cancer and normal cells. Our study revealed that both free EOCs and encapsulated showed activity against cancer colon cells. The use of MSPs as encapsulation system not only protected volatile EOCs enhancing their functionality, but also MSPs allows a controlled release of EOCs into the culture media, which assure higher and sustained effect along the time. In particular, MSPs, both micro- and nano-sized, loaded with cinnamaldehyde and thymol decreased the concentrations necessary to reduce to HCT116 cell population (EC50), without reducing normal colon cells viability. These results open new possibilities for cancer treatments minimizing the adverse effects on non-tumour tissues. In further research, preclinical and clinical studies should provide additional insights for determining the optimal use of EOCs-MSPs.

Acknowledgement

We thank the Spanish Government (projects AGL2015-70235-C2-1-R, AGL2015-70235-C2-2-R and MAT2015-64139-C4-1-R (MINECO/FEDER)) and the Generalitat Valenciana (project PROMETEOII/2014/047) for support. C.A. thanks Colciencias for her predoctoral fellowship. A.B. thanks Generalitat Valenciana and Spanish MINECO for her postdoctoral contracts. The authors also thank the Electron Microscopy Service at the UPV for support.

References

Adorjan, B. & Buchbauer, G., 2010. Biological properties of essential oils: An updated review. *Flavour and Fragrance Journal*, 25(6), pp.407–426.

Arunasree, K., 2010. Anti-proliferative effects of carvacrol on human metastatic breast cancer cell line, MDA-MB 231. *Phytomedicine*, 17(8–9), pp.581–588.

Bernardos, A. et al., 2015. Antifungal effect of essential oil components against *Aspergillus niger* when loaded into silica mesoporous supports. *Journal of the Science of Food and Agriculture*, 95(14), pp.2824–2831.

Bianchini, F. & Vainio, H., 2001. Allium vegetables and organosulfur compounds: do they help prevent cancer? *Environ Health Perspect*, 109, pp.198–902.

Bottone, F.G. et al., 2002. Diallyl disulfide (DADS) induces the antitumorigenic NSAID-activated gene (NAG-1) by a p53-dependent mechanism in human colorectal HCT 116 cells. *The Journal of nutrition*, 132(4), pp.773–778.

Brunauer P.H. Teller, E., S.E., 1938. Adsorption of gases in multimolecular layers. *J. Am. Chem. Soc.*, 60, pp.309–319.

Cabrera, S. et al., 2000. Generalised syntheses of ordered mesoporous oxides: the atrane route. *Solid State Sci.*, 2(4), pp.405–420.

Casella, S. et al., 2013. The role of diallyl sulfides and dipropyl sulfides in the *in vitro* antimicrobial activity of the essential oil of garlic, Allium sativum L., and leek, Allium porrum L. *Phytotherapy Research*, 27(3), pp.380–383.

Dirk, S., 2006. Thermo- and pH- responsive polymers in drug delivery. *Advanced Drug Delivery Reviews*, 58, pp.1655–1670.

Fan, K. et al., 2015. Carvacrol inhibits proliferation and induces apoptosis in human colon cancer cells. *Anti-Cancer Drugs*, 26(8), pp.813–823.

Flesar, J. et al., 2010. *In vitro* growth-inhibitory effect of plant-derived extracts and compounds against Paenibacillus larvae and their acute oral toxicity to adult honey bees. *Veterinary Microbiology*, 145(1–2), pp.129–133.

Geng, F. et al., 2011. Allyl isothiocyanate arrests cancer cells in mitosis, and mitotic arrest in turn leads to apoptosis via Bcl-2 protein phosphorylation. *Journal of Biological Chemistry*, 286(37), pp.32259–32267.

Guimarães, A.G. et al., 2015. Encapsulation of carvacrol, a monoterpene present in the essential oil of oregano, with β-cyclodextrin, improves the pharmacological response on cancer pain experimental protocols. *Chemico-Biological Interactions*, 227, pp.69–76.

Heikkilä, T. et al., 2010. Citotoxicity study of ordered mesoporous silica MCM-41 and SBA-15 microparticles on Caco-2 cells. *European journal of pharmaceutics and biopharmaceutics : official journal of Arbeitsgemeinschaft für Pharmazeutische Verfahrenstechnik e.V*, 74(3), pp.483–494.

Hussain, A. et al., 2011. Eugenol Enhances the Chemotherapeutic Potential of Gemcitabine and Induces Anticarcinogenic and Anti-inflammatory Activity in Human Cervical Cancer Cells. *Cancer Biotherapy & Radiopharmaceuticals*, 26(5), pp.519–527.

Jaganathan, S.K. et al., 2011. Apoptotic effect of eugenol in human colon cancer cell lines. *Cell biology international*, 35(6), pp.607–15.

Jaganathan, S.K. & Supriyanto, E., 2012. Antiproliferative and molecular mechanism of eugenol-induced apoptosis in cancer cells. *Molecules (Basel, Switzerland)*, 17(6), pp.6290–6304.

Janatova, A. et al., 2015. Long-term antifungal activity of volatile essential oil components released from mesoporous silica materials. *Industrial Crops and Products*, 67, pp.216–220.

Jeong, H.-W. et al., 2003. Antitumor effect of the cinnamaldehyde derivative CB403 through the arrest of cell cycle progression in the G2/M phase. *Biochemical Pharmacology*, 65(8), pp.1343–1350.

Jing, L. et al., 2014. Antifungal activity of citrus essential oils. *Journal of Agricultural and Food Chemistry*, 62(14), pp.3011–3033.

Jo, H.J. et al., 2008. Diallyl disulfide induces reversible G2/M phase arrest on a p53-independent mechanism in human colon cancer HCT-116 cells. *Oncology Reports*, 19(1), pp.275–280.

Johnson, A.C. et al., 2008. Do cytotoxic chemotherapy drugs discharged into rivers pose a risk to the environment and human health? An overview and UK case study. *Journal of Hydrology*, 348(1–2), pp.167–175.

Kresge, C. et al., 1992. Ordered mesoporous sieves sinthesized by liquid-crystal template mechanism. *Nature*, 359, pp.710–712.

Kris-Etherton, P.M. et al., 2002. Bioactive compounds in foods: their role in the prevention of cardiovascular disease and cancer. *The American journal of medicine*, 113 Suppl(1), p.71S–88S.

Lai, K.C. et al., 2012. Diallyl sulfide, diallyl disulfide and diallyl trisulfide affect drug resistant gene expression in colo 205 human colon cancer cells in vitro and in vivo. *Phytomedicine*, 19(7), pp.625–630.

Li, J. et al., 2016. Cinnamaldehyde affects the biological behavior of human colorectal cancer cells and induces apoptosis via inhibition of the PI3K/Akt signaling pathway. *Oncology Reports*, 35(3), pp.1501–1510.

Liao, Q.J. et al., 2009. Effect of diallyl disulfide on cell cycle arrest of human colon cancer SW480 cells. *Chinese Journal of Cancer*, 28(2), pp.138–141.

Llana-Ruiz-Cabello, M. et al., 2014. Cytotoxicity and morphological effects induced by carvacrol and thymol on the human cell line Caco-2. *Food and Chemical Toxicology*, 64, pp.281–290.

Llana-Ruiz-Cabello, M. et al., 2015. *In vitro* pro-oxidant/antioxidant role of carvacrol, thymol and their mixture in the intestinal Caco-2 cell line. *Toxicology in Vitro*, 29(4), pp.647–656.

Majeed, H., Antoniou, J. & Fang, Z., 2014. Apoptotic effects of eugenol-loaded nanoemulsions in human colon and liver cancer cell lines. *Asian Pacific Journal of Cancer Prevention*, 15(21), pp.9159–9164.

Maldonado, P.D., Chánez-Cárdenas, M.E. & Pedraza-Chaverrí, J., 2005. Aged garlic extract, garlic powder extract, S-allylcysteine, diallyl sulfide and diallyl disulfide do not interfere with the antibiotic activity of gentamicin. *Phytotherapy Research*, 19(3), pp.252–254.

Marques, H.M.C., 2010. A review on cyclodextrin encapsulation of essential oils and volatiles. *Flavour and Fragrance Journal*, 25(5), pp.313–326.

de Mesquita, M.L. et al., 2009. Cytotoxic activity of Brazilian Cerrado plants used in traditional medicine against cancer cell lines. *Journal of Ethnopharmacology*, 123(3), pp.439–445.

Muñoz, B. et al., 2003. MCM-41 organic modification as drug delivery rate regulator. *Chem Mater.*, 15, pp.500–503.

Musk, S.R.R. & Johnson, I.T., 1993. Allyl isothiocyanate is selectively toxic to transformed cells of the human colorectal tumour line ht29. *Carcinogenesis*, 14(10), pp.2079–2083.

Ogasawara, M., Matsubara, T. & Suzuki, H., 2001. Screening of natural compounds for inhibitory activity on colon cancer cell migration. *Biological & pharmaceutical bulletin*, 24(6), pp.720–3.

Oliveira, P.F. de et al., 2015. Cytotoxicity screening of essential oils in cancer cell lines. *Revista Brasileira de Farmacognosia*, 25(2), pp.183–188.

Park, S.-Y. & Pendleton, P., 2012. Mesoporous silica SBA-15 for natural antimicrobial delivery. *Powder Technology*, 223, pp.77–82.

Park, S.Y., Barton, M. & Pendleton, P., 2011. Mesoporous silica as a natural antimicrobial carrier. *Colloids and Surfaces A: Physicochemical and Engineering Aspects*, 385(1–3), pp.256–261.

Pérez-Esteve, É. et al., 2015. Mesoporous Silica-Based Supports for the Controlled and Targeted Release of Bioactive Molecules in the Gastrointestinal Tract. *Journal of Food Science*, 80(11), pp.E2504–E2516.

Rattanachaikunsopon, P. & Phumkhachorn, P., 2008. Diallyl sulfide content and antimicrobial activity against food-borne pathogenic bacteria of chives (Allium schoenoprasum). *Bioscience, biotechnology, and biochemistry*, 72(11), pp.2987–2991.

Raut, J.S. & Karuppavil, S.M., 2014. A status review on the medicinal properties of essential oils. *Ind. Crop, Prod.*, 62, pp.250–264.

Ravizza, R. et al., 2008. Linalool, a plant-derived monoterpene alcohol, reverses doxorubicin resistance in human breast adenocarcinoma cells. *Oncology Reports*, 20(3), pp.625–630.

Ribes, S., Fuentes, A., Talens, P., Barat, J.M., et al., 2016. Influence of emulsifier type on the antifungal activity of cinnamon leaf, lemon and bergamot oil nanoemulsions against Aspergillus niger. *Food Control*, 73, pp.1–12.

Ribes, S., Fuentes, A., Talens, P. & Barat, J.M., 2016. Use of oil-in-water emulsions to control fungal deterioration of strawberry jams. *Food Chemistry*, 211, pp.92–99.

Salonen, J. et al., 2008. Mesoporous silicon in drug delivery applications. *Journal of pharmaceutical sciences*, 97(2), pp.632–653.

Shaffer, C. V. et al., 2016. Texas Native Plants Yield Compounds with Cytotoxic Activities against Prostate Cancer Cells. *Journal of Natural Products*, 79(3), pp.531–540.

Sherry, M. et al., 2013. Essential oils encapsulated in liposomes: a review. *Journal of liposome research*, 23(4), pp.268–75.

Song, J.-D. et al., 2009. Molecular mechanism of diallyl disulfide in cell cycle arrest and apoptosis in HCT-116 colon cancer cells. *Journal of biochemical and molecular toxicology*, 23(1), pp.71–9.

Suffness, M. & Pezzuto, J., 1990. Assays related to cancer drug discovery. In A. Press, ed. *Methods in Plant Biochemistry: Assays for Bioactivity*. London, UK, pp. 71–133.

Sundaram, S.G. & Milner, J.A., 1996. Diallyl disulfide induces apopotosis of human colon tumor cells. *Carcinogenesis*, 17(4), pp.669–673.

Vallet-Regi F., Arcos, D., M.B. et al., 2007. Mesoporous materials for drug delivery. *Angewandte Chemie - International Edition*, 46(40), pp.7548–7558.

Wong, T.W., Colombo, G. & Sonvico, F., 2011. Pectin matrix as oral drug delivery vehicle for colon cancer treatment. *AAPS PharmSciTech*, 12(1), pp.201–214.

Xiao, D. et al., 2005. Diallyl trisulfide-induced G2–M phase cell cycle arrest in human prostate cancer cells is caused by reactive oxygen species-dependent destruction and hyperphosphorylation of Cdc25C. *Oncogene*, 24, pp.6256–6268.

Xie, X. et al., 2016. EpCAM aptamer-functionalized mesoporous silica nanoparticles for efficient colon cancer cell-targeted drug delivery. *European Journal of Pharmaceutical Sciences*, 83, pp.28–35.

Yang, J.S. et al., 2009. Diallyl disulfide induces apoptosis in human colon cancer cell line (COLO 205) through the induction of reactive oxygen species, endoplasmic reticulum stress, caspases casade and mitochondrial-dependent pathways. *Food and Chemical Toxicology*, 47(1), pp.171–179.

Yu, C. et al., 2014. Cinnamaldehyde/ chemotherapeutic agents interaction and drug-metabolizing genes in colorectal cancer. *Molecular Medicine Reports*, 9(2), pp.669–676.

Zhang, Y., 2010. Allyl isothiocyanate as a cancer chemopreventive phytochemical. *Molecular Nutrition and Food Research*, 54(1), pp.127–135.

4.3 Study of capped mesoporous silica supports as masking garlic-odour system

Study of capped mesoporous silica supports as masking garlic odour system

Carolina Acosta,[a*] Cristian Olguín Pinatti,[b,c] Eduardo García,[b,c] Ramón Martínez-Máñez,[b,d] José M. Barat,[a] Andrea Bernardos[b,d]

[a] Grupo de Investigación e Innovación Alimentaria - Departamento de Tecnología de Alimentos, Universitat Politècnica de València, Camino de Vera S/N, Valencia, Spain.
[b] Instituto Interuniversitario de Investigación de Reconocimiento Molecular y Desarrollo Tecnológico - IDM, Universitat Politècnica de València, Universitat de València, Camino de Vera S/N, Valencia, Spain.
[c] Group of electronic development and printed sensors (ged+ps) Universitat Politècnica de València, Camino de Vera S/N, Valencia, Spain.
[d] CIBER de Bioingeniería, Biomateriales y Nanomedicina (CIBER-BBN), Spain.

Submitted 2017

The masking odour properties of a capped-mesoporous silica support were evaluated. A bioactive component from garlic (diallyl disulphide, **DA**) was encapsulated in mesoporous silica particles. Additionally, the particles' surface was functionalised with a polysaccharide derivative, which has been described as gate-like ensemble for cargo controlled delivery applications. The garlic-associated odour was monitored by sensory analysis, head space solid phase microextraction and electronic nose. The quantitative and qualitative evaluation of functionalised samples did not show volatile components garlic-odour associated. Moreover, panellists from sensory analysis non-differentiate blank samples (bare and empty supports, without **DA**) from functionalised ones, but they did from samples with DA without the functionalised polysaccharide. Hence, surface functionalization was able to mask the unpleased garlic-related odours. In addition, the capped system was able to trigger an on-command delivery in presence of specific enzymatic stimuli. As far as the authors know, this is the first example of odour masking, using an enzyme-induced delivery capped silica-based support, which promotes the use of interesting bioactive components with unpleasant sensorial features for food or pharmaceutical applications.

Keywords: Diallyl disulfide, masking odour, capped mesoporous silica particles, e-nose, headspace.

Introduction

Bioactive components from garlic are interesting because their antimicrobial, antifungal and antibacterial activity (Ankri & Mirelman 1999; Cavallito & Bailey 1944; Yamada & Azuma 1977). Among the garlic bioactive components, the organosulphur derivatives are strongly related to atherosclerosis and thrombosis prevention (Kris-Etherton et al. 2002; Liu et al. 2005; Bayan et al. 2014). In particular, sulphides from allicin decomposition have been recently reported as anticancer agents, and specifically, diallyl disulphide (**DA**) shows promising results against colon cancer cells (Bottone et al. 2002; Yang et al. 2009). However, the sulphur components are the major responsibles of unpleasant garlic-related odour, which limit the industrial applications. Hence, the design of systems able to encapsulate and mask the non-desired odour, results interesting for industrial process.

In relation to encapsulation studies, β-cyclodextrin is mainly used (Hadaruga et al. 2007; Astray et al. 2009), in particular, Ayala-Zavala and co-workers (2010) tested sensory quality of fresh-cut tomato exposed to a cyclodextrine garlic oil-complex. Results indicated that sensorial quality of tomato was not affect, indeed, the tomato samples were recommended for salad mixtures due to compatibility of tomato and garlic flavour (Ayala-Zavala & González-Aguilar 2010). However, the panellists' sensorial acceptability should not

be confussed with a masking garlic-odour capacity of the cyclodextrine complex. So far, results only show the non-detection of unpleasant flavors, but, there are not quantitative evaluations to confirm the masking of garlic components associated to their unpleasant odour. In this context, encapsulation for preserving functional activity while reducing unpleasure sensorial features of organosulphur garlic derived components has been proposed.

Recent works suggest that mesoporous silica-based supports could provide a system for masking sensorial inconvenient of cargo entrapped (Ruiz-Rico et al. 2015). The inorganic mesoporous silica particles (MSPs) have shown to provide unique features such as stability, biocompatibility, high inertness and homogenous porosity (Kresge et al. 1992; Wang 2009; Slowing et al. 2007). Additionally, their surface is easy to functionalise, which make systems able to deliver the entrapped cargo using several external stimuli (Bernardos et al. 2010; Aznar et al. 2009; Pérez-Esteve et al. 2015). In particular, recent studies have encapsulated essential oil components in MSPs, and results have displayed remarkable enhanced antifungal activity and a long-term effectiveness (Bernardos et al. 2015; Janatova et al. 2015; Park et al. 2012). In this sense, MSPs protect bioactive components and their functionalities. However, neither sensorial, nor analytical evaluation has been done on MSPs as encapsulation system for masking odour.

In a previous work, MSPs were used as supports for garlic extract encapsulation and the functionalisation of the surface was developed for a sustained and on-command release of garlic components, which were evaluated as DA (Acosta et al. 2014). Based on that, we hypothesised that surface modifications on MSPs prevent the outflow of sulphurs' volatile components, which mask the unpleasant garlic-related odours.

We herein synthesised micro-sized MSPs, where DA was encapsulated. The particle surface of the loaded MSPs was functionalised with a polysacharide, a hydrolysed starch, named Glucidex 47 (Bernardos et al. 2010; Llopis-Lorente et al. 2017). And the influence of surface functionalization on masking odour features was evaluated.

DA release in headspace was evaluated and results suggest that polysaccharides anchoring on MSPs' surface are responsible for the non garlic-related odour detection. Additionally, only in presence of the specific enzyme stimuli, the MSPs-capped system was able to deliver the DA. As far as we known, it is the first attempt to completely evaluate MSPs as systems with odour masking capacity, besides, it is the first attempt which it is possible mask unpleasant garlic-related odour in function of the absence of specific stimuli; which opens interesting possibilities for industrial applications.

Materials and methods

Chemicals

All chemicals were purchased at the highest grade available and used directly without any further purification. Diallyl-disulphide, **DA**, (tech., 80 %) was purchased from Sigma Aldrich. Acetonitrile and hexane were provided by Fisher Scientific. The chemicals, tetraethylorthosilicate (TEOS), n-cetyltrimethylammonium bromide (CTAB), sodium hydroxide, triethanolamine (TEAH), 3-aminopropyltriethoxysilane (APTES), the phosphate buffered saline (PBS) for molecular biology 0.2 μm filtered (with a phosphate buffer concentration of 0.01 M and a sodium chloride concentration of 0.154 M. The solution pH will be 7.4.), and the enzyme, pancreatin from porcine pancreas were provided by Aldrich. The hydrolysed starch Glucidex-47® (5 % glucose, 50 % maltose, 45 % oligosaccharides and polysaccharides) was provided by Roquette.

Solids characterisation

PXRD measurements were taken on a Seifert 3000TT diffractometer using CuKα radiation. TEM images were obtained under a 100 kV Philips CM10 microscope. N_2 adsorption-desorption isotherms were recorded in a Micromeritics ASAP2010 automated sorption analyser. Samples were degassed at 120 °C in vacuum overnight. The specific surface areas were calculated from the adsorption data within the low pressure range using the BET model (Brunauer & Teller, 1938). Dynamic light scattering (DLS) studies for size distribution were

conducted at 20 °C using a Malvern Mastersizer 2000. Data analysis was based on the Mie theory using refractive indices of 1.33 and 1.45 for the dispersant and MSPs, respectively. To determine the zeta potential (ζ) of solids, a Zetasizer Nano ZS was used. Zeta potential was calculated from the particle mobility values by applying the Smoluchowski model. The average of five recordings was reported as the zeta potential. All the measurements in Malvern Zetasizer Nano ZS and Malvern Mastersizer 2000 were performed at 20 °C in triplicate, samples were dispersed in PBS buffer. Before each measurement, samples were sonicated for 10 min to preclude potential aggregation. Finally, the elemental analysis was performed in a EA-1110 CHN Elemental Analyser.

Synthesis of mesoporous silica micro-sized particles (blank sample, M0)

The mesoporous MCM-41 type support, was first synthesised as micro-sized particles by "atrane route" (Cabrera et al. 2000) in which 4.68 g of CTAB was added at 118 °C to a solution of TEAH (25.79 g) containing 0.045 mol of a silatrane derivative (TEOS, 11 mL). Next, 80 mL of water was slowly added with vigorous stirring at 70 °C. After a few minutes, a white suspension was formed. This mixture was aged at room temperature overnight. The resulting powder was collected by filtration and washed. As-synthesised solid was obtained, it was dried at 70 °C and finally, in order to obtain **M0**, template phase was removed by calcination at 550 °C for 5 h, using an oxidant atmosphere.

Impregnation of garlic components (loaded-solids: M1, M2 and M3)

Diallyl disulphide (**DA**), was suspended in acetonitrile, and three different dissolutions were prepared (0.1 1 and 10 μg·mL^{-1}). Then, based on the impregnation loading procedure described by Pérez-Esteve and co-workers (Pérez-Esteve et al. 2016), 100 mg of **M0** were impregnated with 100 uL of each dissolution, dropped over the solid. To improve the loading yield through porous impregnation, five cycles of addition were carried out (total of 500 μL of DA). After each addition cycle, solids were dried at room temperature to evaporate acetonitrile. Finally, solids **M1**, **M2** and **M3** were obtained, corresponding to loading dissolutions 0.1, 1 and 10 μg of DA·mL^{-1}, respectively.

Synthesis of functionalised-solids (G1, G2 and G3)

Surface functionalisation was developed in two steps. First (Step 1), a solution of 3-aminopropyltriethoxysilane (APTES, 0.14 mL) was added to a dispersion of loaded-solids (**M1, M2** and **M3**) in deionised water (4 mL). The reaction mixture was stirred for 5.5 h at room temperature in an inert atmosphere of nitrogen. The obtained solids were filtered and washed with acid solution at pH 2.0 and dried for 12 h at 35 °C. Intermediated solids obtained after Step 1 of functionalization, were named **g1**, **g2** and **g3**, respectively.

Then (Step 2) a suspension of hydrolysed starch (Glucidex-47) in water (12 mL) was added to in a 1:1 w/w relation (0.6 g of Glucidex and 0.6 g of solids **g1**, **g2** and **g3**).

Final mixture was stirred for 24 h at room temperature in an inert atmosphere of nitrogen. The solids were filtered and washed with deionised water, and dried at for 12 h at 35 ºC, to obtain the final capped solids **G1**, **G2** and **G3,** respectively**.**

Release studies

In a typical experiment, 1 mg of loaded-solids were suspended in 2 mL of PBS and stirred at 200 rpm. On the other hand, delivery evaluation of functionalised-solids (**G1**, **G2**, **G3)** was constituted by 50 mg of solids in 5 mL of PBS buffer. Delivery studies were carried out in PBS with and without enzymatic stimuli (pancreatin at 1 mg per mL PBS). At certain time, suspensions were centrifuged. The supernatant was separated and extracted thrice with hexane, (final volume of 10 mL). The resulting samples (after hexane extraction) were monitored via gas chromatography mass spectrometry (GC/MS).

Release quantification: Hexane extract sample volumes of 1 µl were injected with a pulsed split-less ratio of 10:1 using a hot-needle technique. The GC–MS system consisted of an Agilent7890A gas chromatograph with 5975C Mass Spectrometer. Gas chromatography was performed on a 30 m Agilent BPX5 column with 0.25 mm inner diameter and 0.25 µm film thicknesses. Injection temperature was 240 °C, the interface set to 250 °C and the ion source adjusted to 200 °C. The carrier gas used was helium set at a constant flow rate of 1

ml·min^{-1}. The temperature program was 3 min isothermal heating at 60 °C, followed by a 10 °C·min^{-1} oven temperature ramp to 120 °C, 8 °C·min^{-1} ramp to 180 °C and a final 6 °C·min^{-1} oven temperature ramp to 230 °C with 2 min heating at 230 °C. Mass spectra were recorded at two scans per sec with an m/z 30–600 scanning range and spectra were recorded in selective ion monitoring (SIM) mode: m/z 41, 81 and 146 for diallyl-disulphide (**DA**). The chromatograms and mass spectra were evaluated using the masslab program. A retention time and mass spectral library for automatic peak quantification of metabolite derivatives was implemented within the masslab method format.

Sensory analysis

The triangle different discrimination test was used. Panellists were students and staff members of our department; all of them had good experience in sensory evaluation. The triangle difference test was performed with 24 panellists and each group of samples were tested thrice in a randomized complete block design. No information was given to the panellists about the origin of the samples.

Solids were presented in 10 mL disposable glass cups provided with gas tight cover and coded with 3-digit random numbers. Groups of three samples (0.1 g each) were assessed, and just one sample was different. Each panellist was instructed to open the cover of the cup, to smell the headspace carefully and then

to close it. For nose-clearing, before opening each sample, panellists were asked to smelling their un-fragranced forearm.

The panellists aim was to determine in each group the solid perceived to be different from the other two by smelling only. Two different tests were assessed.

First assay: to measure if people can differentiate between the functionalised-solids and a sample without garlic-loaded (blank sample, M0). Group of samples were formed with two blank-samples and the functionalised-ones. Three groups were disposed for each G1, G2 and G3 solids.

Second assay: to measure differentiation between the loaded- and functionalised-solids. One loaded solid was disposed with two of their corresponded functionalised-solid. Three measurement groups were formed for **M1, M2** and **M3** and their respective functionalised-solid **G1, G2** and **G3.**

Head Space Solid Phase Microextraction (HS-SPME) and GC-MS detection

A known amount (0.1 g) of solid was added to a 10 mL headspace (HS) vial and sealed with a PTFE-faced silicone septum. The vials were maintained at 37 °C and vapour were withdrawn from the vial by fibre assembly 65 um PDMS/DVB, stableflex, 23 Ga and injected in the chromatographic column via a transfer line.

The volatile sulphur-containing compound from solids was analysed using an Agilent Technologies 6890N Network Gas Chromatography System equipped with an Agilent Technologies 5973 inert mass selective detector fitted with an HS-

5MS column (30 m × 0.25 mm × 0.25 µm film thickness, (5 % phenil)-methyl silox Agilent Technologies).

Helium gas was used as a carrier gas at a flow rate of 1 $\mu L \cdot min^{-1}$. The chromatography run was started by warming the column at 40 °C for 1 min, heated to 200 °C at a rate of 10 $°C \cdot min^{-1}$, with 1 min of hold time. Then, increased to 250 °C at a rate 15 $°C \cdot min^{-1}$, and held at 250 °C for 3 min.

The components were identified by comparison with authentic standards. Quantification of flavour components was done by comparing the sample peak area to that of a known amount of pure component in hexane.

Electronic nose detection

A known amount (0.1 g) of solids was added to a 10 mL headspace (HS) vial and sealed with a PTFE-faced silicone septum. The vials were maintained at 25 °C for 20 min, afterwards, vial was placed inside e-nose chamber and headspace was measure along 20 min.

The e-nose system, consists of an array of commercial metal oxide semiconductor (MOS) sensors for different gases (hydrogen, carbon, monoxide, butane, methane, etc.), two LM35DZ for temperature sensing, a sample handling system for the management for the gases to be measured, and a data acquisition system to control the configuration of the sensors and the data collected, in order to manage the sensor cleaning.

Each group of samples (blank sample: **M0**, loaded-solids: **M1**, **M2** and **M3** and functionalised-solids: **G1**, **G2** and **G3**) were evaluated five times.

Data analyses

Statistical analyses from chromatography and sensory data were developed by the SPSS statistical software package. While e-nose data were evaluated by Stand Alone Chemometrics Software (Solo). A first approach used Principal Component Analysis (PCA); the leave one out cross validation was implemented on the entire datasets. We also conducted a Partial Least Square (PLS) analyses, Support Vector Machine Discriminant Analysis (SVMDA) and Multilayer Perceptron (MLP) study. Five sets of measurements were analised, three of them were used to calibration the model and the other two to test the models.

Results and Discussion

Mesoporous silica materials

The mesoporous silica-based particles used in this study were micro-sized MCM-41 type. In this work, solids were synthesised and subsequently, three different DA dissolutions (0.1 1 and 10 □g·mL-1) were used to impregnate in **M0** solids and obtaine **M1**, **M2** and **M3**, respectively. The carbohydrate polymer used for capping the surface particles was hydrolysed starch Glucidex-47 (5 % glucose, 50 % maltose, 45 % oligosaccharides and polysaccharides), a polysaccharide previously reported for capping MSPs (Bernardos et al. 2010). In this approach, loaded-solids (**M1, M2** and **M3**) were functionalised in two steps. First APTES was

anchored to surface particles and solids **g1, g2** and **g3** were obtained, then the hydrolysed starch, Glucidex-47 was covalent bonded to amine and the final functionalised solids **G1**, **G2** and **G3** were obtained (see Scheme 4.3-1).

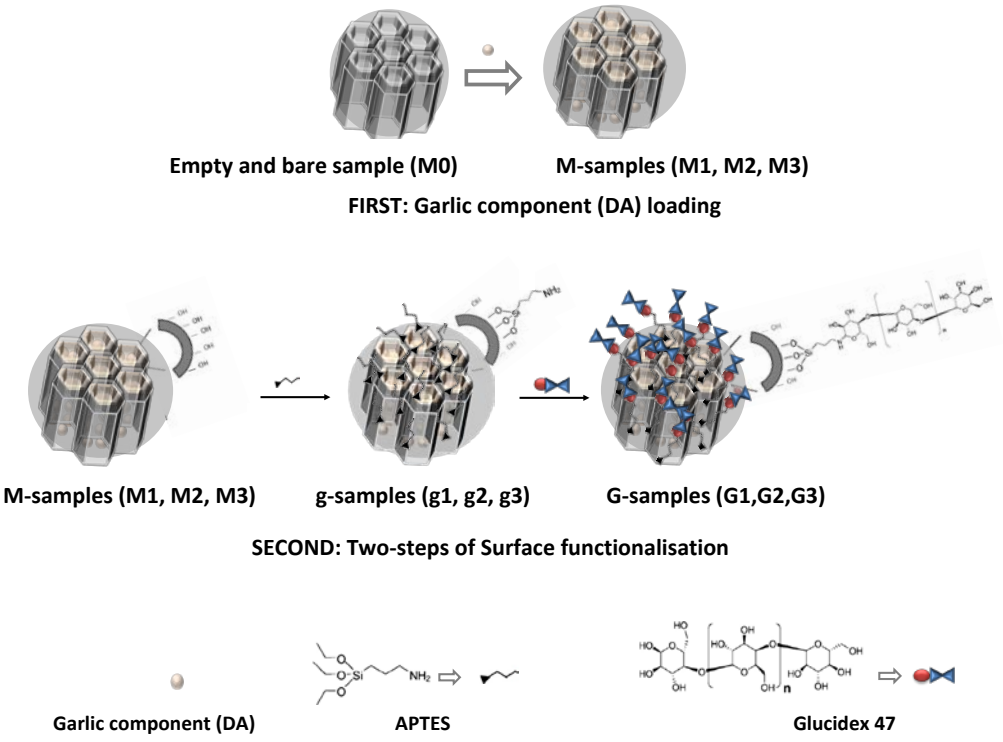

Scheme 4.3-1. Samples synthesis. First: loaded-solids and Second: Two steps to obtain functionalised-solids.

Characterisation of encapsulation system

The characterisation of the solids was performed using well-known techniques. Powder X-ray diffraction (PXRD) patterns of the prepared silica mesoporous MCM-41 type micro-sized particles (as-synthesised and calcined) are shown in Figure 4.3-1A. The PXRD of as-synthesised solids shows four low-angle

reflections typical of a hexagonal array that can be indexed as (100), (110), (200) and (210). A significant shift of the (100) reflection in the PXRD of the **M0** calcined solid is observed (Figure 4.3-1A), corresponding to an approximate cell contraction of ca. 4.9 Å. PXRD pattern of loaded and functionalised solids (Figure 4.4-1A) only shows the characteristic (100) reflection. The presence of this peak indicates that the mesoporous structure was preserved through the filling process with the garlic component (**DA**) and after the anchoring of hydrolysed starch. Figure 4.3-1B shows the typical porosity associated with the pseudo hexagonal array of calcined mesoporous silica particles (**M0**), TEM images show that mesoporous structure remains after loading and functionalization. Additionally, TEM images indicate that solids were obtained as micrometric particles of ca. 1000-4000 nm (Figure 4.3-1B).

N_2 adsorption–desorption isotherms of the **M0** calcined phase shows typical curves which can be related to the nitrogen condensation inside the mesopores by capillarity, as corresponds to a type IV isotherm (see Figure 4.3-1C). The absence of a hysteresis loop in this interval and the narrow pore distribution suggests the existence of uniform cylindrical mesopores (2.71 nm, 0.88 $cm^3 \cdot g^{-1}$).

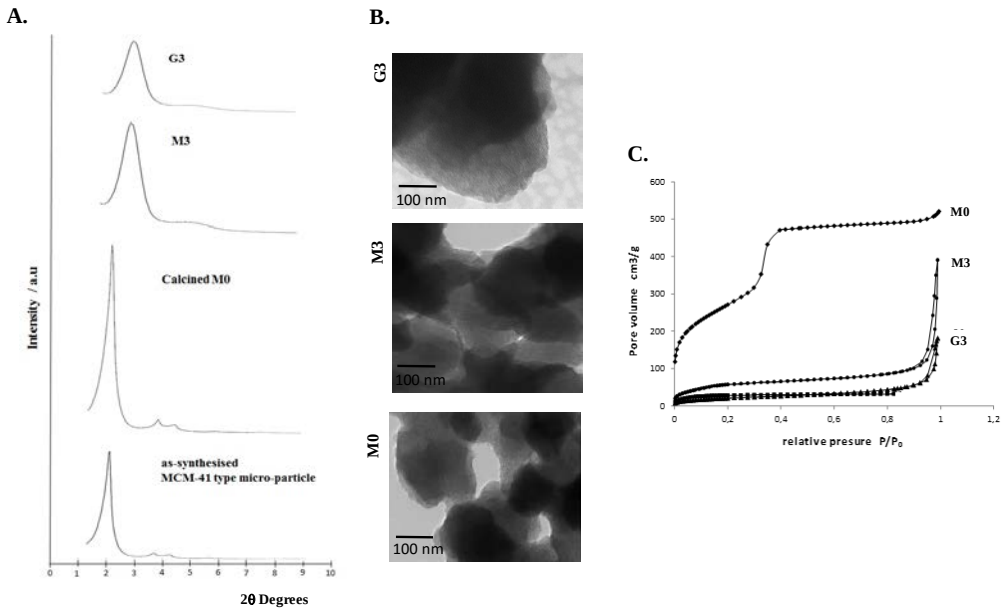

Figure 4.3-1. Materials characterisation: A. Powder X-ray patterns, B. TEM images of micro-sized particles (empty and bare particles, M0; loaded-solids, M3 and functionalised-solids, G3), C. Nitrogen adsorption-desorption isotherms: Calcined material M0 [●], Solid M3 [■] and solid G3 [◆].

A total specific surface of 989.4 $m^2 \cdot g^{-1}$ was obtained by using the BET model to calcined material. In contrast, the N_2 adsorption–desorption isotherms of the loaded-solids and the final functionalised-solids, show in each case a flat curve with specific surfaces of 220 and 100 $m^2 \cdot g^{-1}$ and pore volumes of 0.25 and 0.17 $cm^3 \cdot g^{-1}$ for **M3** and **G3**, respectively (data non shown for other samples). Decrease of surface and pore volume confirm the significant pore blocking due molecular gates anchorage.

Finally, zeta potential (ζ) was performed in aqueous dispersion (PBS), data shown in Table 4.3-1. Calcined and loaded-solids had a negative zeta potential due

to the presence of anionic silanol groups on their surface. Upon functionalisation, the surface potential changed from negative to positive, which was ascribed to the grafting of starch onto the surface of solids.

Table 4.3-1. Characteristics of synthesised solids

	S_{BET} (m^2g^{-1})	Pore volume (cm^3g^{-1})	Mean size (nm)*	Z potential (ζ) (mV)
M0	989.419	0.884	2566	-18.60
M3	220.089	0.248	1930	-8.06
G3	100.081	0.171	1189	11.06

* Single-particle size determined by TEM

Diallyl disulphide encapsulation

Based on the **DA** concentration used for loading **M1**, **M2** and **M3** solids, the theoretical amount of **DA** encapsulated was determined as 0.5, 5 and 50 μg of **DA** per mg of solid, respectively. Then, to identify the loading-yield, elemental analysis (EA) was performed. Based on sulphur content obtained by EA, the real **DA** amount was determined and loading-yield was calculated (see Table 4.3-2A).

In addition, the steps of gate-anchorage were monitored through sulphur and nitrogen content from EA data. Functionalised-solids showed a **DA** decreased amount, mainly from **M3** to **G3** (see Table 4.3-2B). Based on loading yield of **M3** and **G3**, we hypothesised that the highest **DA** concentration tested (10 $\mu g \cdot mL^{-1}$) did not was effectively encapsulated, and some leaks along functionalised process may decrease the encapsulation yield. Despite **DA** loses, the sulphur content

inside **G1**, **G2** and **G3** solids confirms the **DA** presence after the surface functionalization.

Table 4.3-2. Encapsulated content of garlic, as diallyl disulphide (DA) loaded concentration.

A	Garlic content (μg DA·mg solid^{-1})	Loading yield (%)
M1	0.46	91.2
M2	0.91	18.2
M3	13.23	26.5

B	Garlic content (μg DA·mg solid^{-1})	Loading yield (%)
G1	0.45	90.0
G2	0.81	16.2
G3	5.47	10.9

On the other hand, the nitrogen amount was associated with APTES content, which did not change from first (Intermediate solids: **g1**, **g2** and **g3**) to second (Final solids: **G1**, **G2** and **G3**) step of functionalization. In this sense, the functionalization through 2-steps, should works as the 1-step method, previously reported (Bernardos et al. 2010; Acosta et al. 2014).

Controlled release studies

The gate-like system is associated to enzymatic stimuli. A polysaccharide (hydrolysed starch Glucidex 47) is grafted on MSPs surface and inhibits cargo delivery due to the formation, around the pore outlets, of a dense monolayer of sugar molecules. In the presence of pancreatin (a pool of enzymes that contain amylases), the 1→4 glycosidic bond between α-D-glucoses from the starch is hydrolysed with the subsequent uncapping of the pores and cargo delivery (Bernardos et al. 2010), as Scheme 4.3-2 shows.

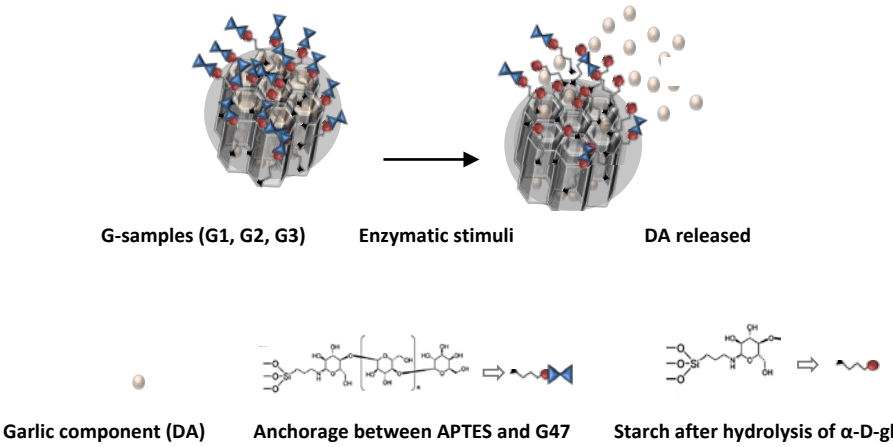

Scheme 4.3-2. Representation of uncap system after hydrolysis of the saccharide anchored on the MSPs surface

Based on the **DA** amount calculated by EA, the maximum capacity of release (mrc) was determined (See Figure 4.3-2).

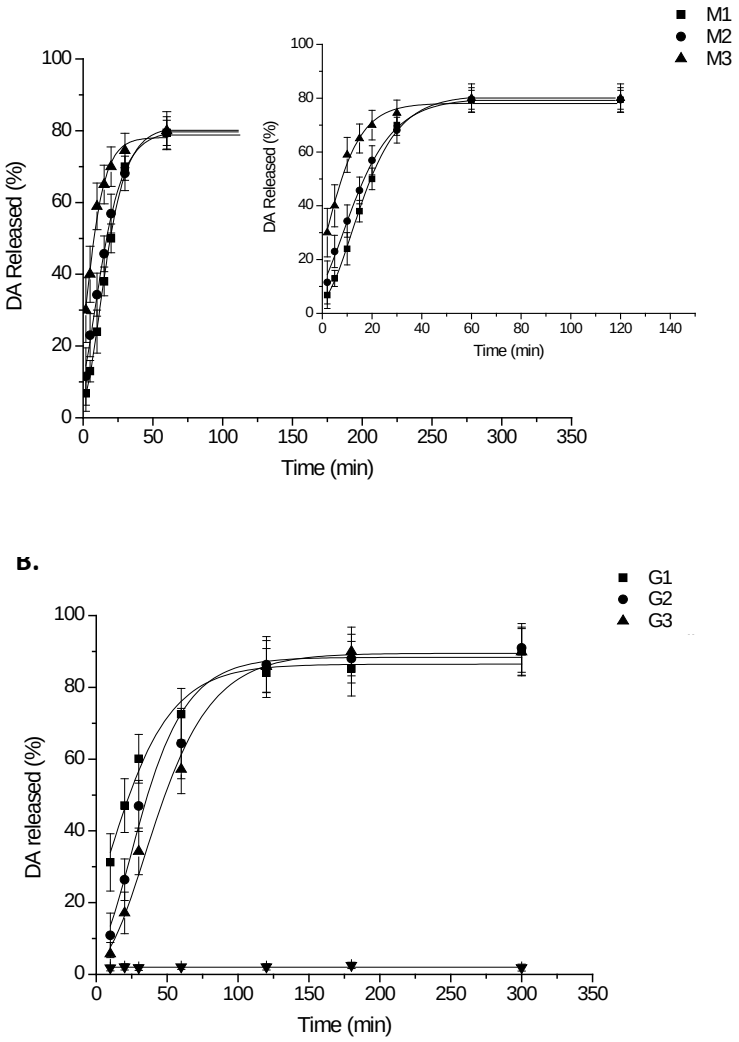

Figure 4.3-2. Release evaluation: A. Loaded-solids suspended in PBS, (inset shows a zoom of the boost release at first 40 min) and B. Functionalised-solids suspended in PBS with pancreatin (maximum release after 150min); the mean release of G1, G2 and G3 in PBS (without enzyme stimuli) [▼].

Loaded-solids showed a 60 % of release within the first 20 min; and ca. 80 % of maximum release capacity (mrc) was released in one hour, see Figure 4.3-2A.

On the other hand, functionalised-solids did not show a **DA** release in PBS (Figure 4.4-2B), but once they were dispersed in PBS dissolution with pancreatin enzyme, a controlled released was identified. Along first hour, just the 40 % of mrc was released, and the next two hours 60 % of mrc was achieved. Finally, after 5 h, the maximum release (80 % of mrc) was achieved. As Figure 4.3-2 shows, a controlled release was observed, which is in line with previous systems based on Glucidex-47 (Bernardos et al. 2010).

Sensory evaluation

To evaluate the effect of gate-like system on the garlic-related odour detection, two triangle different discrimination tests were done. According to statistical tables for triangle tests, for 24 panellists, the number of correct responses should be at least 14.[1] In relation to Table 4.3-3A, 80 % of panellists did not identify any characteristic odour in functionalised-solids, so, functionalised-solids were non significantly different from solids with anything encapsulated inside their pores (blank samples, **M0**).

On the other hand, Table 4.3-3B shows the differences between loaded solids with and without capped system. Results were not statistical significantly to declare differences either **G1** to **M1** nor **G2** to **M2**. Except to **G3** from **M3**, where

[1] *http://www.fao.org/docrep/v7180e/V7180E12.HTM ; http://www.mikromarkt.eu/pdfs/uk_modul_9_t4.pdf*

results indicated a significant differentiation of functionalised-solid from the loaded-solid.

Table 4.3-3. Sensory results from triangle different discrimination tests.

A.

	Correct answers
G1 - B - G1	4.0 ± 1.2
G2 - B - G2	5.0 ± 0.6
G3 - B - G3	5.0 ± 0.6

B.

	Correct answers
G1 - M1 - G1	9.0 ± 0.6
G2 - M2 - G2	11.0 ± 0.7
G3 - M3 - G3	18.0 ± 0.9

In this regard, panellists recognise a slight and strange but not unpleasant odour in **M1** and **M2** samples. They did not associate any garlic-odour to **M1** or **M2** samples, however they did not clearly identify the blank sample. On the other hand, panellists identify a garlic-related odour from **M3**, and the absence to strange odour in **G3** samples. As Table 4.3-2 shows, **DA** content in **M1** and **M2** is significantly lower than **M3**. We therefore assume that small **DA** amount is not easily recognised by panellists, as they certainly did with the largest **DA** concentration, in **M3** sample.

Here, the ability of functionalisation for masking garlic odour is demonstrated. However, the inconclusive results from sensory analyses with loaded-solids **M1** and **M2**, show that sensory results are not enough to confirm our hypothesis, and it is needed the use of analytical and quantitative studies.

Head Space Evaluation (HS-SPME with GC-MS detection)

Taking into account the above results, it is needed to confirm that the non-detection of garlic-related odour, is a result of masking effect and not as a consequence of small amount of **DA** encapsulated nor due to **DA** losses.

In this context, **DA** evaluation of loaded-solids (**M1**, **M2**, and **M3** solids) and functionalised-solids (**G1**, **G2** and **G3**) using headspace HS-SPME was performed. Also, solids obtained after the first step of functionalization, **g1**, **g2** and **g3** dispersed in PBS with and without pancreatin, were evaluated.

Figure 4.3-3 shows the intensity response related to **DA** detection. The three loaded-solids (**M1**, **M2** and **M3**) showed the major **DA** detection. As well as results were correlated with **DA** content. It confirms the significant high **DA** content of **M3**. Then, after the complete surface functionalization, any of three functionalised-solids (**G1**, **G2** and **G3**) did not show any **DA** detection.

Despite this, results from testing solids **g1**, **g2** and **g3**, after the first step of surface functionalization (with only APTES anchorage), a small **DA** amount was detected. It confirms not only the **DA** presence, (there are not lack of **DA** along functionalization steps), but also, results indicate that first step of APTES functionalization is not enough to mask the complete garlic-related odour detection. In relation to detection of **DA**-released, PBS dispersions had non-**DA** detection, but a significant **DA** signal was detected for enzyme suspensions.

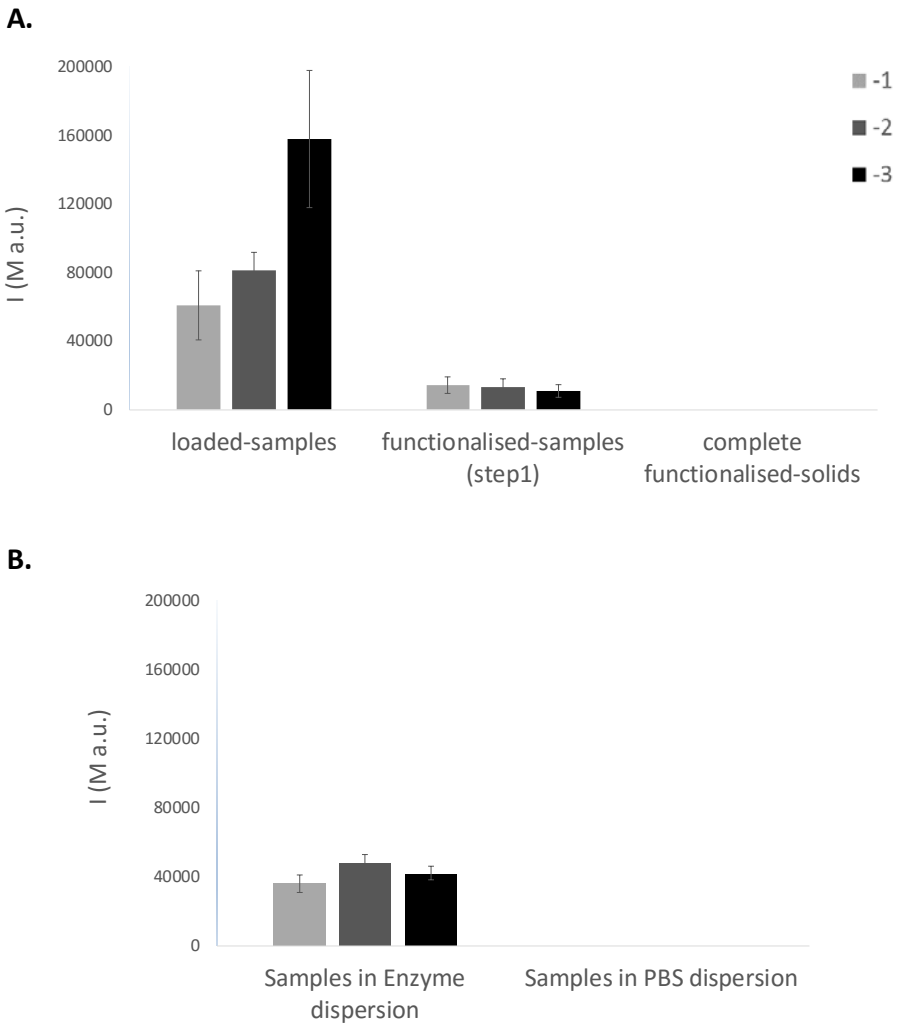

Figure 4.3-3. Head space of garlic-related odour detection, evaluated as diallyl disulphide content. A. Head-space detection of dry-samples: Loaded-solids (M1, M2 and M3), intermediate solids after first step of functionalization (g1, g2 and g3) and Final functionalised solids (G1, G2, G3). B. Head-space detection of functionalised samples on PBS suspensions: With and without enzyme presence.

Grey bars correspond to solids of DA dispersion of loading of 0.1 µg·mL^{-1} (M1, g1 and G1), Dark grey bars are solids of DA loading dispersion of 1 µg·mL^{-1} (M2, g2 and G2), and black bars are of DA loading dispersion of 10 µg·mL^{-1} (M3, g3 and G3).

Hence, the HS-SPME monitoring confirms the masking odour due to surface functionalization. Results also indicated that a complete surface capping is needed for enhancing the masking properties of gate-like systems. Moreover, monitoring of release dispersions not only validate the on-command delivery but also confirms that **DA** component remains inside the pores. Additionally, results showed that capped-system mask the unpleasant odour unless the specific enzymatic stimulus appears.

Electronic nose evaluation

In order to get a rapid system to detect the presence or odour absence. An electronic nose (e-nose) was used to evaluate the headspace. First, a protocol was developed to detect **DA** disolutions in hexane. A dynamic data analysis showed that e-nose was able to differentiate **DA** in function to three different concentrations. The protocol established was able to differentiate **DA** solutions from their respective controls (hexane without **DA**). It means that the developed e-nose protocole has a dose-manner response.

Data exploration and dimension reduction on the datasets were performed by Principal Components Analysis (PCA). Attending to the three **DA** concentrations and all the functionalised-samples. This model had four principal components whit a cumulative variance of 91.4 %, a Root Mean Square Error of Calibration (RMSEC) of 0.276 and a Root Mean Square Error of Cross Validation of 2.071, and

a 67.5 % of representatively from the datasets. Due to low representatively of two components, see Appendix 4.3-Figure S1, we tried a concretely PCA with three components. Figure 4.3-4 shows the data clustering for each loaded-samples (**M1**, **M2** and **M3**). The cluster corresponding to functionalised-samples, show a reliable result. Which confirms the differences between the loaded and functionalised-samples.

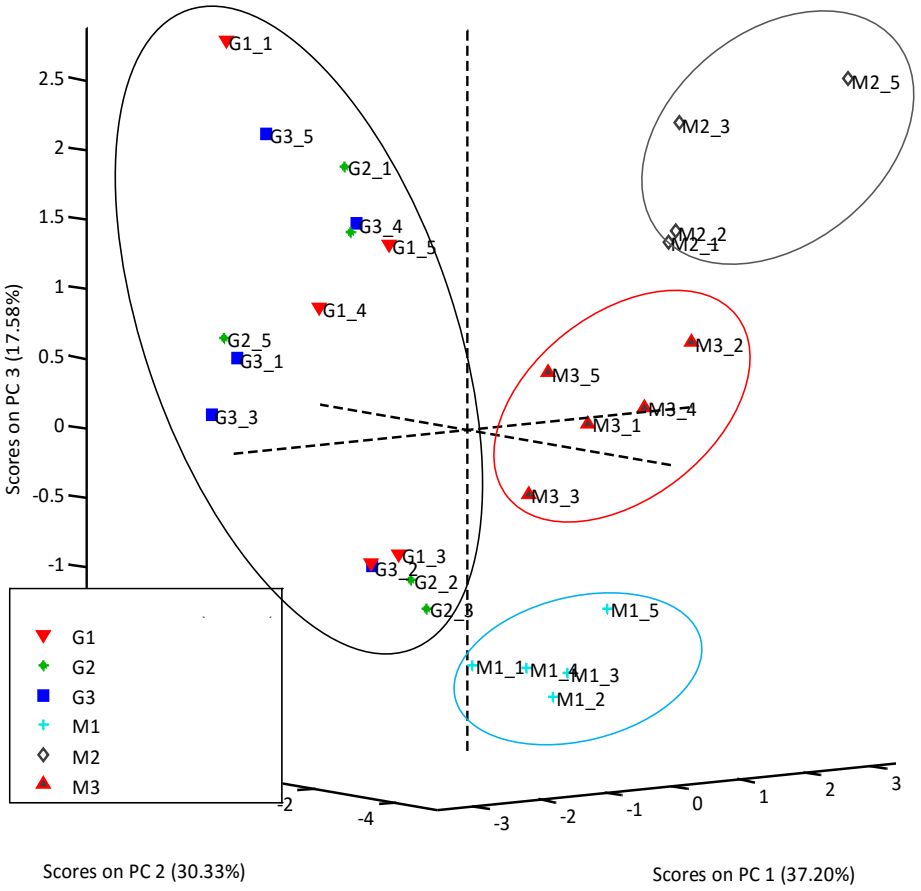

Figure 4.3-4 Principal Components Analyse with 3 principal components to differentiate two main groups: The bigger circle with all the functionalised- samples, and clearly

differentiate, on the other side: the loaded-samples, without surface functionalization are grouped in function of concentration of DA loaded.

We also conducted a Partial Least Square (PLS), see Appendix 4.3-Figure S2, analysis attending to the four different classes assuming that functionalised-samples should take the same response, ideally. In this case, the model had a R^2 of 0.79 which indicate the probability level to predict the right sample using the model obtained, (taking into account a Cross Validation). PLS model had four principal components whit a cumulative variance of 87.6 %, a Root Mean Square Error of Calibration (RMSEC) of 1.063 and a Root Mean Square Error of Cross Validation of 1.882 (Supplementary information, Appendix 4.3-Figure S3). A SVMDA analyses was also carried out (Supplementary information, Appendix 4.3-Figure S4), it indicated that 90 % of samples were properly classified among the four classes defined.

Finally, we carried out a Multilayer Perceptron (MLP). Bearing in mind that when MLP is used as a classification tool, the numbers of neurons in the input layer is equal to the dimension of the feature space and the number of neurons in the output layer is usually chosen to be the number of classes. In our case we define architecture of twelve inputs neurons, six neurons in one hidden layer and four output neurons. We achieved, with all samples measured, a 100 % classification accuracy through leave-one-out cross validation method.

Table 4.3-4 shows the confusion matrix of MLP classifier using leave-one-out cross validation method. Hence, e-nose responses confirmed the differences along samples with garlic odour and samples with non-garlic detection. Based on results obtained with electronic nose, we conducted a PLS, using data from DA release quantification studies, to obtain a real approaching.

Table 1.3-4 Confusion matrix of MLP

Target Output	**M1**	**M2**	**M3**	**Loaded-solids**
M1	5	0	0	0
M2	0	5	0	0
M3	0	0	5	0
Loaded-solids	0	0	0	15

In this case, although the model had a R2 of 0.794, RMSEP and RMSECV were high; hence, using a real approach to the samples measured, e-nose method developed is able to identify garlic odour.

Conclusions

A masking encapsulation system for garlic-related odour was described. Major bioactive component in garlic (diallyl disulphide, **DA**) was encapsulated in mesoporous silica supports, and the surface functionalisation not only provides an on-command release by enzyme presence, but also retains the DA inside the pores which mask the garlic-related odour.

Sensory and headspace monitoring of **DA** showed that MSPs support by itself does not represent a masking odour solution, but surface functionalisation achieves the non-odour detection. Additionally, this study showed that electronic-nose can be used as a rapid system for monitoring.

Acknowledgements

The authors wish to express their gratitude to the Spanish Government (MINECO Projects AGL2012-39597-C02-01, AGL2012-39597-C02-02, AGL2015-70235-C2-1, MAT2012-38429-C04-01, MAT2015-64139-C4-1 and MAT2015-64139-C3-R MINECO/FEDER), the Generalitat Valencia (Project PROMETEOII/2014/047) and Colombian Administrative Department of Science, Technology and Research which supported Ms. Acosta Scholarship. Ms. Bernardos thanks Generalitat Valenciana and Spanish MINECO for her postdoctoral contracts. We would also like to thank the Instituto de Conservación y Mejora de la Agrodiversidad Valenciana (COMAV), and the Microscopy Service of the Universitat Politècnica de València, for technical support, and Roquette for the Glucidex samples.

References

Acosta, C., Perez-Esteve, E., Fuenmayor, C. A., Benedetti, S., Cosio, M. S., Soto, J., … Martínez-Máñez, R. (2014). Polymer Composites Containing Gated Mesoporous Materials for On-Command Controlled Release. *ACS Appl Mater Interfaces*, 6(9), 6452–60.

Ankri, S., & Mirelman, D. (1999). Antimicrobial properties of allicin from garlic. *Microbes and Infection*, 1(2), 125–129.

Astray, G., Gonzalez-Barreiro, C., Mejuto, J. C., Rial-Otero, R., & Simal-Gándara, J. (2009). A review on the use of cyclodextrins in foods. *Food Hydrocolloids*, 23(7), 1631–1640.

Ayala-Zavala, J. F., & González-Aguilar, G. A. (2010). Optimizing the use of garlic oil as antimicrobial agent on fresh-cut tomato through a controlled release system. *Journal of Food Science*, 75(7).

Aznar, E., Martínez-Máñez, R., & Sancenón, F. (2009). Controlled release using mesoporous materials containing gate-like scaffoldings. *Expert Opin Drug Deliv*, 6(6), 643–655.

Bayan, L., Koulivand, P. H., & Gorji, A. (2014). Garlic: a review of potential therapeutic effects. *Avicenna Journal of Phytomedicine*, 4(1), 1–14.

Bernardos, A., Marina, T., Žáček, P., Pérez-Esteve, É., Martínez-Mañez, R., Lhotka, M., … Klouček, P. (2015). Antifungal effect of essential oil components against *Aspergillus niger* when loaded into silica mesoporous supports. *Journal of the Science of Food and Agriculture*, 95(14), 2824–2831.

Bernardos, A., Mondragon, L., Aznar, E., Marcos, M. D., Martínez-Manez, R., Sancenón, F., … Amoros, P. (2010). Enzyme-responsive intracellular controlled release using nanometric silica mesoporous supports capped with "saccharides." *ACS Nano*, 4(11), 6353–6368.

Brunauer P.H. Teller, E., S. E. (1938). Adsorption of gases in multimolecular layers. *J. Am. Chem*. Soc., 60, 309–319.

Bottone, F.G., Baek, S.J., Nixon, J.B., Elling, T.E. (2002). Diallyl disulphide (DADS) Induces the antitumorigenic NSDAID-activated gene (NAG-1) by a p53-dependent mechanism in human colorectal HCT116 cells. *The Journal of nutrition*., 132 (4), 773-778.

Cabrera, S., El Haskouri, J., Guillem, C., Latorre, J., Beltrán, A., Beltrán, D., … Amorós, P. (2000). Generalised syntheses of ordered mesoporous oxides: the atrane route. *Solid State Sci*., 2(4), 405–420.

Cavallito, C. J., & Bailey, J. H. (1944). Allicin, the Antibacterial Principle of Allium sativum. I. Isolation, Physical Properties and Antibacterial Action. *J Am Chem Soc*, 66(11), 1944–1952.

Hadaruga, D. I., Hadaruga, N. G., Rivis, A., Gruia, A., & Pinzaru, I. A. (2007). Thermal and oxidative stability of the Allium Sativum L. bioactive compounds/alfa- and beta-Cyclodextrin nanoparticles. *Rev. Chim.*, 58(11), 1009–1015.

Janatova, A., Bernardos, A., Smid, J., Frankova, A., Lhotka, M., Kourimsk, L., … Kloucek, P. (2015). Long-term antifungal activity of volatile essential oil components released from mesoporous silica materials. *Industrial Crops and Products*, 67, 216–220.

Kresge, C. T., Leonowicz, M. E., Roth, W. J., Vartuli, J. C., & Beck, J. S. (1992). Ordered mesoporous molecular sieves synthesized by a liquid-cristal template mechanism. *Nature,* 359, 710–712.

Kris-Etherton, P. M., Hecker, K. D., Bonanome, A., Coval, S. M., Binkoski, A. E., Hilpert, K. F., … Etherton, T. D. (2002). Bioactive compounds in foods: their role in the prevention of cardiovascular disease and cancer. *The American Journal of Medicine*, 113 Suppl(1), 71S–88S.

Liu, C. T., Hse, H., Lii, C. K., Chen, P. S., & Sheen, L. Y. (2005). Effects of garlic oil and diallyl trisulfide on glycemic control in diabetic rats. *European Journal of Pharmacology*, 516(2), 165–173.

Llopis-Lorente, A., Lozano-Tprres, B., Bernardos, A., Martínez-Máñez, R., & Sancenón, F. (2017). Mesoporous silica materials for controlled delivery based on enzymes. *Journal of Materials Chemistry B*, 5(17), 3069–3083.

Park, S. Y., Barton, M., & Pendleton, P. (2012). Controlled release of allyl isothiocyanate for bacteria growth management. *Food Control*, 23(2), 478–484.

Pérez-Esteve, É., Fuentes, A., Coll, C., Acosta, C., Bernardos, A., Amorós, P., … Barat, J. M. (2015). Modulation of folic acid bioaccessibility by encapsulation in pH-responsive gated mesoporous silica particles. *Microporous and Mesoporous Materials*, 202, 124–132.

Pérez-Esteve, É., Ruiz-Rico, M., de la Torre, C., Villaescusa, L. A., Sancenón, F., Marcos, M. D., … Barat, J. M. (2016). Encapsulation of folic acid in different silica porous supports: a comparative study. *Food Chemistry,* 196, 66–75.

Ruiz-Rico, M., Fuentes, C., Pérez-Esteve, É., Jiménez-Belenguer, A. I., Quiles, A., Marcos, M. D., … Barat, J. M. (2015). Bactericidal activity of caprylic acid entrapped in mesoporous silica nanoparticles. *Food Control*, 56, 77–85.

Slowing, I. I., Trewyn, B. G., Giri, S., & Lin, V. S.-Y. (2007). Mesoporous silica nanoparticles for drug delivery and biosensing applications. *Adv. Funct. Mater.*, 17(8), 1225–1236.

Wang, S. (2009). Ordered mesoporous materials for drug delivery. *Microporous and Mesoporous* Materials, 117, 1–9.

Yamada, Y., & Azuma, K. (1977). Evaluation of the in vitro antifungal activity of allicin. *Antimicrobial Agents and Chemotherapy*, 11(4), 743–749.

Yang, J.S., Chen, G.W., Hsia, T.C., Ho, H.C., Lin, M.W., Lin, S.S., Yeh, R.D., Ip, S.W., Lu, H.F., Chung, J.G. (2009). Diallyl disulfide induces apoptosis in human colon cancer cell line (COLO 205) through the induction of reactive oxygen species, endoplasmic reticulum stress, caspases casade and mitochondrial-dependent pathways. *Food and Chemical Toxicology*, 47(1),171–179

4.4 Polymer composites containing gated mesoporous materials for on-command controlled release

Polymer composites containing gated mesoporous materials for on-command controlled release

*Carolina Acosta,[*a,b] Edgar Pérez-Esteve,[a,b] Carlos A. Fuenmayor,[d] Simona Benedetti,[d] Maria Stella Cosio,[d] Juan Soto,[b] Félix Sancenón,[b,c] Saverio Mannino,[d] José Barat,[a] María D. Marcos,[b,c] Rámon Martínez-Máñez.[b,]*

[a] *Grupo de Investigación e Innovación Alimentaria (CUINA), Universitat Politècnica de València, Camino de Vera s/n, E-46022 Valencia, Spain.*

[b] *Instituto de Reconocimiento Molecular y Desarrollo Tecnológico (IDM), Unidad Mixta Universitat Politècnica de València – Universitat de València, Camino de Vera s/n, E-46022 Valencia, Spain.*

[c] CIBER de Bioingeniería, Biomateriales y Nanomedicina (CIBER-BBN), Spain

Department of Food, Environmental and Nutritional Sciences – DeDENS. University of Milan

Published in ACS Applied Materials & Interfaces. 2014 May 14;6(9):6453-60.

Polyamidic nanofibrous membranes containing gated silica mesoporous particles, acting as carriers, are described as novel hybrid composite materials for encapsulation and on-command delivery of garlic extracts. The carrier system consists of MCM-41 solids functionalized in the outer surface, with linear polyamines (Solid **P1**) and with hydrolyzed starch (Solid **P2**), both acting as molecular gates. Those particles were adsorbed on electospun nylon-6 nanofibrous membranes yielding to composite materials **M1** and **M2**. FE-SEM analysis confirmed the presence of particles incorporated on the nylon nanofibers. The release of the entrapped molecules (garlic extract) from the **P1**, **P2**, **M1** and **M2** materials was evaluated using cyclic voltammetry measurements. Electrochemical studies showed that at acidic pH **P1** and **M1** were unable to release their entrapped cargo (closed gate), whereas at neutral pH both materials release their loading (open gate). Dealing with **P2** and **M2** materials, in the absence of pancreatin a negligible release is observed (closed gate), whereas in the presence of enzyme the load is freely to diffuse to the solution. These newly developed composite nanomaterials, provide a homogeneous easy-to-handle system with controlled delivery and bioactive-protective features, having potential applications on pharmacology, medical and engineering fields.

Introduction

In the last years, anchoring organic or biological molecules on certain inorganic supports has resulted in the design of hybrid materials which show advanced cooperative functional behaviors (Descalzo et al., 2006). One appealing concept in this area is related with the design of gated supports for advanced delivery applications (Aznar et al., 2009; Coti et al., 2009). These new materials contain switchable molecular-based entities which control the on-command release of previously entrapped guests. These gated materials are based on the combination of two components: (i) a suitable inorganic support acting as a container (for loading the cargo) and (ii) a switchable "gate-like" ensemble able to be "opened" upon the application or the presence of a predefined stimulus (Coll et al., 2013). Selection of both components is important and determines the controlled release performances of the final support.

As inorganic scaffolds, mesoporous silica of different pore sizes and morphologies have been widely used (Carino et al., 2007; Heikkila et al., 2007; Tang et al., 2012). Mesoporous supports can be prepared in different forms (from nanometric to micrometric) with tailor-made pores in the 2-10 nm range. Moreover, they have a very high specific surface area (up to 1200 m2g-1), have homogeneous porosity, high inertness, a large loading capacity and are easy to functionalize (Kresge et al., 1992). These properties make silica mesoporous

structures ideal candidates as scaffolds for delivery applications. In relation to the gated ensemble, currently several molecular, supramolecular and nanoparticulated systems have been used. Those systems are able to deliver the entrapped cargo using several external stimuli such as light (Agostini et al., 2012; Mal et al., 2003), pH (Angelos et al., 2009; Casasús et al., 2008), changes in redox potential (Fujiwara et al., 2006; Giri et al., 2005), temperatura (Aznar et al., 2011; Fu et al., 2003) and the presence of certain ions, molecules or biomolecules (Oroval et al., 2013; Park et al., 2009; Schlossbauer et al., 2009).

In particular, the design of gated mesoporous materials has been proved to be a promising starting point for applying the versatility of molecular and supramolecular concepts to the design of gating solids, and a way of studying the factors that can influence the design of molecular gating functions with advanced delivery functionalities. These concepts contrast with the design of traditional delivery systems which are often based on simple diffusion controlled processes (Muñoz et al., 2003).

On the other hand, nanofibers are especially appealing for the development of novel composites with potential applications on areas such as vascularization, cell migration and attachment processes (Arecchi et al., 2010; Loh et al., 2010; Venugopal and Ramakrishna, 2005). There are a number of different processing techniques used for the synthesis of nanofibers including drawing, self-assembly

or phase separation, however electrospining is probably the most widely studied (Kriegel et al., 2008). Electrospun nanofibers have surface properties that can be specially tailored to adjust and control porosity, composition and morphology, with a highly controllable three-dimensional structure and high surface area-to-volume ratios, for providing support on the inclusion of antimicrobial agents, drugs, flavors, colors, antioxidants, enzymes and other functional compounds (Jia et al., 2002; Price et al., 2003; Rajesh and Dhirendra, 2006). Nanofibers have also been used in delivery applications, however there are few examples where release only occurs triggered by specific and selected stimuli and as stated above, sustained delivery is still the most common principle. Very recently, nanofibers that incorporate different types of silica mesoporous materials have been prepared and characterized (Kim et al., 2011; Madhugiri et al., 2003; Zhuang et al., 2010). However, in these papers only the synthesis and the physical properties of the prepared fabrics are studied.

Taking into account the above mentioned facts we believe that a new range of potential applications can be envisioned by the combination of nanofibers to support gated silica mesoporous particles in order to obtain composites with the potential ability to deliver a certain cargo upon the application of target stimuli while cargo is protected until its specific delivery. In order to achieve this goal and as a proof of concept we have selected for this particular work two mesoporous

systems able to protect and deliver the cargo upon changes in the pH or in the presence of a target enzyme (vide infra) (Bernardos et al., 2010, 2008). Those mesoporous scaffolds are then supported on nylon-6 nanofibers to provide a homogenous material for delivery.

As cargo we selected a garlic extract whose bioactive components have been reported to have antimicrobial, antiatherosclerotic and antioxidative properties (Block, 2010; Feldberg et al., 1988). Garlic extract contain among other substances allicin and diallyl disulfide, organosulfurs responsible of the functional properties of garlic. However, some of these functional compounds from garlic extract are unstable and have sensorial trouble for certain applications. In this context, the design of supports able to protect the cargo and induce delivery on-command is of importance.

Experimental Procedure

All chemicals were purchased at the highest grade available and used directly without any further purification. Diallyldisulfide (tech., 80%) and NaClO4 (ACS Reagent, 98%) were purchased from Sigma Aldrich, NaBr was purchased from May and Baker Ltd, UK. All solutions were prepared with acetonitrile (HPLC Gradient grade, Fisher Scientific) and deionized water of resistivity not less than 18.2 MΩ·cm^{-1} at 25 °C (Millipore UHQ, Vivendi, UK). The chemicals nylon-6, formic acid (98 %), tetraethylorthosilicate (TEOS), n-cetyltrimethylammonium bromide

(CTAB), sodium hydroxide, triethanolamine (TEAH3), 3-aminopropyltriethoxysilane, 3-[2-(2-aminoethylamino) ethylamino]-propyl-trimethoxysilane and pancreatin from porcine pancreas were provided by Aldrich. The hydrolyzed starch Glucidex@ 47 (5% glucose, 50% maltose, 45% oligosaccharides and polysaccharides) was provided by Roquette.

Synthesis of mesoporous silica microparticles

The mesoporous MCM-41 type support, was first synthesized by "atrane route" (Cabrera et al. 2000) in which 4.68 g of CTAB was added at 118 °C to a solution of TEAH3 (25.79 g) containing 0.045 mol of a silatrane derivative (TEOS, 11 mL). Next 80 mL of water was slowly added with vigorous stirring at 70 °C. After a few minutes, a white suspension was formed. This mixture was aged at room temperature overnight. The resulting powder was collected by filtration and washed. Solid was dried at 70 °C and finally, in order to remove the template phase was calcined at 550 °C for 5 h using an oxidant atmosphere.

Synthesis of starch derivative (Glu-N1)

A solution of 3-aminopropyltriethoxysilane (**N1**, 5.85 mL, 25 mmol) was added to a suspension of hydrolyzed starch (Glucidex@ 47) in ethanol. The reaction mixture was stirred for 24 h at room temperature and heated at 60 °C for 30 min. The solvent was evaporated under reduced pressure.

Garlic bioactive compounds extraction

Garlic was obtained in local market. The garlic cloves were peeled and chopped. A certain amount of acetonitrile was used to crush the garlic and get a sample with a garlic acetonitrile relation of 1:10 w/v where principal organosulfures were extracted. Solution was shaken by vortex for 3-5 min and then filtered and kept at 4 °C.

Garlic bioactive compounds loading (P0)

100 mg of mesoporous particle MCM-41 were suspended in 40 mL of garlic acetonitrile extract inside a round-bottom flask. The mixture was stirred for 24 h at room temperature. This mixture was filtered and dried at room temperature for 12 h.

Synthesis of P1

An excess of 3-[2-(2-aminoethylamino)-ethylamino]-propyl-trimethoxysilane (**N3**, 0.43 mL) was added to 0.1 g **P0** in 40 ml acetonitrile. The final mixture was stirred for 5.5 h at room temperature in an inert atmosphere of nitrogen. Solid was filtered and washed with acid solution at pH 2.0 (acidified with sulfuric acid) and dried for 12 h at 35 °C.

Synthesis of P2

Glu-N1 was added to **P0** in a 1:1 w/w relation. The final mixture was stirred for 5.5 h at room temperature under argon. The solid was filtered and washed with deionised water, and dried at for 12 h at 35 °C.

Particles immobilization – Composites M1 and M2

Polymer solution was made with 8 g of nylon-6 pellets dissolved in 26.6 mL of a formic acid (88 %) aqueous solution. The dispersion obtained was stirred for about 24 h to make a clear sol–gel. Then 80 mg of solid (**P1** for membrane **M1** and **P2** for membrane **M2**) were added and stirred for 5 h at 300 rpm. 5 mL syringe (Hamilton) was filled with the entire composite polymer solution and placed in a KDP100 syringe pump (KD-Scientific) at a flow rate of 0.20 mL min^{-1}. The needle of the syringe was linked to the Spellman SL150 high voltage power supply by an alligator clip, while a copper lamina, positioned at 11 cm in front of the needle, was used as collector and grounded. The electrical potential was set at 25 kV. Production time of a single membrane was stopped at 10 min.

Release studies

Aqueous suspensions of the four materials were stirred for 5 h at 200 rpm. Each hour an aliquot from solution was taken, passed through nylon 0.45 um filters and then evaluated by cyclic voltammetry. Delivery sample was constituted by 12 mg of solid **P1** or **P2** and 30 cm^2 for **M1** or **M2** and suspended in 30 mL of the corresponding release solution. Delivery studies of solid **P1** and membrane **M1** were carried out in aqueous solution containing sulfate anion (10^{-2} M) and at pH 7.0 and pH 2.0. Solid **P2** and membrane **M2** were suspended in aqueous solutions at pH 7.0 in the absence and in the presence of pancreatin.

Cyclic voltammetry

A CHI 1010 Electrochemical Analyzer (CH Instruments, Austin Texas) with a three electrode setup consisting of a glassy carbon working electrode, platinum auxiliary electrode and an Ag/AgCl reference electrode was employed. Cyclic voltammogram experiments were acquired with a scan rate of 50 mVs^{-1} and were obtained by running a series of FIA. Experiments in which the potential was stepped incrementally from -0.1 to +1.5 V (vs. Ag/AgCl) and the current was measured.

Experiments were performed in aqueous reference solution with acetonitrile (50:50), sodium bromide 15 mM in 0.1 M of sodium perchlorate (Martindale et al., 2011). The measure solution has a 1:1 v/v ratio between reference solution (blank) and sample.

Characterization of materials

PXRD measurements were performed on a Seifert 3000TT diffractometer using CuKα radiation. Field Emission Scanning Electron Microscope images were acquired by FE-SEM ULTRA 55-44-22, evaluated by secondary (SE2) and backscattered electrons (AsB) detectors. Samples were coated with platinum and examined at 5kV. An X-ray EDS detector was used for qualitative elements analysis. Dynamic Light Scattering (DLS) studies were conducted at 25 °C using a Malvern Zetasizer Nano ZS. Back-scattered light was detected at 173 °, and the mean particle diameter was calculated from the quadratic fitting of the

correlation function over 3 runs of 10 s duration. All measurements were performed in triplicate on previously sonnicated highly dilute aqueous dispersions. Thermogravimetric analyses were carried out on a TGA/SDTA 851e Mettler Toledo balance, using an oxidant atmosphere (air, 80 $mL \cdot min^{-1}$) with a heating program consisting of a heating ramp of 10 °C per minute from 393 to 1273 K and an isothermal heating step at this temperature for 30 min. TEM images were obtained with a 100 kV Philips CM10 microscope. N2 adsorption-desorption isotherms were recorded with a Micromeritics ASAP2010 automated sorption analyzer. The samples were degassed at 120 °C in vacuum overnight. The specific surface areas were calculated from the adsorption data in the low pressure range using the BET model (Brunauer & Teller, 1938).

Results and Discussion

The gated materials

In this approach, MCM-41 was used as inorganic scaffold in the form of microparticles. The prepared MCM-41 support contains mesopores in the 2-3 nm range which allow the encapsulation of certain guests. In relation to the capping component two previously reported gates were selected; one based in the use of linear polyamines (for the preparation of **P1** material) and other based in the use of hydrolyzed starch (for the preparation of **P2** material). Scheme 4.4-1 shows the proposed paradigm for the preparation of the gated materials.

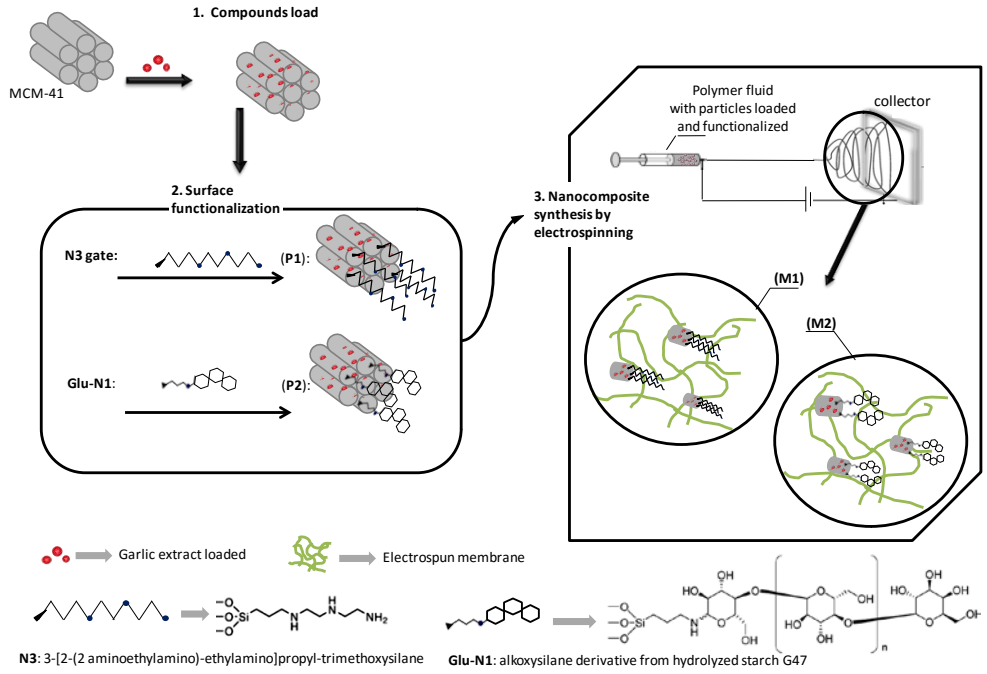

Scheme 4.4-1. Synthesis of mesoporous particles P1 (capped with N3) and P2 (capped with Glu-N1). Preparation of the composites M1 and M2 is also shown.

For the synthesis of the pH-responsive gated material (**P1**) the derivative 3-[2-(2 aminoethylamino)-ethylamino]propyl-trimethoxysilane (**N3**) was selected as simple, yet suitable, open-chain molecular pH-responsive system that was anchored through covalent bonds on the pore outlets of the MCM-41 support. For the preparation of the enzyme-responsive material (**P2**) the commercially available hydrolyzed starch Glucidex® 47 was selected. The hydrolyzed starch was properly derivatized, through reaction with 3-aminopropyltriethoxysilane (**N1**), in

order to yield the alkoxysilane derivative (**Glu-N1**) which was then anchored on the external surface of the MCM-41 support.

In the **P1** solid changes in the pH control the state of the gate (open or closed). In particular, open-closed cycle relies on protonation/deprotonation processes of the grafted polyamines. At acidic pH, the nitrogen atoms of the polyamines are fully protonated and strong electrostatic repulsions between the grafted polyamines occur. These strong repulsions pushed away the protonated polyamines blocking the pores of the inorganic support and, as a consequence, inhibit cargo release. Also certain anion-controlled outcome is observed because negatively charged anions interact with the positively charged ammonium moieties leading to a more pronounced pore blocking. At neutral pH the polyamines are only partly deprotonated and the electrostatic repulsions are highly diminished. This allow pore opening due to the more flexible conformational of polyamines (when compared with polyammonium) with the subsequent cargo release.

In solid **P2**, the opening mechanism deals with an enzymatic hydrolysis of the grafted starch, which acts as molecular gate. The anchoring of the saccharides inhibits cargo delivery due to the formation, around the pore outlets, of a dense monolayer of starch molecules. In the presence of pancreatin (a pool of enzymes that contain amylase), the 1→4 glycosidic bond between β-D-glucoses present in

the starch is hydrolyzed with the subsequent uncapping of the pores and cargo delivery. Scheme 4.4-2 shows the release mechanism.

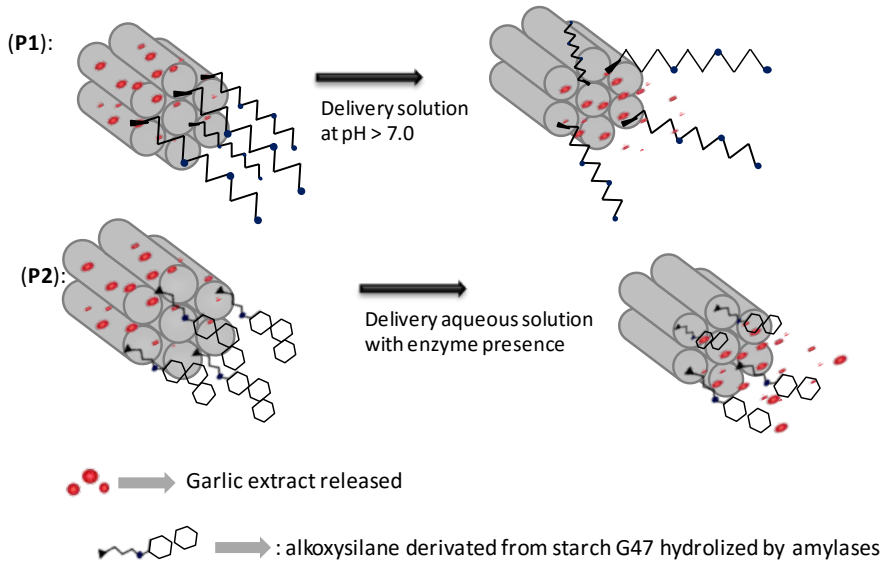

Scheme 4.4-2. Mechanism of pH and enzyme induce release of the entrapped cargo from P1 and P2.

The composite materials

The final goal of this work was to incorporate the materials **P1** and **P2** on nanofibers as a suitable approach for the development of composite fabrics able to deliver the cargo upon the presence of specific stimuli. Polymer solutions were made based on one of the most standardized protocols. Nylon-6 pellets were dissolved in an aqueous solution containing formic acid. The dispersion obtained was stirred for ca. 24 h to make a clear sol–gel. Then 80 mg of solids **P1** or **P2** were added and the mixture was stirred. The final composites **M1** (containing

solid **P1**) and **M2** (containing solid **P2**) were obtained by exposition of the prepared mixtures on an electrical field using the well-known electrospinning technique and collected as non-woven membranes on a plate that acts as the counter electrode.

Materials characterization

The characterization of the materials **P1** and **P2** was performed using well-known techniques. Powder X-ray diffraction (PXRD) patterns of the prepared silica mesoporous MCM-41 solids are shown in Figure 4.4-1. The PXRD of siliceous as synthesized MCM-41 shows four low-angle reflections typical of a hexagonal array that can be indexed as (100), (110), (200) and (210). A significant shift of the (100) reflection in the PXRD of the MCM-41 calcined sample is clearly observed (curve b in Figure 4.4-1) corresponding to an approximate cell contraction of ca. 5 Å. This displacement and the broadening of the (110) and (200) peaks are most likely related to condensation of silanols during the calcination step, when CTAB is removed. In the case of **P1** and **P2**, the PXRD pattern (Figure 4.4-1C and 1D) only shows the characteristic (100) reflection. The presence of this peak indicates that the mesoporous structure was preserved through the filling process with the garlic extract and the anchoring of molecular gates.

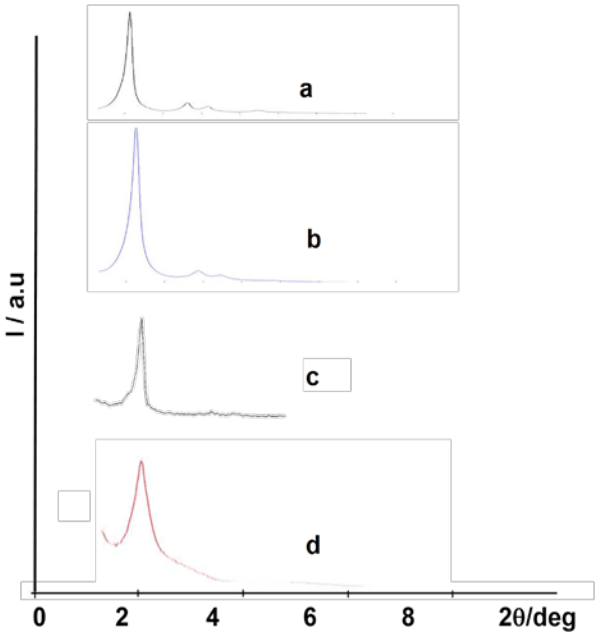

Figure 4.4-1. Powder X-ray patterns of a) as-synthesized MCM-41, b) calcined MCM-41, c) solid P2, and d) solid P1.

Figure 4.4-2 shows TEM images of MCM-41 solid support showing the typical porosity associated with this type of inorganic support. The images also show that the mesoporous solid was obtained as micrometric particles. In fact, Dynamic Light Scattering (DLS) studies carried out with the starting MCM-41 confirmed the presence of micrometric particles with a mean average diameter of ca. 1 μm (see Figure 4.4-2).

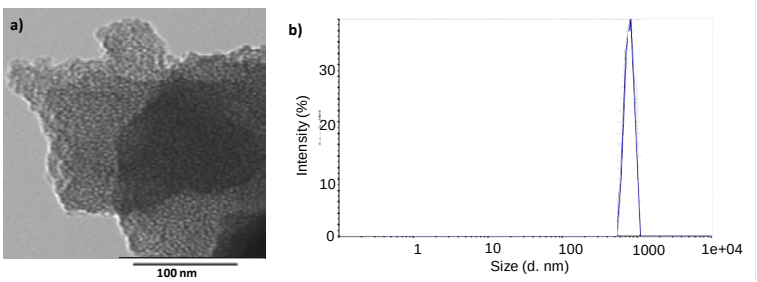

Figure 4.4-2 A. TEM image of MCM-41 particles and B. statistical representation of particle size of MCM-41obtained by DLS (Dynamic Light Scattering) studies.

N_2 Adsorption–desorption isotherms of the MCM-41 calcined phase show typical curves consisting of one single adsorption step at the intermediate P/P_0 value (0.1-0.4) which can be related to the nitrogen condensation inside the mesopores by capillarity, as corresponds to a type IV isotherm (see Figure 4.4-3). The absence of a hysteresis loop in this interval and the narrow pore distribution suggests the existence of uniform cylindrical mesopores (2.71 nm, 0.88 $cm^3\ g^{-1}$). The application of the BET model to calcined material gave a value for the total specific surface of 979.6 $m^2\ g^{-1}$. In contrast, the N_2 adsorption–desorption isotherms of the loaded solid **P0** and the final functionalized solids (**P1** and **P2**), show in each case a flat curve with specific surfaces of 220, 100 and 193 $m^2\ g^{-1}$ and pore volumes of 0.25 0.17 and 0.19 $cm^3\ g^{-1}$ for **P0**, **P1** and **P2**, respectively. This not only shows an appreciable absence of mesopority but also indicates a significant pore blocking due molecular gates anchorage being as decrease of

specific surface and volume pore from solid loaded **P0** to final functionalized solids **P1** and **P2**.

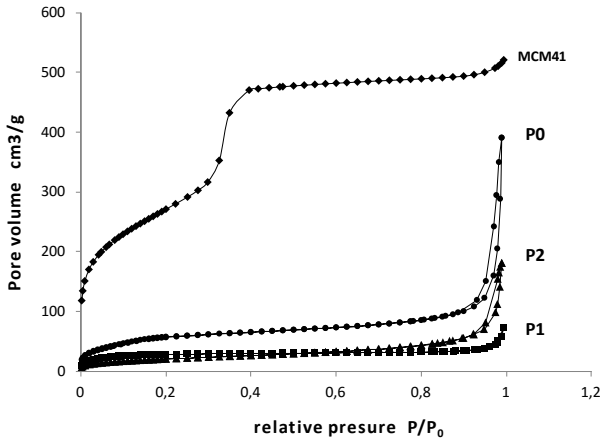

Figure 4.4-3. Nitrogen adsorption-desorption isotherms: (◆) MCM-41 calcined material, (●) P0 solid, (■), P1 solid, and (▲) P2 solid.

The organic contents in the loaded solid were determined through thermogravimetric studies. TGA curves showed a weight loss between 100-600 °C due to the organic matter combustion corresponding to the entrapped cargo in **P0** and, in the case of **P1** and **P2**, corresponding to the entrapped cargo and the molecular gate. In particular, the amount of organic matter in the MCM-41 scaffolding loaded with the garlic extract was of ca. 0.18 g garlic extract/g SiO_2, whereas the final gated materials **P1** and **P2** have a content of organic matter of 0.38 and 0.25 g/g SiO_2, respectively. (See Appendix 4.4-Figure S1, for TGA curves).

The morphology of composites **M1** and **M2** was studied by means of FE-SEM. Micrographs of the nanofibrous structures are shown in Figure 4.4-4. Nylon-6 ultra-thin fibers, with an average thickness of 160 nm (Figure 4.4-4A), exhibited a non-woven arrangement. Several chain entanglements can be observed, which results in a highly porous structure. The absence of beads and fiber bundles indicated that the electrospinning conditions were adequate for a proper and stable solvent evaporation. FE-SEM images of **M1** and **M2** (Figure 4.4-4B) show the presence of entrapped **P1** and **P2** particles, distributed randomly across the nanofibrous matrix. The gated silica particles appear to be partially wrapped in the fibers external surface, suggesting the occurrence of relatively strong adhesive forces. The presence of hydrogen bonding interactions between the polyamide chains of the fibers and the capping molecules covering **P1** and **P2** (polyamines and polysaccharides, respectively) cannot be excluded. The formation of covalent bonds between the fibers and the capping molecules is unlikely considering the preparation conditions for the final **M1** and **M2** composites. It should be noticed that, regardless the nature of the interactions occurring between particles and fibers, the adhesion forces seem to be strong enough for maintaining the composite structure together after the release procedure (Figure 4.4-4C). This was confirmed by FE-SEM-EDX studies that showed the presence of silicon in the composite membranes after release completion, and even after long-term (24h)

soaking, in the different release environments tested. (See Appendix 4.4-Figure S2 for EDX spectra)

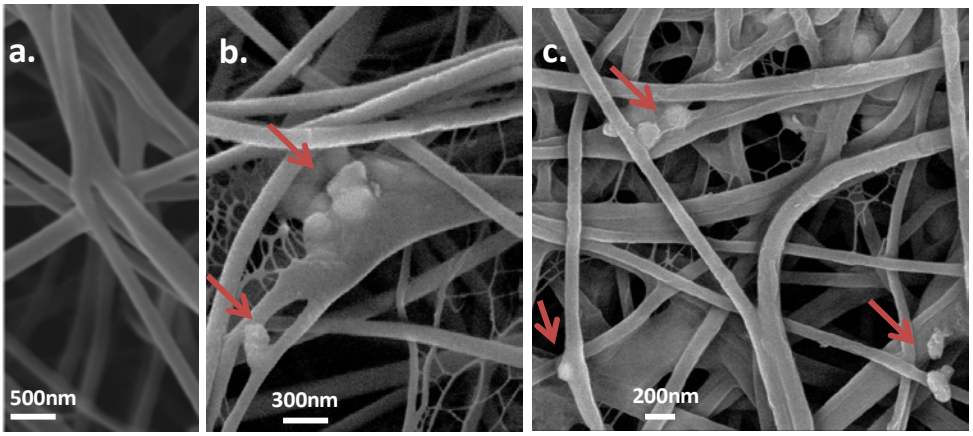

Figure 4-4-4. Representative FE-SEM images of a) nylon6 nanofiber, b) composite with entangled microparticles before the released procedure, and c) the same composite after the release procedure.

Controlled release behavior

Controlled release studies were performed on **P1**, **P2** and **M1** and **M2**. Cargo delivery was monitored by cyclic voltammetry studies using a reported procedure based in the detection of disulfides (diallyl disulfide – DA, is one of the major components of the garlic extract) in the presence of bromide. The detection is based on the electrogeneration of bromine on a carbon electrode, which reacts with disulfides to catalytically regenerate bromide. This redox reaction induced the appearance of a peak in the voltammogram in the 1.0-1.2 V range, whose intensity is proportional to the amount of disulfides present in the garlic extract. (See Appendix 4.4-Figure S3, for Voltammetric evaluations).

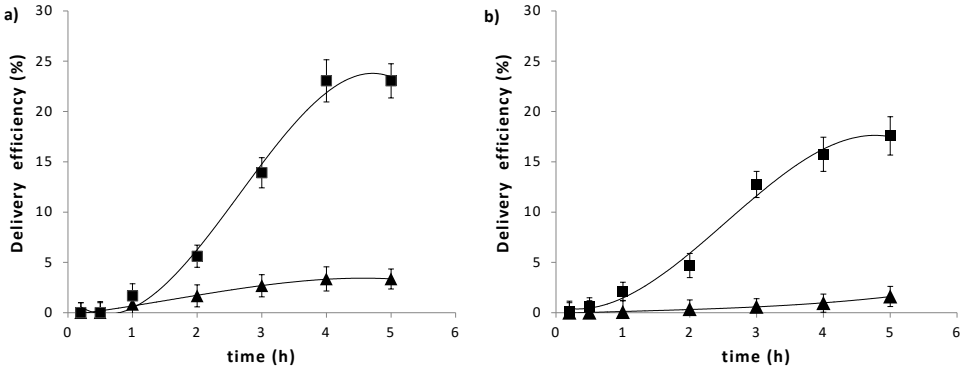

Figure 4.4-5. Efficiency delivery curves of diallyl disulfide (DA) in garlic extract from pH-sensitive materials a) P1 particles and b) M1 composites. Release at pH 7.0 (■) and pH2.0 (▲).

In a first step controlled release features of the pH-sensitive materials **P1** and **M1** were evaluated. In a typical experiment 12.5 mg of **P1** or 80 mg of **M1** were suspended in 25 mL of water at pH 2.0 and pH 7.0 (in the presence of sulfates). Then at certain time intervals, fractions of both suspensions were taken and the solid (**P1** or **M1**) was removed. Cargo delivery into the solution was then measured via the electrochemical procedure described above. Diallyl disulfide delivery process was followed by voltammetric responses of the clear solutions. In Figure 5 the delivery profiles at pH 2.0 and 7.0 for **P1** and **M1** are displayed. The results have been represented as the delivery efficiency, the percentage of the voltammetry signal of each aliquot relative to the signal that would be obtained for the complete delivery of the cargo for each material.

From Figure 4.4-5 it can be seen that aqueous suspensions of solid **P1** at pH 2.0 show a poor release of the garlic extract even after some hours in solution (see Figure 5a). This very low release is clearly related with the presence of the polyamine-based gated ensemble. However, when the experiments are carried out in water suspensions at pH 7.0 a release of the cargo is observed as indicated by the time-dependent enhancement of the intensity of the oxidation peak in the 1.0-1.2 V range. In the case of composite **M1**, similar delivery profiles have been obtained this fact clearly indicating that the release process has not been modified when the microcarriers have been dispersed into the membrane. As it can be seen in the FE-SEM images (Figure 4.4-4) the particles are not embedded within the fibers but only located on the fiber outer surfaces, so the gated mesopores of the microcarriers are accessible and the opening/closing mechanism is fully operational. However, some differences between **P1** and **M1** delivery profiles may be observed. Release from **M1** composite reaches a lower efficiency and the process looks slower, than for **P1** solid. The curve for **M1** does not clearly reach the saturation as it does for **P1** delivery. This fact could be related with some kinetic difficulties for the cargo to be delivered from the **M1** composite due to the intricate morphology of the membrane.

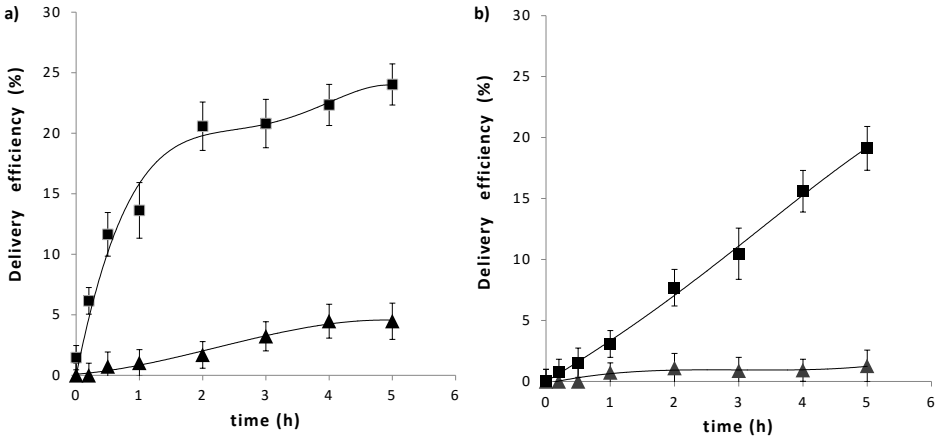

Figure 4.4-6. Delivery of garlic extract from enzyme-response materials a) P2 particles and b) M2 composite. Release in the presence of pancreatine (■) and release in the enzyme absence (▲).

Similar delivery experiments were carried out with materials **P2** and **M2**. In particular, 12.5 mg of **P2** or 80 mg of **M2** were suspended in 25 mL of water in the presence and in the absence of pancreatin at neutral pH. Then, at a certain time, aliquots of both suspensions were taken and the solid materials (**P2** or **M2**) removed. As in the above case cargo release was measured via the electrochemical procedure described previously.

The delivery profiles for **P2** and **M2** in the presence and absence of pancreatin are displayed in Figure 4.4-6. Suspensions of **P2** at neutral pH in the absence of enzyme shows no delivery of the garlic extract which is attributed to the presence of the starch derivative anchored on the external surface of the mesoporous material. In contrast, when the experiments are carried out in the

presence of pancreatin a clear release of the cargo is observed and attributed to the enzyme-induced hydrolysis of glycosidic bonds of the grafted polysaccharides. In the case of **M2**, the same basic behavior can be observed, the lack of delivery in the absence of the enzyme and the delivery when the enzyme is present, so the release mechanism may not be affected by the fact of having the micro-carriers embedded into the membrane. However, in this case we can observe a higher difference in the delivery speed for **M2** when comparing with **P2** than for the **P1/M1** system. This, in fact supports the explanation given above for the **M1** behavior. As in the case of **M2** composite the mechanism for opening the gate is more complex than for **M1** because it needs the enzyme to get the micro-carrier surface in order to get the gate open, the intricate morphology of the composite produce a higher effect giving rise to a more pronounced slowdown of the whole process.

This slightly different behavior of the composites **M1** and **M2** respect to the parent **P1** and **P2** materials could be seen as an appropriate method to get a better control of the delivery process, enhancing the closed conditions and allowing a more maintained released of the cargo.

Conclusions

Two new composite materials (**M1** and **M2**) based on the incorporation of two gated silica mesoporous hybrid solids (**P1** and **P2**) on a electrospun

polyamidic nanofiber have been prepared and their controlled release behaviour studied. Those composites presented a fibrous structure with entangled microparticles. At pH 2.0 aqueous suspensions of **M1** showed negligible release of the entrapped extract whereas when the pH is increased to 7.0 a clear cargo delivery from **M1** is observed. In the case of **M2**, the mesoporous gated microparticles are equipped with a polysaccharide able to inhibit cargo release. Addition of pancreatin to aqueous suspensions of **M2** induced cargo delivery due to the progressive enzyme-induced hydrolysis of the grafted polysaccharide. We believe that the development of composite materials based on silica mesoporous microparticles equipped with gate-like systems is an interesting way to prepare smart fabrics showing "zero" release that can be opened at will using appropriate stimuli. These systems are homogenous and offer an efficient way for the cargo protection, opening a wide range of research opportunities for this delivery concept to be applied in several industries.

Acknowledgements

The authors wish to express their gratitude to the Generalitat Valenciana (Grisolia scholarship 2011/012, project PROMETEO/2009/016), Spanish Government (MINECO Projects AGL2012-39597-C02-01, AGL2012-39597-C02-02 and MAT2012-38429-C04-01) and the CIBER-BBN for their support. IILA thanks DISTAM and Università degli di Milano for a specialization scholarship. We would

also like to thank the Institut de Cieǹ cia dels Materials (ICMUV) and to the Microscopy Service of the Universitat Politecnica de Valencia for technical support. We thank Roquette for the Glucidex samples.

References

Agostini, A., Sancenón, F., Martínez-Máñez, R., Marcos, M.D., Soto, J., Amorós, P., 2012. A photoactivated molecular gate. Chem Eur J 18, 12218–12221.

Angelos, S., Khashab, N.M., Yang, Y.-W., Trabolsi, A., Khatib, H.A., Stoddart, J.F., Zink, J.I., 2009. pH clock-operated mechanized nanoparticles. J Am Chem Soc 131, 12912–12914.

Arecchi, A., Scampicchio, M., Drusch, S., Mannino, S., 2010. Nanofibrous membrane based tyrosinase-biosensor for the detection of phenolic compounds. Anal Chim Acta 659, 133–136. doi:S0003-2670(09)01550-5 [pii]10.1016/j.aca.2009.11.039

Aznar, E., Martínez-Máñez, R., Sancenón, F., 2009. Controlled release using mesoporous materials containing gate-like scaffoldings. Expert Opin Drug Deliv 6, 643–655. doi:10.1517/17425240902895980

Aznar, E., Mondragón, L., Ros-Lis, J. V., Sancenón, F., Marcos, M.D., Martínez-Máñez, R., Soto, J., Pérez-Payá, E., Amorós, P., Mondragõn, L., Ros-Lis, J. V., Sancenõn, F., Marcos, M.D., Martínez-Máñez, R., Soto, J., Pérez-Payá, E., Amorõs, P., 2011. Finely tuned temperature-controlled cargo release using paraffin-capped mesoporous silica nanoparticles. Angew Chem Int Ed Engl. 50, 11172–11175. doi:10.1002/anie.201102756

Bernardos, A., Aznar, E., Coll, C., Martínez-Manez, R., Barat, J.M., Marcos, M.D., Sancenón, F., Benito, A., Soto, J., 2008. Controlled release of vitamin B2 using mesoporous materials functionalized with amine-bearing gate-like scaffoldings. J Control Release 131, 181–189. doi:S0168-3659(08)00420-3 [pii]10.1016/j.jconrel.2008.07.037

Bernardos, A., Mondragon, L., Aznar, E., Marcos, M.D., Martínez-Manez, R., Sancenón, F., Soto, J., Barat, J.M., Perez-Paya, E., Guillem, C., Amoros, P., 2010. Enzyme-responsive intracellular controlled release using nanometric silica mesoporous supports capped with "saccharides." ACS Nano 4, 6353–6368. doi:10.1021/nn101499d

Block, E., 2010. Garlic and other alliums. RSC Publishing, Cambridge.

Brunauer P.H. Teller, E., S.E., 1938. Adsorption of gases in multimolecular layers. J. Am. Chem. Soc. 60, 309–319.

Cabrera, S., El Haskouri, J., Guillem, C., Latorre, J., Beltrán, A., Beltrán, D., Marcos, M.D., Amorós, P., 2000. Generalised syntheses of ordered mesoporous oxides: the atrane route. Solid State Sci. 2, 405–420.

Carino, I.S., Pasqua, L., Testa, F., Aiello, R., Puoci, F., Iemma, F., Picci, N., 2007. Silica-based mesoporous materials as drug delivery system for methotrexate release. Drug Deliv 14, 491–495. doi:785910210 [pii]10.1080/10717540701606244

Casasús, R., Climent, E., Marcos, M.D., Martínez-Máñez, R., Sancenón, F., Soto, J., Amorós, P., Cano, J., 2008. Dual aperture control on pH- and anion-driven supramolecular nanoscopic gate-like ensambles. J Am Chem Soc 130, 1903–1917.

Coll, C., Bernardos, A., Martínez-Manez, R., Sancenón, F., 2013. Gated silica mesoporous supports for controlled release and signaling applications. Acc Chem Res 46, 339–349. doi:10.1021/ar3001469

Coti, K.K., Belowich, M.E., Liong, M., Ambrogio, M.W., Lau, Y.A., Khatib, H.A., Zink, J.I., Khashab, N.M., Stoddart, J.F., 2009. Mechanised nanoparticles for drug delivery. Nanoscale 1, 16–39. doi:10.1039/b9nr00162j

Descalzo, A.B., Martínez-Mañez, R., Sancenón, F., Hoffmann, K., Rurack, K., 2006. The supramolecular chemistry of organic-inorganic hybrid materials. Angew Chem Int Ed Engl 45, 5924–5948. doi:10.1002/anie.200600734

Feldberg, R., Chang, S., Kotik, A., Nadler, M., Neuwirth, Z., Sundstrom, D., Thompson, N., 1988. In vitro mechanism of inhibition of bacterialcell growth by allicin. Antimicrob. Agentes Chemother. 32, 1763–1768.

Fu, Q., Rao, V.R., Ista, L.K., Wu, Y., Andrzejewski, B.P., Sklar, L.A., Ward, T.L., López, G.P., 2003. Control of Molecular Transport Through Stimuli-Responsive Ordered Mesoporous Materials. Adv Mater 15, 1262–1266.

Fujiwara, M., Terashima, S., Endo, Y., Shiokawa, K., Ohue, H., 2006. Switching catalytic reaction conducted in pore void of mesoporous material by redox gate control. Chem commun. 44, 4635–4637.

Giri, S., Trewyn, B.G., Stellmaker, M.P., Lin, V..-Y., 2005. Stimuli-responsive controlled-release delivery system based on mesoporous silica nanorods capped with magnetic nanoparticles. Angew Chem Int Ed. 44, 5038–5044.

Heikkila, T., Salonen, J., Tuura, J., Kumar, N., Salmi, T., Murzin, D.Y., Hamdy, M.S., Mul, G., Laitinen, L., Kaukonen, A.M., Hirvonen, J., Lehto, V.P., 2007. Evaluation of mesoporous TCPSi, MCM-41, SBA-15, and TUD-1 materials as API carriers for oral drug delivery. Drug Deliv 14, 337–347. doi:781274082 [pii]10.1080/10717540601098823

Jia, H., Zhu, G., Vugrinovich, B., Kataphinan, W., Reneker, D.H., Wang, P., 2002. Enzyme-carrying polymeric nanofibers prepared via electrospinning for use as unique biocatalysts. Biotechnol Prog 18, 1027–1032. doi:bp020042m [pii]10.1021/bp020042m

Kim, B.H., Yang, K.S., Woo, H.G., 2011. Preparation and electrochemical properties of carbon nanofiber composite dispersed with silver nanoparticles using polyacrylonitrile and beta-cyclodextrin. J Nanosci Nanotechnol 11, 7193–7197.

Kresge, C., Leonowicz, M., Roth, W., Vartuli, J., Beck, J., 1992. Ordered mesoporous sieves sinthesized by liquid-crystal template mechanism. Nature 359, 710–712.

Kriegel, C., Arecchi, A., Kit, K., McClements, D.J., Weiss, J., 2008. Fabrication, functionalization, and application of electrospun biopolymer nanofibers. Crit Rev Food Sci Nutr 48, 775–797. doi:902001968 [pii]10.1080/10408390802241325

Loh, X.J., Peh, P., Liao, S., Sng, C., Li, J., 2010. Controlled drug release from biodegradable thermoresponsive physical hydrogel nanofibers. J Control. Release 143, 175–182. doi:http://dx.doi.org/10.1016/j.jconrel.2009.12.030

Madhugiri, S., Dalton, A., Gutierrez, J., Ferraris, J.P., Balkus Jr., K.J., 2003. Electrospun MEH-PPV/SBA-15 composite nanofibers using a dual syringe method. J Am Chem Soc 125, 14531–14538. doi:10.1021/ja030326i

Mal, N.K., Fujiwara, M., Tanaka, Y., 2003. Photocontrolled reversible release of guest molecules from coumarin-modified mesoporous silica. Nature 421, 350–353.

Martindale, B., Neil, L., Compoton, R., 2011. Towards the electrochemical quantification of the strenght of garlic. Analyst 136, 128–133.

Muñoz, B., Rámila, A., Pérez-Pariente, J., Díaz, I., Vallet-Regí, M., 2003. MCM-41 organic modification as drug delivery rate regulator. Chem. Mater. 15, 500–503. doi:10.1021/cm021217q

Oroval, M., Climent, E., Coll, C., Erijta, R., Aviñó, A., Marcos, M.D., Sancenón, F., Martínez-Máñez, R., Amorós, P., 2013. An aptamer-gated silica mesoporous material for thrombin detection. Chem commun. 49, 5480–5482.

Park, C., Kim, H., Kim, S., Kim, C., 2009. Enzyme responsive nanocontainers with cyclodextrin gatekeepers and synergistic effects in release of guests. J Am Chem Soc 131, 16614–16615.

Price, R.L., Waid, M.C., Haberstroh, K.M., Webster, T.J., 2003. Selective bone cell adhesion on formulations containing carbon nanofibers. Biomaterials 24, 1877–1887. doi:S0142961202006099 [pii]

Rajesh, V., Dhirendra, S.K., 2006. Nanofibers and their applications in tissue engineering. Int J Nanomedicine 1, 15–30.

Schlossbauer, A., Kect, J., Bein, T., 2009. Biotin-avidin as a protease-responsive cap system for controlled guest release from colloidal mesoporous silica. . Angew Chem Int Ed. 48, 3092–3095.

Tang, F., Li, L., Chen, D., 2012. Mesoporous silica nanoparticles: synthesis, biocompatibility and drug delivery. Adv Mater 24, 1504–1534. doi:10.1002/adma.201104763

Venugopal, J., Ramakrishna, S., 2005. Applications of polymer nanofibers in biomedicine and biotechnology. Appl Biochem Biotechnol 125, 147–158. doi:ABAB:125:3:147 [pii]

Zhuang, X., Cheng, B., Kang, W., Xu, X., 2010. Electrospun chitosan/gelatin nanofibers containing silver nanoparticles. Carbohydr Polym 82, 524–527. doi:http://dx.doi.org/10.1016/j.carbpol.2010.04.085.

5 SECTION II

Nanotoxicological evaluation of mesoporous silica supports

5.1 Introduction: Understanding the MSPs' toxicicity

Extended use of nanomaterials have increased the interest to regulate nanotechnology applications and the associated toxicity. In particular, the toxic responses of many silica nanomaterials has not yet been fully evaluated. To address this issue, some companies are participating in the European Nanosafe consortium, which evaluates the health risks of nanomaterials (Sahoo, Parveen, & Panda, 2007). Along with JRC the European Nanotechnology Gateway and European Nanobusiness Association (ENA), have been established general parameters for working nanoparticles materials, defining physical and chemical properties to identify its behaviour as metabolisable compound. Focus on identify reliably methods which predict the possible spectra of toxic risks and health hazard associated for persistence, bio-acumulation and translocation of these particles by current exposure ways such as dermal contact, inhalation or ingestion, where *in-vitro* and *in-vivo* techniques to identify effects on exposure target (organism, organ, tissue or cell) are widely used (Cushen, Kerry, Morris, Cruz-Romero, & Cummins, 2012).

5.1.1 MSPs' toxicity: *In vitro* studies

In vitro assays are used to evaluate cell viability and cell damage. Cell viability is mainly based on compounds present in healthy cells that be directly related with metabolic activity, biological functionality of membranes or cells as

well as compounds related with the physiological function of the respiratory chain. But, cell viability is not always based on the integrity of the metabolism compounds, it could also be measure by the leakage of components that go out from cytoplasm when the cellular metabolism is affected. All those compounds are the markers used to evaluate the cell viability.

Currently, direct and indirectly reactions conducted by dye compounds are used for identify the markers of cell viability. Colorimetrical or fluorescently methods relate the light emission or fluorescent response with concentration of markers, which is proportional to number of living cells (X. He et al., 2008; Mönkäre et al., 2011; Totsuka et al., 2009). *In vitro* assays use different cell types include phagocytic, neural, hepatic, epithelial, endothelial and red blood cells as well cancer cell lines. The identification from cell endpoints that reflect physiological stress, toxicity or some other phenomenon try to model what is developed in human body (Heikkilä et al., 2010).

On the other hand, damage in cellular activity is not only related with decreasing in cell viability, is also related with apoptotic process. Apoptosis reachs a general collapse, which affects nucleus process and could trigger necrotic activity. Apoptosis is a biochemical reactions set that include alteration in cell membrane, cytosol condensation and collapse of chromatin and shrinkage cellular. Cell is disintegrated into vesicles (apoptotic bodies), which are engulf and

removed by phagocytic cells. The spilling out of that content into surrounding cells increases the damage and conduce a necrotic cell level. Necrosis is a form of traumatic cell death, it results from acute cellular injury and generates defence responses as inflammation. Death cells by necrosis usually don't send the same chemical signals to the immune system that cells undergoing apoptosis do. Necrosis typically has disruption of the chromatin, the plasma membrane and also the organelle membranes. Late necrosis is characterized by extensive DNA hydrolysis, vacuolation of the endoplasmic reticulum, organelle breakdown, and cell lysis. The release of intracellular content after plasma membrane rupture is the cause of inflammation in necrosis (Kim, Nam, & An, 2012).

In cases of cell damage, caspases are a family of cysteine proteases that play essential roles in inflammation, apoptosis and necrosis. Among the caspases family, effector caspases cleavage the cytosolic and nuclear proteins to intra-nucleosomal degradation of DNA and leads the apoptosis process. Based on the evaluation of those enzymes activity, is determinate the relation between apoptotic and necrotic cells.

Cell viability studies

Cell viability evaluated for silica nanoparticles showed a significant descended in metabolic activity, where smallest size particles and highest doses represent the major damage (Oberdorster et al., 2005). Those studies have

revealed that viability drop is caused meanly by internalization of particles. Once particles go inside the cells a loss of mitochondrial membrane is produced and the mitochondrial membrane potential is reduced. The decrease of deshydrogenase activity in mitochondria trigger a dysfunction and posterior damage cellular.

Human neuroblastom cells showed a viability decrease from 92 % to 40 % before exposure to MCM-41 nanoparticles (Q. He, Zhang, Gao, Li, & Shi, 2011), and analyses realized in fibroblasts show a viability decreased to 83.8 and 73.9 % by particles under 80 nm. However, 500 nm particles showed weak effects, with 91.4 % of cell viability, even at 200 $ug \cdot ml^{-1}$ (Q. He et al., 2011; Li et al., 2011). Other studies have revealed that particles larger than 1000 nm were unable to pass tissues as intestinal mucus barrier (Release, Medicine, Damm, Received, & Szentkuti, 1997), which confirms the size-effect relation.

It is important to determinate the risk related as a function of whole particle features. Latest studies showed that metabolic activity decrease is due not only by smallest size particles and high concentrations but also by all the entire interaction cell-particle. An interesting behaviour showed by silica particles is related to surfactant removing; when solids were treated with refluxing in acidified methanol, generates a 60 % of cell depletion, while through the calcined procedure, silica particles kept the cell survival percentage above 80 % (Savolainen et al., 2010). Another important factor on toxic response is the

interaction with chemical surface structure. Recent studies shown a significant influence in ATP drop depends on the particles' surface treatment; thus, carbonized particles affect in different manner than oxidized particles (Santos et al., 2010). Alike when surface is functionalized, particles change the way to endocytoses (Tao, Toms, Goodisman, & Asefa, 2009) and the cell damage could decrease. In this context, nanoparticles have been functionalized with different systems such as amino-propyl and mercaptopropyl to decrease the dose lethal in neuroblastoma cells (Di Pasqua et al., 2008).

Cell damage studies

Size particle still as an important feature to determine toxicity, studies revealed that particles under 21 nm exposed to myocardial cells showed damage for nuclear condensation as an increase in cell debris. It has beed related with cycle arrest, where there was a significantly decrease of cell percentage in S phase cycle. Besides, monitoring of p53 and p21 protein levels became more marked with doses increased with these particles (Takagi et al., 2008; Ye, Liu, Chen, Sun, & Lan, 2010)(Ye et al., 2010), which are related with arrest cycle in G1-phase. On the other hand, the apoptosis process was induced for a time and concentration dependent, with an early apoptotic rate for 100 $\mu g \cdot ml^{-1}$ and necrosis process above 200 $\mu g \cdot ml^{-1}$ in HEPG2 cells. Throug caspase-3 expression by western blot analyses, human endothelial cells also showed a necrosis process with the smaller

particles. So the smallest nanoparticles develop apoptotic and necrotic effects (Marquis, Love, Braun, & Haynes, 2009; Napierska et al., 2009).

Caspases activity indicate similar effect between different silica materials such as MCM or SBA, not only by size-relation but also by chemical structure differences. In cases of cell viability decrease the surface chemistry is important to determinate the toxicity of particles. Hydrophilic/hydrophobic character induces the way they interact with cells; depends on surface structure there are differences into influence in cell-particle interactions, which is stronger with Si-C-Hx and Si-Cx bonds in surface's particle, than Si-Ox surfaces, which is less harmful. Surface structure influences the cellular damage by apoptosis and necrotic cells produced, as well as decrease of cellular viability (Bimbo et al., 2010).

Hydrophilicity facilitate protein adsorption and cell-adhesion whereas hydrophobic particle could form links with proteins which may cause conformational changes or denaturation . Hydrophobic surfaces have been shown increment in apoptotic cells, more evident in smaller size fractions, and related with amount of particles in contact with each cell. However it is needed to identify not only acute effects but only chronic responses, which needs *in vivo* assays.

Oxidative studies

Another important factor to consider in cell damage is the influence of the oxidative state regulated by the electron transport chain (ETC). ETC is a complex of redox reactions in which electrons are transferred from a donor molecule to an acceptor molecule. In mitochondria, it is the conversion of oxygen to water, NADH to NAD+ and succinate to fumarate that generates an electrochemical proton gradient to form energy as ATP. Atomic oxygen, a strong oxidizing agent is the electron acceptor. In ETC, it has two unpaired electrons in separate orbits in its outer electron shell. This electron structure makes oxygen susceptible to radical formation. The sequential reduction of oxygen through the addition of electrons leads to the formation of a number of reactive oxygen species, ROS including: superoxide, hydrogen peroxide, hydroxyl radical, hydroxyl ion and nitric oxide. Superoxide radical is an oxidative specie precursor and the most proximal ROS considering the mitochondrial function (Thannickal & Fanburg, 2000).

The deleterious effect of oxidative stress on the proper function of cells is well known, Caco-2 cells have been reported as sensitive by silica as initiators of ROS generation and O_2 formation, at highest doses of MCM41 and SBA15 (Gebhardt J. Caspary, W.F. Boehles, H. Stein, J., 1999). As well as smallest particles can trigger the release of reactive oxygen species and cause oxidative

stress. It also trigger an inflammation response by means of interaction with the reticule-endothelial system.

Similarly, ROS could be related with chemical surface. In fact, ROS can be induced by hydrophobic/hydrophilic interactions and/or redox reactions between cell and the particles surface. Process to craft surface, influence oxidation or thermally oxidation surface treatments reduce the efficiency electron transfer from the excitons to the surface molecules, which decrease ROS production. For instance, carbonized surface particles increased amounts of hydrogen peroxide and superoxide anion, which induces a mitochondrial dysfunction. Mitochondrial damages increase cell apoptosis and subsequent cell membrane damage and cell death (Santos 2010). Further oxidative stress could generate deleterious by lipid in membrane, causing injury to lipids, proteins and DNA (Bayir & Kagan, 2008).

So that, the principal evaluation for particles in *in-vitro* assays is the response as cell viability and cell damage as well as ROS production to identify the principal cellular risks that influence injuries in organs and target tissues.

5.1.2 MSPs' toxicity: *In vivo* studies

Toxicity evaluation requires not only a cellular level analyse but also needs real scenery to study the adverse effects on living beings. *In vivo* assays are developed principally on mice, raised in specific conditions by care procedures accord with the local care committee. Weigh, temperature, age of treatment and

quarantine conditions before analyses are the control parameters to take in count.

In vivo analyses expose the target component in selected animals by direct ingestion or intravenously or subcutaneous injection. Time and doses are defined and a monitoring in blood and tissues is done (Aillon, Xie, El-Gendy, Berkland, & Forrest, 2009). Fixation and freezing preserve tissues samples before are staining and sectioned for microscope analyze in the histopathological examinations.

Organs such as liver, spleen, kidney, intestine, heart and lungs are exciding to determinate lesions, congestion or haemorrhage (Cha & Myung, 2007). Specific studies, separate into organs tissues by parenchymal and non-parenchymal cells trough procedures that allow analyse a subcellular level the toxicological damage.

Genotoxic and mutation evaluation apply PCR analyses to determinate DNA sequences on mouse model, known as GPT delta mice, which deletions in lambda DNA integrated in the chromosome are preferentially selected for molecular analysis (Ogawara et al., 1999; Totsuka et al., 2009).

Some MSPs studies have been developed in mice by subcutaneous administration and direct ingestion, and it has not shown a significant damage by exposure of microparticles for 2 and 4 weeks (Kilpeläinen et al., 2009). However, silica nanoparticles oral administered in rats (Aleshin, Lee, Park, & Akagi, 2004), reported particles distribution to kidneys, liver, lungs and spleen. It is important to

notice that silica particles were easily decomposed and eliminated via urinary and faecal excretion after oral exposure. The smaller the particles, the more rapidly they are secreted, presumably because they are more easily decomposed. Those studies shown that once absorbed, particles are transported via the portal vein to the liver and are then eliminated during a 7-day period by faecal excretion, and also through urine, without changing the kidney microstructure.

In line with this, an *in vivo* study with male nude mice (Souris et al., 2010), confirmed that after oral administration, silica nanoparticles located in the liver could be excreted into the intestine by the hepatobiliary excretion process.

Although in most of cases particle size is determining to concern about pass through essential human barriers; shape, surface coating, charges associated and much more features associated with physical and chemical behaviour influence the toxic response, even more deep than size distribution, because not only small size has tendency to diffuse faster through mucus layers, also particle charge influence the diffusion.

Some anionic particles have been shown to reach the epithelial surface, whereas cationic particles were trapped in the mucus (Hagens, Oomen, de Jong, Cassee, & Sips, 2007). When particles go through the mucus layer, they cross by paracellular or transcellular route, first one is modulated by polymers that act as expanders into the tight junctions of the epithelium (Salamat-Miller & Johnston,

2005), reason why nanomaterials cannot be excluded from that way. Second route is the endocytosis, where attachments of ligands or coating surfactants by charge particles could influence the transcellular uptake and depending the material characteristic could enter both the blood and lymphoid circulation intact (Joye, Davidov-Pardo, & McClements, 2014) besides interaction with body-components depend on surface chemistry, hydrophobic surfaces are susceptible to opsonization and clearance by the reticulo-endothelial system, resulting driving particles to liver and spleen (Letchford & Burt, 2007).

5.1.3 Potential risks of MSPs due to oral intake

Gastrointestinal tract (GIT) is complex and also includes the resident microbiome/microbiota; accordingly, evaluation of oral nanomaterials uptake has to considerate not only cell absorption and extra intestinal organ accumulation but also the potential alteration of gut microbes and the effects on the host (Bergin & Witzmann, 2013).

5.1.4 Some concerns about gastrointestinal tract (GIT) and oral intake pathways

GIT is composed of the oral cavity, the oesophagus, the stomach and the intestine. Liver and pancreas are extra intestinal organs involved in gastrointestinal functions of digestion, absorption, distribution, metabolism and excretion of the swallowed substances. GIT is a selective mucosal barrier, consist

of epithelium and mucus layer, which mechanically protect and lubricate the entire tract and the underlying tissue (Bergin & Witzmann, 2013; Eleonore Roblegg., 2012).

Mucosal barrier has an estimated surface area of 200 m^2, which gives a potential interaction with ingested substances. In addition, studies have shown that mucus barrier allows a selectively materials permeation (Kaunitz, 1999; Macierzanka et al., 2011; Sigurdsson, Kirch, & Lehr, 2013). Epithelium represent the highest resistance against it; so it is necessary identify the entire tract features to understand the interaction of ingested nanomaterials and their potential risks.

Brief physicochemical considerations

GIT activity begins in the mouth where the ingested food is chewed and mixed with saliva (Humphrey and Williamson 2001; Chen 2009). Saliva mainly consists in water (98 %) and inorganic salts, organic substances, including proteins, enzymes, mucins and others (Levine et al. 1987). Saliva also contains enzymatic activity of lipases and amylases, however residence time in the oral cavity is short (2-5 min). Thus enzyme activity is low and the influence of the mouth on the translocation pathways is negligible.

Once substances are swallowed, they pass through the oesophagus, which have a mucus layer produced by oesophageal and exocrine glands. Substances directly pass to the stomach, where the residence time varies between 2 to 6 h.

Protein digestion starts by protease action, which depends of hydrochloric acid secretion from epithelium, which confers an intensive acidic medium (pH 1-2). The stomach mucus layer and posterior small and large intestine mucus is secreted mainly by intraepithelial cells. However, thickness and composition of mucus layer varies along GIT. As well as thickness increase from proximal to distal parts of the intestine, maximal thickness has been reported in the stomach (Eleonore Roblegg., 2012). Likewise, thickness of epithelium also varies along the GIT (Diaz del Consuelo et al., 2005) (Atuma et al., 2001; Matsuo et al., 1997).

The mucosal surface area in small intestine significantly increases, due to folds and elongation to facilitate the absorption by enterocytes (gut epithelial cells). Mucus layer of small intestine has several enzymes, to finish the digestive process. Most substances absorption takes place in the upper small intestine, where the mucus pH is around to 6 (within the 5.7 to 6.2 range) and gradually increases through the small intestine to pH 7.5 (within the 7.3 to 7.7 range) (Fallingborg., 1999).

Otherwise, small intestine has a large number of cell associations, enterocytes, intraepithelial lymphocytes, goblet cells, dendritic cells and cells belonging to the immune system (M-cells), are linked together. M-cells are located in the epithelium overlying the follicle associated epithelium (FAE) or Peyer's Patches. M-cells are responsible to initiate mucosal immunity responses,

allowing the substances transport across the epithelial cell layer (Hazzard, Hodges, Scott, McGuinness, & Carr, 1996). In particular, the small intestine is where mostly occurs the digestion and absorption, with a residence time of ingested substances between 2 to 5 h. However, distal small intestine and colon have specialized absorptive roles in water, vitamins, and fatty acid absorption (Bergin & Witzmann, 2013). Even though, the main barriers for GIT permeation are the mucus layer and the epithelium, this barrier resides in a basal membrane, separated from connective tissue; hence, for reaching the systemic circulation by capillaries substances have not only to cross entire epithelium but also the basal membrane.

5.1.5 Oral intake of MSPs

Studies suggest tha once MSPs are ingested they are absorbed through gut enterocytes and through epithelial cells of the Peyer's patches in the gut-associated lymphoid tissue, which mainly reach liver, kidney and spleen (Jani, Halbert, Langridge, & Florence, 1990). Also, the absorbed particles stimulate phagocytosis at gastrointestinal mucosa to cause antigen-antibody trigger inflammation responses (Hussain et al., 2011). Other studies report that MSPs are taken up by recticuloendothelial system, where, the smaller is the ingested material the maximal is the absorption (Vong, Yoshitomi, Matsui, & Nagasaki, 2015; Yu, Hubbard, Ray, & Ghandehari, 2012).

Mucus membrane pathway elucidates MSPs behavior through the endodermal cells, where absorption and secretion are involved. In fact, depends on mucus - MSPs interaction, muco-adhesive capacity changes and facilitate translocation which promotes the cytotoxic effects (Sigurdsson et al., 2013). In the same way, phagocytosis and contact fibroblasts B cells are interesting patways due to their association with gut lymphoid tissue and blood circulatory system (Murdock, Braydich-Stolle, Schrand, Schlager, & Hussain, 2008; Oberdorster et al., 2005).

Once particles pass through cell membrane, they affect the cellular activity. This cell-particle interaction generates membrane perturbations, modification on signalling responses by influence on the cellular electron transfer and vesicle trafficking pathways. It induces the release of endosomal substances, reactive oxygen species, cytokines and chemokines, thus stimulate inflammatory responses and metabolism damage. The intercellular transport of those substance affect the gene regulation of cellular injuries and could trigger the apoptosis and necrosis process (Fruijtier-Pölloth, 2012; Jones, Grainger, & Clinton D., 2009).

References

Aillon, K. L., Xie, Y., El-Gendy, N., Berkland, C. J., & Forrest, M. L. (2009). Effects of nanomaterial physicochemical properties on in vivo toxicity. Advanced Drug Delivery Reviews, 61(6), 457–66.

Aleshin, A. N., Lee, H. J., Park, Y. W., & Akagi, K. (2004). One-dimensional transport in polymer nanofibers. Phys Rev Lett, 93(19), 196601.

Bayir, H., & Kagan, V. E. (2008). Bench-to-bedside review: Mitochondrial injury, oxidative stress and apoptosis--there is nothing more practical than a good theory. Critical Care (London, England), 12(1), 206.

Bergin, I. L., & Witzmann, F. A. (2013). Nanoparticle toxicity by the gastrointestinal route: evidence and knowledge gaps. Int J Biomed Nanosci Nantechnol., 3(1–2).

Bimbo, L. M., Sarparanta, M., Santos, H. A., Airaksinen, A. J., Mäkilä, E., Laaksonen, T., … Salonen, J. (2010). Biocompatibility of thermally hydrocarbonized porous silicon nanoparticles and their biodistribution in rats. ACS Nano, 4(6), 3023–3032.

Boya, P., Andreau, K., Poncet, D., Zamzami, N., Perfettini, J.-L., Metivier, D., … Kroemer, G. (2003). Lysosomal membrane permeabilization induces cell death in a mitochondrion-dependent fashion. The Journal of Experimental Medicine, 197(10), 1323–1334.

Cha, K. E., & Myung, H. (2007). Cytotoxic effects of nanoparticles assessed in vitro and in vivo. J Microbiol Biotechnol, 17(9), 1573–1578.

Cushen, M., Kerry, J., Morris, M., Cruz-Romero, M., & Cummins, E. (2012). Nanotechnologies in the food industry – Recent developments, risks and regulation. Trends in Food Science & Technology, 24(1), 30–46.

Di Pasqua, A. J., Sharma, K. K., Shi, Y.-L., Toms, B. B., Ouellette, W., Dabrowiak, J. C., & Asefa, T. (2008). Cytotoxicity of mesoporous silica nanomaterials. Journal of Inorganic Biochemistry, 102(7), 1416–23.

Eleonore Roblegg., F. E. (2012). Models for oral uptake of nanoparticles in consumer products. Toxicology, 291, 10–17.

Elias O. Daniere, M.C. Terzetti, F. Marande, A.M. Dzwigaj, S. Pezerat, H. Fenoglio, I. Fubini, B., Z. P. (2000). Cytotoxicity and transforming effects of silica particles with different surface properties in Syrian hamster ambryo (SHE) cells. Toxicology in Vitro, 14, 409–422.

Fruijtier-Pölloth, C. (2012). The toxicological mode of action and the safety of synthetic amorphous silica-a nanostructured material. Toxicology, 294(2–3), 61–79.

Fubini A., B. H. (2003). Reactive oxygen species (ROS) and reactive nitrogen species (RNS) generation by silica in inflamation and fibrosis. Free. Radic. Biol. Med., 34, 1507–1516.

Fujii N. Fumon, H. Hayashi, S. Kovalev, D. Goller, B. Diener, J., M. N. (2006). Dynamics of photosensitized formation of singlet oxygen by porous silicon in aqueous solution. Journal of Applied Physics, 100(12), 124302–1243025.

Gebhardt J. Caspary, W.F. Boehles, H. Stein, J., B. R. (1999). Superoxide: a major factor for stress protein induction in reoxygenation injury in the intestinal cell line Caco-2. Digestion, 60, 238–245.

Hagens, W. I., Oomen, A. G., de Jong, W. H., Cassee, F. R., & Sips, A. J. (2007). What do we (need to) know about the kinetic properties of nanoparticles in the body? Regulatory Toxicology and Pharmacology, 49(3), 217–229.

Hazzard, R. A., Hodges, G. M., Scott, J. D., McGuinness, C. B., & Carr, K. E. (1996). Early intestinal microparticle uptake in the rat. Journal of Anatomy, 189 (Pt 2, 265–271.

He, Q., Zhang, Z., Gao, F., Li, Y., & Shi, J. (2011). *In vivo* biodistribution and urinary excretion of mesoporous silica nanoparticles: Effects of particle size and PEGylation. Small, 7(2), 271–280.

He, X., Nie, H., Wang, K., Tan, W., Wu, X., & Zhang, P. (2008). In vivo study of biodistribution and urinary excretion of surface-modified silica nanoparticles. Analytical Chemistry, 80(24), 9597–603.

Heikkilä, T., Santos, H. a H. A., Kumar, N., Murzin, D. Y., Salonen, J., Laaksonen, T., … Lehto, V.-P. (2010). Citotoxicity study of ordered mesoporous silica MCM-41 and SBA-15 microparticles on Caco-2 cells. European Journal of Pharmaceutics and Biopharmaceutics : Official Journal of Arbeitsgemeinschaft Für Pharmazeutische Verfahrenstechnik e.V, 74(3), 483–494.

Hussain, A., Brahmbhatt, K., Priyani, A., Ahmed, M., Rizvi, T. a., & Sharma, C. (2011). Eugenol Enhances the Chemotherapeutic Potential of Gemcitabine and Induces Anticarcinogenic and Anti-inflammatory Activity in Human Cervical Cancer Cells. Cancer Biotherapy & Radiopharmaceuticals, 26(5), 519–527.

Jani, P., Halbert, G. W., Langridge, J., & Florence, A. T. (1990). Nanoparticle uptake by the rat gastrointestinal mucosa: quantitation and particle size dependency. J Pharm Pharmacol, 42(12), 821–826.

Jones, C. F., Grainger, D. W., & Clinton D., J. G. (2009). In vitro assessments of nanomaterial toxicity. Advanced Drug Delivery Reviews, 61(6), 438–56.

Joye, I. J., Davidov-Pardo, G., & McClements, D. J. (2014). Nanotechnology for increased micronutrient bioavailability. Trends in Food Science & Technology.

JRC. (2011). Challenges of Regulation and risk assessment of nanoparticles. (Join Research Center publishes summary, Ed.), JRC Enlargement and Integration Action,. Varese.

Kaunitz, J. D. (1999). Barrier function of gastric mucus. Keio Journal of Medicine, 48(2), 63–68.

Kilpeläinen, M., Riikonen, J., Vlasova, M. A., Huotari, A., Lehto, V. P., Salonen, J., … Jarvinen, K. (2009). In vivo delivery of a peptide, ghrelin antagonist, with mesoporous silicon microparticles. Journal of Controlled Release : Official Journal of the Controlled Release Society, 137(2), 166–70.

Kim, S. W., Nam, S. H., & An, Y. J. (2012). Interaction of Silver Nanoparticles with Biological Surfaces of Caenorhabditis elegans. Ecotoxicology and Environmental Safety, 77, 64–70.

Letchford, K., & Burt, H. (2007). A review of the formation and classification of amphiphilic block copolymer nanoparticulate structures: micelles, nanospheres, nanocapsules and polymersomes. Eur J Pharm Biopharm, 65(3), 259–269.

Li, Y., Sun, L., Jin, M., Du, Z., Liu, X., Guo, C., … Sun, Z. (2011). Size-dependent cytotoxicity of amorphous silica nanoparticles in human hepatoma HepG2 cells. Toxicology in Vitro : An International Journal Published in Association with BIBRA, 25(7), 1343–52.

Linsinger, T. P., Chaudhry, Q., Dehalu, V., Delahaut, P., Dudkiewicz, A., Grombe, R., … Weigel, S. (2013). Validation of methods for the detection and quantification of engineered nanoparticles in food. Food Chem, 138(2–3), 1959–1966.

Macierzanka, A., Rigby, N. M., Corfield, A. P., Wellner, N., Böttger, F., Mills, E. N. C., & Mackie, A. R. (2011). Adsorption of bile salts to particles allows penetration of intestinal mucus. Soft Matter, 7(18), 8077.

Marquis, B. J., Love, S. A., Braun, K. L., & Haynes, C. L. (2009). Analytical methods to assess nanoparticle toxicity. Analyst, 134(3), 425–439.

Mönkäre, J., Riikonen, J., Rauma, E., Salonen, J., Lehto, V.-P., & Järvinen, K. (2011). In vitro dissolution methods for hydrophilic and hydrophobic porous silicon microparticles. Pharmaceutics, 3(2), 315–25.

Murdock, R. C., Braydich-Stolle, L., Schrand, A. M., Schlager, J. J., & Hussain, S. M. (2008). Characterization of nanomaterial dispersion in solution prior to in vitro exposure using dynamic light scattering technique. Toxicological Sciences, 101(2), 239–253.

Napierska, D., Thomassen, L. C., Rabolli, V., Lison, D., Gonzalez, L., Kirsch-Volders, M., … Hoet, P. H. (2009). Size-dependent cytotoxicity of monodisperse silica nanoparticles in human endothelial cells. Small, 5(7), 846–853.

Noda, T., Iwakiri, R., Fujimoto, K., & Aw, T. A. K. Y. E. E. (2001). Induction of mild intracellular redox imbalance inhibits proliferation of CaCo-2 cells. The FASEB Journal, 15(12), 2131–2139.

Oberdorster, G., Maynard, A., Donaldson, K., Castranova, V., Fitzpatrick, J., Ausman, K., … Yang, H. (2005). Principles for characterizing the potential human health effects from exposure to nanomaterials: elements of a screening strategy. Part Fibre Toxicol, 2, 8.

Ogawara, K., Yoshida, M., Higaki, K., Kimura, T., Shiraishi, K., Nishikawa, M., … Hashida, M. (1999). Hepatic uptake of polystyrene microspheres in rats: effect of particle size on intrahepatic distribution. J Control Release, 59(1), 15–22.

Release, C., Medicine, V., Damm, B., Received, G., & Szentkuti, L. (1997). Light microscopical observations on luminally administered dyes, dextrans, nanospheres and microspheres in the pre-epithelial mucus gel layer of the rat distal colon. Journal of Controlled Release, 46(3), 233–242.

Sahoo, S. K., Parveen, S., & Panda, J. J. (2007). The present and future of nanotechnology in human health care. Nanomedicine, 3(1), 20–31.

Salamat-Miller, N., & Johnston, T. P. (2005). Current strategies used to enhanced the paracellular transport of therapeutic polypeptides across the intestinal epithelium. International Journal of Pharmaceutics, 294(1–2), 201–216.

Savolainen, K., Alenius, H., Norppa, H., Pylkkänen, L., Tuomi, T., & Kasper, G. (2010). Risk assessment of engineered nanomaterials and nanotechnologies—A review. Toxicology, 269(2–3), 92–104.

Sigurdsson, H. H., Kirch, J., & Lehr, C. M. (2013). Mucus as a barrier to lipophilic drugs. International Journal of Pharmaceutics.

Soji, T., Murata, Y., Ohira, A., Nishizono, H., Tanaka, M., & Herbert, D. C. (1992). Evidence that hepatocytes can phagocytize exogenous substances. Anatomical Record, 233(4), 543–546.

Souris, J. S., Lee, C.-H. H., Cheng, S.-H. H., Chen, C.-T. T., Yang, C.-S. S., Ho, J. A. A., … Lo, L.-W. W. (2010). Surface charge-mediated rapid hepatobiliary excretion of mesoporous silica nanoparticles. Biomaterials, 31(21), 5564–5574.

Takagi, A., Hirose, A., Nishimura, T., Fukumori, N., Ogata, A., Ohashi, N., … Kanno, J. (2008). Induction of mesothelioma in p53+/- mouse by intraperitoneal application of multi-wall carbon nanotube. J Toxicol Sci, 33, 105–116.

Tao, Z., Toms, B. B., Goodisman, J., & Asefa, T. (2009). Mesoporosity and functional group dependent endocytosis and cytotoxicity of silica nanomaterials. Chem Res Toxicol, 22(11), 1869–1880.

Thannickal, V. J., & Fanburg, B. L. (2000). Reactive oxygen species in cell signaling. Am J Physiol Lung Cell Mol Physiol, 279(6), L1005-28.

The royal society. (2004). Nanoscience and nanotehcnologies: opportunities and uncertainties.

Totsuka, Y., Higuchi, T., Imai, T., Nishikawa, A., Nohmi, T., Kato, T., … Wakabayashi, K. (2009). Genotoxicity of nano/microparticles in in vitro micronuclei, in vivo comet and mutation assay systems. Particle and Fibre Toxicology, 6(1), 23.

Vong, L. B., Yoshitomi, T., Matsui, H., & Nagasaki, Y. (2015). Development of an oral nanotherapeutics using redox nanoparticles for treatment of colitis-associated colon cancer. Biomaterials, 55, 54–63.

Ye, Y., Liu, J., Chen, M., Sun, L., & Lan, M. (2010). In vitro toxicity of silica nanoparticles in myocardial cells. Environmental Toxicology and Pharmacology, 29(2), 131–7.

Yu, T., Hubbard, D., Ray, A., & Ghandehari, H. (2012). In vivo biodistribution and pharmacokinetics of silica nanoparticles as a function of geometry, porosity and surface characteristics. Journal of Controlled Release : Official Journal of the Controlled Release Society, 163(1), 46–54.

Zegura, B., Volcic, M., Lah, T. T., & Filipic, M. (2008). Different sensitivities of human colon adenocarcinoma (CaCo-2), astrocytoma (IPDDC-A2) and lymphoblastoid (NCNC) cell lines to microcystin-LR induced reactive oxygen species and DNA damage. Toxicon, 52(3), 518–525.

5.2 Effect of capped mesoporous silica particles on colon cells viability

Effect of capped mesoporous silica particles on colon cells viability

Carolina Acosta[a], Jose M. Barat[a],
Ramón Martínez-Máñez[bc], Mar Orzaez[d]

[a]Grupo de Investigación e Innovación Alimentaria – Departamento de tecnología de Alimentos
[b]Centro de Reconocimiento Molecular y Desarrollo Tecnológico – Unidad Mixta Universitat de València Universitat Politècnica de Valencia, Camino de Vera S/N, Valencia, Spain
[c]CIBER de Bioingeniería, Biomateriales y Nanomedicina (CIBER-BBN), Spain
[d]Laboratorio de Química de Péptidos y Proteínas del Centro de Investigación Príncipe Felipe. C\ Eduardo Primo Yúfera 3, Valencia, Spain[d]

Evaluation of cell viability of colon cancer cells exposed to mesoporous silica particles was determined. The effect of size, doses and surface functionalisation of mesoporous silica particles was studied. Cells were incubated with concentrations range between 0.1 to 10 $mg \cdot mL^{-1}$ of micro- and nano-sized particles dispersions. In addition, surface of particles was capped with a polysaccharide molecule. Results indicate that depletion of cell viability depends of size and surface characteristics. These effects were significant in a doses-manner after 24 to 48 h exposure times. Thus, data shown that metabolic cell activity reduction and subsequent toxicity can be lowered through synthesis pathway changes and surface modification.

Introduction

Silicon element exhibits a vast array of different chemistries, in which size, shape, and surface of the nano- and micro-structures can be easily manipulated. Among its oxide forms, silicon dioxide, also known as silica (-SiO_2-), can be prepared as porous structure in different forms (from nanometric to micrometric size). In particular, the mesoporous support has pores in the 2-10 nm range which means a very high specific surface area (up to 1200 $m^2 \cdot g^{-1}$) (Perez-Pariente 2006). These properties make silica mesoporous structures ideal candidates as carriers for delivery applications.

In food and pharmaceutical industry, mesoporous silica-based supports are interesting devices. In contrast to current organic polymer supports, the inorganic structure of silica-based supports resists the harsh conditions of the gastrointestinal tract, while their high surface area allows a large encapsulation capacity. In addition, the surface structure is easy to functionalise with organic molecules, which can be attached after cargo encapsulation and are able to release the entrapped guest in function of specific targets such as, enzymatic or pH changes (Vallet-Regi F. Arcos, D. et al. 2007). These features can be used to modulate the bioaccessibility of target molecules along the gastrointestinal tract.

In particular, silica-based materials in form of synthetic amorphous silica are recognized as safe for food use (GRAS by FDA regulations), and it is also an

authorised additive in Europe, E-551 classification (Contado et al., 2013). However, according to current regulation, mesoporous silica particles (MSPs), both, micro and nano-sized, they can be intentionally synthesised to modulate porous above the order of 100 nm, which is associated to engineered nanomaterials. In this context, physicochemical properties can differ from those of the non-nanoscale as well as can differ the toxic effects. Thus, in order to use MSPs for oral delivery applications, they need a nanotoxicological evaluation to assure their safety.

In particular, *in vitro* cytotoxic studies of MSPs has shown mainly a dose-dependent effect and particle size influence (smaller particles showed higher cytotoxicity). And citotoxic effects have been related to particles-cells interactions, which trigger apoptotic signalling. Studies on colon cell lines pointed to mitochondrial disruption due to ATP depletion due as well as reactive oxygen species production induced by MSPs' surface features.

So far, the potential biological effects of MSPs with surface modifications have not been widely studied in the gastrointestinal tract (GIT). To our knowledge, the *in vitro* quantification of capped MSPs hve been reported for four types of micro-sized mesoporous silica-based particles. Pérez-Esteve and coworkers (2016) encapsulate folic acid and functionalised the particles' surface with amine molecules. They suggested that cells from gastrointestinal tract tolerated the

particles at concentrations of 50, 100, 150 and 200 $\mu g \cdot mL^{-1}$ (Pérez-Esteve et al. 2016).

Similar levels of biocompatibility of functionalised porous silica have been reported by other authors (Souris et al. 2010; Si et al. 1997; Xie et al. 2016). This high biocompatibility is most likely related with both, the particle size employed and the surface functionalisation. The cytotoxic effect of MSPs (190 and 420 nm) showed significant cytotoxicity at concentrations above 25 $mg \cdot mL^{-1}$, while micro-scale particles of 1220 nm showed only slight cytotoxicity due to decreased endocytosis (He et al. 2011; He et al. 2008). Moreover, the interaction of silanol groups (ca. 6% of total MSPs' surface) with biological molecules, such as cellular membrane lipids and proteins, may strongly interact and modify the structure of these molecules. But the functionalisation could prevent those effects. The purpose of the present study was to compare *in vitro* data on the effects of the ordered mesoporous silica-based micro and nanoparticles, both with and without surface functionalisation, on intestinal epithelial cells (colon cell lines).

Herein, we wanted to evaluate a doses range to define a particle concentration threshold for cytotoxic effects on cell lines with similarities in morphology and physiology than gastrointestinal tract.

Materials and methods

All the chemicals were purchased at the highest possible grade available and were directly used with no further purification. Chemicals tetraethylorthosilicate (TEOS), N-cetyltrimethylammonium bromide (CTABr), sodium hydroxide (NaOH), triethanolamine (TEAH), 3-aminopropyl-triethoxysilane (APTES) and N-((3-trimethoxysilylpropyl) diethylenetriamine) (N3), were provided by Aldrich. Hydrolysed starch Glucidex® 47 (5 % glucose, 50 % maltose, 45 % oligosaccharides and polysaccharides) was provided by Roquette.

Mesoporous silica-based particles synthesis

MSPs were synthesised as micro and nano sized particles. Following the so-called ‘‘atrane route”(Cabrera et al. 2000), microparticles (**M**) were obtained. 4.68 g of CTABr was used as the structure-directing agent, and added at 118 ºC to a TEAH solution (25.79 g) that contained 0.045 mol of a silatrane derivative (TEOS, 11 mL). The molar ratio of the reagents was fixed to 7 TEAH3:2 TEOS:0.52 CTABr:0.5 NaOH:180 H2O. After dissolving CTABr in the solution, water was slowly added with vigorous stirring at 70 °C. After a few minutes, a white suspension was formed. This mixture was aged in an autoclave at 100 °C for 24 h.

Nanoparticles (**N**) were obtained using the following procedure: CTABr (2.00 g, 5.48 mmol) was first dissolved in 960 mL of deionised water. NaOH (aq) (2.00 M, 7.00 mL) was added to the CTABr solution, followed by adjusting the

solution temperature to 95 °C. TEOS (10.00 mL, 44.8 mmol) was then added dropwise to the surfactant solution. The mixture was allowed to stir for 3 h to give a white precipitate. The product was centrifuged, and washed with deionised water and ethanol. And the resulting powder (as-synthesised) was dried at 60 °C.

For all samples (**M** and **N**) to prepare the final mesoporous materials, the as-synthesized solids were calcined at 550 °C using an oxidant atmosphere for 5 h in order to remove the template phase.

Synthesis of functionalised particles (M1, N1)

An excess of 3-[2-(2-aminoethylamino)-ethylamino]-propyl-trimethoxysilane (N3, 0.43 mL) was added to 0.1 g bare particles (**M** and **N**) in 40 ml acetonitrile. The final mixture was stirred for 5.5 h at room temperature in an inert atmosphere of nitrogen. Solid was filtered and washed with acid solution at pH 2.0 (acidified with sulfuric acid) and dried for 12 h at 35 °C.

Methods to characterise

Powder X-ray diffraction (PRXD), transmission electron microscope (TEM), N_2 adsorption-desorption isotherms, thermogravimetric analyses (TGA) and Z-potential measurements were employed to characterize the synthesised supports. PXRD measurements were taken on a Seifert 3000TT diffractometer using CuKα radiation. The TEM images were obtained with a 100 kV Philips CM10 microscope. The equilibrium adsorption isotherms of nitrogen were measured at -196 °C using

static volumetric adsorption systems (ASAP 2020 analyser, Micrometrics). TGA were carried out on a TGA/SDTA 851e Mettler Toledo balance in an oxidant atmosphere (air, 80 $mL \cdot min^{-1}$) with a heating program that consisted of a heating ramp of 10 °C per minute from 120 to 1000 °C, and an isothermal heating step at this temperature for 30 min. Finally, to determine the zeta potential (ζ) of the bare and functionalised MSPs, a Zetasizer Nano ZS equipment (Malvern Instruments, Malvern, UK) was used. Samples were dispersed in distilled water at a concentration of 1 $mg \cdot mL^{-1}$. Before each measurement, samples were sonicated for 15 min to preclude aggregation. The zeta potential was calculated from the particle mobility values by applying the Smoluchowski model. The average of five recordings was reported as zeta potential. The measurements were performed at 25 °C. Measurements were performed in triplicate.

Cell culture

The human colon cell lines were obtained from ATCC–LGC Standards. HCT116 and CaCO2 cells were grown in McCoy's 5A culture medium, and DMEM, respectively. Culture medium was supplemented with 10 % FBS and antibiotics (100 $U \cdot mL^{-1}$ of penicillin, 100 $\mu g \cdot mL^{-1}$ of streptomycin). Cells were maintained at 37 °C in an atmosphere of 5 % CO_2 and 95 % air and undergone passage twice a week.

WST-1 Cell Viability Assay

Cells were cultured in sterile 96-well plates at a seeding density of 2.5×10^{3} cells per well, and they were allowed to settle for 24 h. Equivalent concentration of particles were added to cells in range from 0.1 to 10 $mg\cdot mL^{-1}$. After 24 and 48 h, WST-1 (10 μL) was added to each well; cells were further incubated for 2 h and absorbance was measured at 450 and 620 nm.

Statistical analyses

Cell viability was evaluated through sigmoidal fit of dose-response curves, and the Origin software package was used. Statistical analyses were determined by One-Way and factorial ANOVA through SPSS software.

Results and discussion

Particles characterisation

The particles were characterised by TEM, powder X-ray diffraction (PXRD) and N_2 adsorption-desorption studies (see Figure 5.2-1). The X-ray patterns the typical four low-angle reflections of hexagonal array. Which remains after surface functionalisation. TEM images confirm the hexagonal porous structures, visualised as alternate black and white stripes (see Figure 5.2-1A and 1B). As TEM images show, micro-sized particles were obtained as irregular micrometric particles with a size in the 1000 – 3000 nm range, whereas nano-sized ones were obtained as spherical particles with diameters ranging from 80 to 100 nm. And

functionalisation did not affect the size range. On the other hand, adsorption-desorption isotherms, shows typical type IV curves, they consisting of one single adsorption step at the intermediate P/P_0 value (0.1-0.4). In contrast, the isotherms of the functionalised particles (**M1** and **N1**), shows a flat curve which indicates the pore blocking due functionalisation on particles' surface.

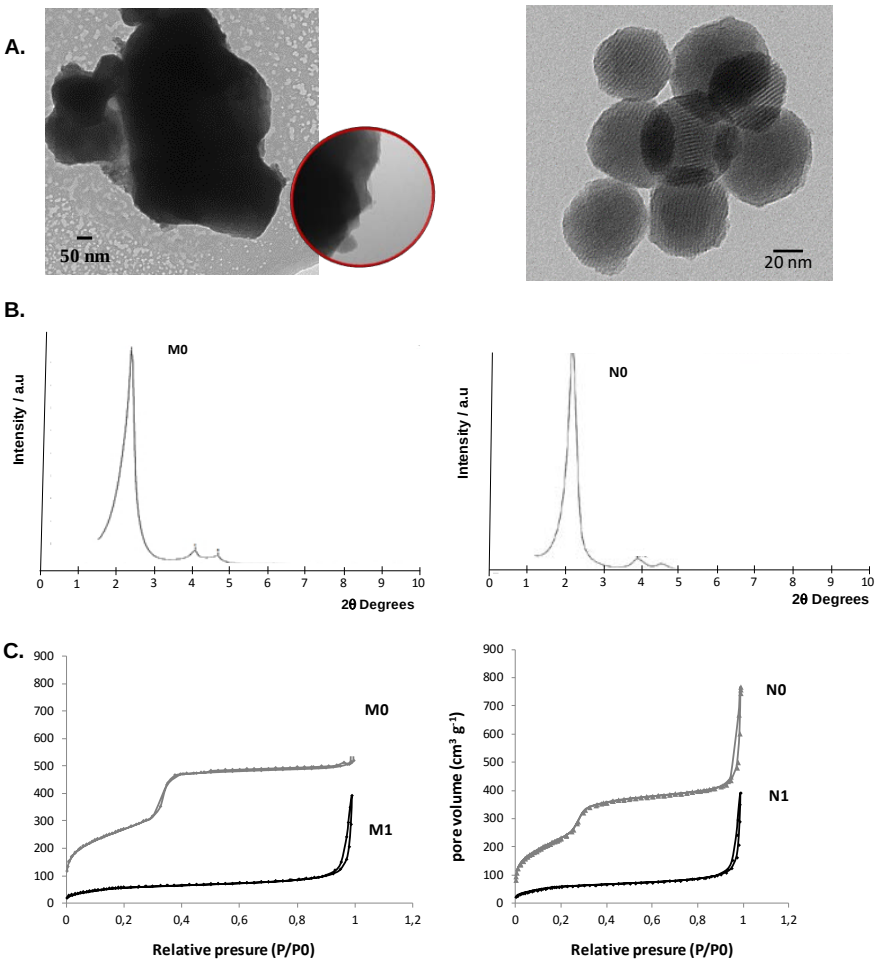

Figure 5.2-1. Characterisation of MSPs A. TEM images of micro and nano-particles (inset shows the porosity of micro particles). B. X-ray diffraction patterns of micro (M0) and

nano (N0) particles. C. Absorption-desorption curves for bare (M0 and N0) and functionalised (M1 and N1) particles.

In addition, the zeta potential value changes in function of surface structure. Bared particles have a negative zeta potential (about -18 mV), while functionalisation increase the values to positive ranges (Above 15 mV). (Supporting info, Apendix 5.2 S1)

Cell viability studies

In vitro data, showed a significant reduction of cell viability, both in HCT-116 and Caco-2 cell lines, for doses higher of 2 $mg \cdot mL^{-1}$ (See figure 5.2-2), and with higher viability reduction for nano-sized particles. However, independent of size the threshold dose for mesoporous silica particles, MCM-41 type, was about 1 to 2 $mg \cdot mL^{-1}$.

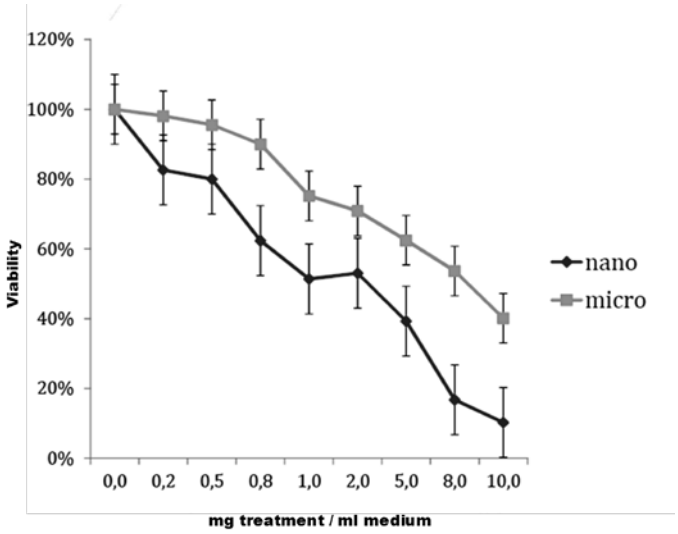

Figure 5.2-2. Doses and size-effect on HCT116 cell viability when nano and micro-sized MSPs are incubated for 24h at 37 °C.

Results suggest no significant differences between cell lines. But, studies above particles concentrations of 1 mg·mL^{-1} showed the visible effect of surface, incubation time and size on cells. In addition, results showed that after 48 h, the complete effect of particles presence was evidenced. Based on that, the concentration through half of population is reduced (the lethal dose LD50) was determined at 48 h (See Table 5.2-1). But Caco-2 cell line showed differences related with time only, no differences showed the concentration increase, and viability reduction there was no remarkable, in all cases cell viability was up to 80%.

Table 5.2-1. Lethal dose (LD50) on colon cancer cells incubated with mesoporous silica particles

	At 24 h ($mg \cdot mL^{-1}$)	**After 48 h** ($mg \cdot mL^{-1}$)
M0	0.8	1.2
M1	0.9	1.5
N0	0.3	0.5
N1	0.7	0.9

First, lowest doses did not show a significant cell viability reduction. This was generally between 0.02 to 0.08 $mg \cdot mL^{-1}$. Beyond 0.3 to 1.0 $mg \cdot mL^{-1}$, the size effect was confirmed, nano-sized particles caused more damage than micro-ones. However, the surface functionalization increases the particles' biocompatibility, more significant to nano-sized particles.

Global results indicated that features such as size and surface structure of mesoporous silica particles MCM41 type, are modifiable tools for synthesizing particles with low cytotoxic impact. Studies on epithelial cells of gastrointestinal tract elucidate the particles' behavior after being oral ingested. However, to confirm the non-toxicity of these particles, it is need to go a step forward and evaluate the oral intake through *in vivo* models.

Acknowledgement

We thank the Spanish Government (projects AGL2015-70235-C2-1-R, AGL2015-70235-C2-2-R and MAT2015-64139-C4-1-R (MINECO/FEDER)) and the Generalitat Valenciana (project PROMETEOII/2014/047) for support. C.A. thanks Colciencias for her predoctoral fellowship. The authors also thank the Electron

Microscopy Service at the UPV for support and We thank Roquette for the Glucidex samples.

References

Cabrera, S. et al., 2000. Generalised syntheses of ordered mesoporous oxides: the atrane route. *Solid State Sci.*, 2(4), pp.405–420.

He, Q. et al., 2011. In vivo biodistribution and urinary excretion of mesoporous silica nanoparticles: Effects of particle size and PEGylation. *Small*, 7(2), pp.271–280.

He, X. et al., 2008. In vivo study of biodistribution and urinary excretion of surface-modified silica nanoparticles. *Analytical chemistry*, 80(24), pp.9597–603

Pérez-Esteve, É. et al., 2016. Encapsulation of folic acid in different silica porous supports: a comparative study. *Food Chemistry*, 196, pp.66–75.

Perez-Pariente, J., Materiales mesoporosos de óxido de silicio. *Liberación de fármacos en matrices biocerámicas: avances y perspectivas*, pp.39–64.

Si, U. et al., 1997. Comprehensive Study of Surface Chemistry of MCM-41 Comprehensive Study of Surface Chemistry of MCM-41 Using. , 5647(97), pp.6525–6531.

Souris, J.S. et al., 2010. Surface charge-mediated rapid hepatobiliary excretion of mesoporous silica nanoparticles. *Biomaterials*, 31(21), pp.5564–5574.

Vallet-Regi F. Arcos, D., M.B. et al., 2007. Mesoporous materials for drug delivery. *Angewandte Chemie - International Edition*, 46(40), pp.7548–7558.

Xie, X. et al., 2016. EpCAM aptamer-functionalized mesoporous silica nanoparticles for efficient colon cancer cell-targeted drug delivery. *European Journal of Pharmaceutical Sciences*, 83, pp.28–35.

5.3 A C. elegans in vivo nanotoxicology evaluation of bare and functionalised micro and nano mesoporous silica particles

A C. elegans in vivo nanotoxicology evaluation of bare and functionalised micro and nano mesoporous silica particles

Carolina Acosta,[a*] Jose M. Barat,[a] Ramón Martínez-Máñez,[b,c] Félix Sancenón,[b,c] Silvia Llopis,[d] Nuria González,[d] Salvador Genovés,[d] Daniel Ramón,[d] and Patricia Martorell[d]

[a]Grupo de Investigación e Innovación Alimentaria - Departamento de Tecnología de Alimentos, Universitat Politècnica de València, Spain
[b]Instituto Interuniversitario de Investigación de Reconocimiento Molecular y Desarrollo Tecnológico (IDM). Universitat Politecnica de València, Universitat de València, Camino de Vera s/n, 46022-Valencia, Spain
[c]CIBER de Bioingeniería, Biomateriales y Nanomedicina (CIBER-BBN), Spain
[d]Department of Food Biotechnology, Biopolis S.L., Parc Científic Universitat de València, Spain
* Corresponding author: cararo@upvnet.upv.es

Submitted 2017

Here we show a study about the toxicologic evaluation of mesoporous silica particles (MSPs) in the nematode *C. elegans*. The effect on *C. elegans* ageing parameters of bare micro- (**M0**) and nano-sized (**N0**) MSPs, and the corresponding functionalised particles with a starch derivative (**Glu-N**) (**M1** and **N1),** was investigated. To analise the toxicity of MSPs, their impact on *C. elegans* lifespan, movement capacity, progeny and ability to survive upon an acute oxidative stress was assesed. This study demonstrated that both size of particles (**M0** and **N0)**, labelled with rhodamine and monitored through fluorescence microscopy, are ingested by nematodes. Moreover, toxicity assays indicated that bare nano-sized particles (**N0**) have a negative impact on *C. elegans* lifespan, reducing mobility and progeny production in nematodes. Contrary, micro-sized particles **(M0)** are inocuous for the nematodes. Furthermore, functionalization of nanoparticles with starch derivative reduced their toxicity on *C. elegans*. Thus, oral intake of **N1** considerably increased the mean lifespan and movement activity as well as the resistance to oxidative stress. The overall findings here presented pointed out the influence of size and surface of MSPs on their potential toxicity *in vivo*, and evidenciate the silica-based mesoporous particles as a potential support for encapsulation in life sciences applications. Furthermore, the good correlation obtained between healthy aging variables and viability (mean lifespan) validates the use of *C. elegans* as a multicellular organism for nanotoxicology studies.

Introduction

In recent years, inorganic nanomaterials have drawn the attention as suitable tools for developing delivery systems (Mo et al., 2014). Among inorganic supports for controlled release applications, mesoporous silica particles (MSPs) have received great interest (Valtchev et al., 2013; Stein et al., 2003; Soler-Illia et al., 2011; Angelos et al., 2007). MSPs have tunable and homogeneous pore size distribution (in the 2–10 nm range in diameter), and high specific surface area and volume, which provide large loading capacity (Salonen et al., 2008; Wight et al., 2002). Apart from voids, MSPs highlights for exhibiting a high concentration of structural defects on their surface in the form of silanol (Si-OH) groups that can easily react with trialkoxysilane derivatives ((R'O)3-Si-R), allowing the possibility of generating organic−inorganic hybrid supports (Vinu et al., 2005; Kickelbink et al., 2004). This strategy offers a wide range of new perspectives in the development of delivery systems (Coll et al., 2013), while opening the design of on-command release particles to control the delivery of previously entrapped guest (Angelos et al., 2007; Aznar et al., 2016; Sancenón et al., 2015). In line with this concept, examples of MSPs functionalised with a number of different molecules and biomolecules able to deliver the cargo upon the applications of physical (light, temperature, magnetic fields, ultrasounds) (Mal et al., 2003; Agostini et al., 2012; Fu et al., 2003; Aznar et al., 2011; Giri et al., 2005), chemical (anions, cations,

neutral molecules, redox-active species and pH) (Fujiwara et al., 2006; Angelos et al., 2009) and biochemical (such as enzymes, DNA and antibodies) (Oroval et al., 2013; Schlossbauer et al., 2009; Bernardos et al., 2010; Park et al., 2009) stimuli have been reported.

However, in spite of the promising applicability of MSPs as advanced delivery systems, and despite silica not being considered harmful for humans, the effect of particle size and surface functionalisation of MSP on *in vivo* toxicity after MSP is oral administered remains poorly understood, and more studies in this context are essential to obtain useful information for the future design of safe and non-toxic oral delivery systems based in MSP.

From another point of view, the nematode *Caenorhabditis elegans* has emerged as a well-suited *in vivo* model for toxicological studies owing to its established biology and readily scorable life traits. *C. elegans* is a multicellular organism with a short lifespan (21 days), a well-studied biological system and is simple to maintain. In addition, experiments with *C. elegans* are less expensive than those carried out with vertebrate models and allow to carrying out a wide set of tests at different conditions in a short time (*C. elegans Consortium*, 1998). Moreover, it has been reported that results obtained with *C. elegans* can be predictive of those in higher eukaryotes because many physiological processes, signal transduction pathways and genes are conserved (Leung et al., 2008). These

features have led to an increasing use of *C. elegans* as a suitable model in toxicological studies. Quantitative parameters of *C. elegans* that can be assayed include gene expression, growth, size, progeny production, and mortality. Moreover, behavioural parameters related with toxicity on healthy aging (healthspan), such as changes on movement capacity and sensitivity to oxidative stress can also be easily determined.

Recent studies have confirmed that different inorganic nanomaterials are efficiently ingested by *C. elegans* and toxicological studies using different materials have been carried out (Cha et al., 2012; Wang et al., 2009; Gonzalez-Moragas et al., 2015). Nonetheless, very few studies have been reported with *C. elegans* and silica-based particles. In particular, toxicological studies have been carried out with amorphous (non-porous) silica nanoparticles (Pluskota et al., 2009; Scharf et al., 2013). These studies suggested that these nanoparticles (smaller than 50 nm) induce premature aging, due to progeny reduction and alterations of phenotypes related to aging. However, as far as we know, there are not studies with *C. elegans* and mesoporous silica-based particles nor about the nematodes' lifespan after fed with MSPs neither studies of nematodes' behaviour in relation to different features associated to MSPs such as size or particles' surface functionalisation.

In this scenario, and taking into account the above mentioned facts and out interest in the design and use of mesoporous silica particles for delivery applications, we report herein a study on the interaction of *C. elegans* with nano- and micro-sized MSP after particles were oral administered. Moreover, both, bare particles and particles functionalised in the external surface with hydrolysed starch, have been studied. We have carried out studies not only on population viability by lifespan, but also studied worm's behaviour by healthspan variables (movement capacity, resistance to acute oxidative stress and offspring). The results showed that surface functionalisation of MSPs is a suitable procedure to significantly reduce toxicity of these particles in *C. elegans*. This is especially so for mesoporous silica in the form of nanoparticles.

Materials and methods

Chemicals

All the chemicals were purchased at the highest possible grade available and were directly used with no further purification. Chemicals tetraethylorthosilicate (TEOS), N-cetyltrimethylammonium bromide (CTABr), sodium hydroxide, triethanolamine (TEAH), 3-aminopropyl-triethoxysilane (APTES) were provided by Aldrich. Hydrolysed starch Glucidex® 47 (5% glucose, 50% maltose, 45% oligosaccharides and polysaccharides) was provided by Roquette.

C. elegans strain and maintenance

C. elegans strain Bristol (wild-type) N2 was obtained from the Caenorhabditis Genetics Center at the University of Minnesota and was maintained at 20 °C on nematode growth medium (NGM). Strain *Escherichia coli* OP50 used as normal diet for nematodes was obtained from the Caenorhabditis Genetics Center.

Synthesis of micro-sized mesoporous silica particles (M0)

Micro-sized mesoporous silica particles were synthesised by the "atrane route" [32] in which 4.68 g of CTABr were added at 118 °C to a TEAH solution (25.79 g) that contained 0.045 mol of a silatrane derivative (TEOS, 11 mL). Next 80 mL of water were slowly added with vigorous stirring at 70 °C. After a few minutes, a white suspension formed. This mixture was aged at room temperature overnight. The resulting powder (as-synthesised material) was collected by filtration and washed. The solid was dried at 70 °C and was finally calcined at 550 °C for 5 h in an oxidant atmosphere in order to remove the template phase.

Synthesis of nano-sized mesoporous silica-based particles (N0)

Nano-sized mesoporous silica particles were synthesised by the following procedure: N-cetyltrimethylammoniumbromide (CTABr, 1.00 g, 2.74 mmol) was first dissolved in 480 mL of deionised water. Then 3.5 mL of a NaOH 2.00 $mol \cdot L^{-1}$ solution was added, followed by an adjustment of temperature to 80 °C. TEOS (5.00 mL, 22.4 mmol) was then added dropwise to the surfactant solution. The

mixture was stirred for 2 h to give a white precipitate. Finally, the solid was collected by centrifugation, washed with deionised water and dried at 70 °C overnight (as-synthesised material). To prepare the final mesoporous nanoparticles (**N0**), the as-synthesised solid was calcined at 550 °C in an oxidant atmosphere for 5 h to remove the template phase.

Synthesis of the starch derivative (Glu-N)

A solution of APTES (5.85 mL, 25 mmol) was added to a suspension of hydrolysed starch (Glucidex@ 47) in ethanol (Bernardos et al., 2010). The reaction mixture was stirred for 24 h at room temperature and heated at 60 °C for 30 min. The solvent was evaporated under reduced pressure.

Synthesis of starch-functionalized mesoporous silica particles (M1, N1)

To prepare the starch-functionalised mesoporous silica particles **M1** and **N1**, **Glu-N** was added to **M0** and **N0** in a 1:1 w/w ratio. The final mixture was stirred for 5.5 h at room temperature under argon. The solid was filtered, washed with abundant deionised water and dried for 12 h at 35 °C.

Synthesis of labelled particles (M0-rhd and N0-rhd)

Particles **M0** and **N0** were labelled with rhodamine B using a similar procedure to that reported by Xu and co-workers (Xu et al., 2014). First the solid surface was modified with APTES. For this purpose, **M0** or **N0** nanoparticles were suspended in toluene (30 mL) and APTES (0.19 mL, 0.8 mmol) was added. The final suspension was refluxed at 110 °C for 20 h. Afterward 50 mg of the corresponding

solid was suspended in ethanol with 50 mg B rhodamine isothiocyanate (RITC) for 20 h to obtain **M0-rhd** and **N0-rhd**.

Finally, ethanol suspensions were filtered and solids were washed with abundant deionised water, and dried for 12 h at 35 °C.

Materials characterisation

PXRD measurements were taken on a Seifert 3000TT diffractometer using CuKα radiation. TEM images were obtained under a 100 kV Philips CM10 microscope. Thermogravimetric analyses were carried out on a TGA/SDTA 851e Mettler Toledo balance in an oxidant atmosphere (air, 80 mL·min-1) with a heating program that consisted of a heating ramp of 10 °C per minute from 120 to 1000 °C, and an isothermal heating step at this temperature for 30 min.

N_2 adsorption-desorption isotherms were recorded in a Micromeritics ASAP2010 automated sorption analyser. Samples were degassed at 120 °C in vacuum overnight. The specific surface areas were calculated from the adsorption data within the low pressure range using the BET model (Brunauer et al., 1938).

Dynamic light scattering (DLS) studies for size distribution were conducted at 25 °C using a Malvern Zetasizer Nano ZS and Malvern Mastersizer 2000. Data analysis was based on the Mie theory using refractive indices of 1.33 and 1.45 for the dispersant and MSP, respectively. To determine the zeta potential (ζ) of bare and functionalised MSP, a Zetasizer Nano ZS was used. Zeta potential was

calculated from the particle mobility values by applying the Smoluchowski model. The average of five recordings was reported as the zeta potential. All the measurements in Malvern Zetasizer Nano ZS and Malvern Mastersizer 2000 were performed at 20 °C in triplicate, samples were dispersed in M9 buffer at concentration of 1 $mg \cdot L^{-1}$. Before each measurement, samples were sonicated for 10 min to preclude potential aggregation.

Particles suspension

Particles **M0**, **M1**, **N0** and **N1** were sterilised by UV for 30 min after particles were dispersed at a known volume fraction of M9 buffer ($KHPO_4$ 3 $g \cdot L^{-1}$, Na_2HPO_4 6 $g \cdot L^{-1}$, NaCl 5 $g \cdot L^{-1}$, $MgSO_4$ 1 mmol), and disposed in an ultrasound bath with 2 pulses of 15 min to reduce particle aggregates. The required amount of the corresponding suspension was used to prepare each doses evaluated (three doses: 0.5, 5.0 and 50 $\mu g \cdot mL^{-1}$ of **M0**, **N0**, **M1** and **N1**). For better handling, dispersions were aliquoted and stored at -20 °C until used.

Worms synchronisation

Ten reproductive worms of the wild-type strain were laid on NGM agar plates (nematode growth medium: agar 17.5 $g \cdot L^{-1}$, sodium chloride 3.0 $g \cdot L^{-1}$, peptone 2.5 $g \cdot L^{-1}$, cholesterol 0.005 $g \cdot L^{-1}$) with *E. coli* OP50. Worms were incubated for 2.5 h and then the initial population was eliminated. Laid eggs and the larvae were raised to young adulthood at 20 °C for 72 h. After the final larval molt, when animals became reproductive adults, worms were considered

synchronised and were selected for the assays. Worms were selected and placed on NGM plates for evaluations, and *C. elegans* was defined as young adults (0-day adults).

Lifespan assays in C. elegans

Synchronised worms of the wild-type strain were grown at 20 °C and transferred to NGM agar. For control population (standard feeding, without particles), worms were just transferred to NGM plates (10 worms per plate). Worms fed with MSPs were transferred to NGM plates supplemented with the corresponding particle suspension (i.e. **M0**, **M1**, **N0** or **N1**). Animals were moved periodically to new plates and scored every 2 days, and were considered dead if they failed to respond to a platinum wire. Three independent assays (10 plates per assay) were carried out for 21 days (lifespan extension) for control population and for each dose and each particle (and three doses: 0.5, 5.0 and 50 $\mu g \cdot mL^{-1}$ of **M0**, **N0**, **M1** and **N1**). Every 2 days, the initial population was transferred to fresh NGM plates and addition of the particles was maintained.

Oxidative stress on C. elegans

To measure the survival rates of *C. elegans* after exposure to oxidative stress, synchronised worms, which had hatched in NGM on the agar plates that contained the *E. coli* OP50 strain, and in the presence or absence of the corresponding particles (i.e. **M0**, **N0**, **M1** or **N1**) were used. After 5 days of growth at 20 °C, worms were transferred to MB medium (Basal medium: agar 17 $g \cdot L^{-1}$,

sodium chloride 5.85 $g \cdot L^{-1}$, cholesterol 0.005 $g \cdot L^{-1}$) plates that contained 2 mM H_2O_2, and were incubated for 5 h. Then viability of worms was measured. Worms were considered dead when they no longer responded to prodding. Each experiment was done with 70 individuals and evaluations were carried out in triplicate for control population, and for each dose and each particle.

Healthspan studies

A synchronised nematode population was obtained. For all the studies, young adult worms (0-day adults) were selected and transferred to plates for each dose and each particle (three doses: 0.5, 5.0, 50 $\mu g \cdot mL^{-1}$ of **M0**, **N0**, **M1** and **N1**). A control population was also evaluated. **Movement activity**: Locomotion activity was monitored on 2-day adult and 9-day adult worms. Synchronised worms (70 individuals) were transferred to plates containing the particles and movement was determined as the total right bends achieved in 35 seconds. Evaluations were made in triplicate. **Offspring:** Synchronised worms were selected and individually transferred to NGM plates daily for 5 days (10 plates per each dose and each particle). The progeny (larvae) laid in each plate was counted to determine the offspring. Evaluations were made in triplicate.

Fluorescence Microscopy

A 5 $\mu g \cdot mL^{-1}$ solution of **M0-rdh** or **N0-rhd** was seeded on NGM plates. Synchronised worms were transferred to the plates (5 plates per each solid). Worms were treated and transferred as in lifespan assays. After 5 days of

incubation, worms (10 worms per plate) were placed in a sample-holder with 2% agarose pads, and were anesthetised with levamisol solution; a coverslip was overlaid to fix the worms' position. Finally, DIC (Nomarsky) and epi-fluorescence digital images were acquired with an Eclipse 90i Nikon microscope with an 20x objective equipped with a digital camera (Nikon DS-5Mc) and a fluorescence filter TRITC (G-2E/C). Images were processed and analysed by the Nis Elements BR 2.32 software.

Statistical analysis

Statistical analyses were determined by One-Way ANOVA. Survival curves were evaluated by the Kaplan Meier model and compared using the log rank survival significance test. The SPSS statistical software package was used.

Results and discussion

Mesoporous silica synthesis

Bare micro- (**M0**) and nano-sized (**N0**) MSPs, were synthesised using well-known procedures. Moreover, both **M0** and **N0** particles were functionalised with hydrolysed starch to obtain the corresponding micro- (**M1**) and nano-sized (**N1**) starch-functionalised particles. Functionalisation was carried out by simple reaction of **M0** and **N0** with **Glu-N** that was prepared by reaction of APTES with hydrolysed starch (Glucidex@ 47) in ethanol (see Scheme 5.3-1). The solids were thoughtfully washed with water and dried before use. ^{1}H NMR spectrum of **Glu-N** was consistent with that described in the literature (Appendix 5.3-Figure S1)

(Bernardos et al., 2010). Moreover, particles **M0** and **N0** were labelled with a red fluorescent dye (i.e. rhodamine B isothiocyanate, RITC) (Xu et al.,2014), to obtain **M0-rhd** and **N0-rhd**, respectively.

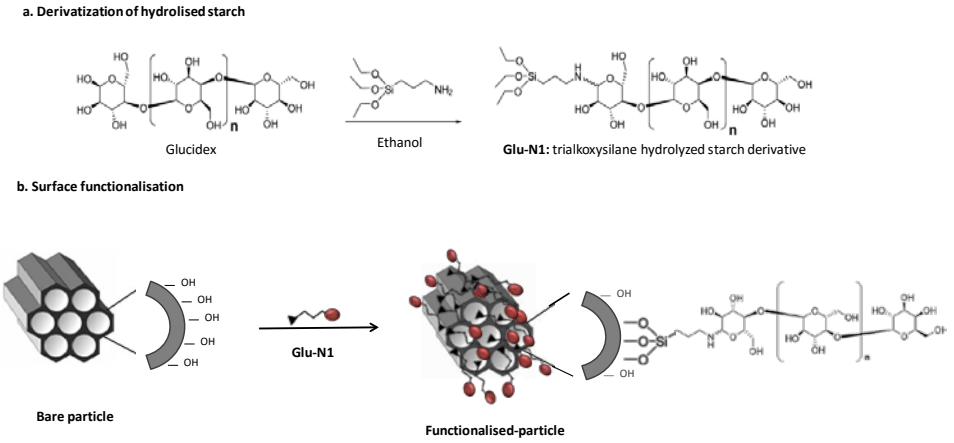

Scheme 5.3-1. Synthesis of mesoporous silica particles capped with Glu-N

Material characterisation

The characterisation of the synthesised materials was performed by well-known standard techniques. Powder X-ray diffraction (PXRD) patterns of bare **M0** and **N0** (as-synthesised and calcined) and starch-functionalised **M1** and **N1** particles are shown in Figure 5.3-1A. PXRD patterns of bare particles show the typical four low-angle reflections of mesoporous silica solids, which can be indexed as (100), (110), (200) and (210) Bragg peaks. From the PXRD data, a_0 cell parameters of 47.89 and 49.73 Å (d100 spacing of 41.48 and 43.07 Å) were calculated for as-synthesised **M0** and **N0**, respectively. A significant shift of the (100) reflection in the PXRD in the calcined samples was clearly observed which

corresponds to an approximate cell contraction of ca. 4.8 and 4.5 Å for calcined **M0** and **N0**, respectively (see Figure 5.3-1A). This is related to the condensation of silanols in the calcination step when CTABr was removed. For the starch-functionalised **M1** and **N1** particles, PXRD patterns showed only the characteristic (100) reflection. However, the presence of this peak clearly indicated that the mesoporous structure was preserved after anchoring of the **Glu-N** derivative. TEM images also showed, for all particles, the typical porosity associated with this type of inorganic supports as a pseudo hexagonal array of pore voids. TEM images also showed that **M0** and **M1** are irregular micrometric particles, whereas **N0** and **N1** are spherical nano-size particles (see Figure 5.3-1B for typical TEM images of **M0** and **N0**).

N_2 adsorption–desorption isotherms of **M0** and **N0** showed typical curves consisting of one single adsorption step at intermediate P/P0 values (0.1-0.4), which is related to nitrogen condensation inside mesopores by capillarity (Figure 5.3-1C). Absence of a hysteresis loop in this interval and a narrow pore distribution suggested the existence of uniform cylindrical mesopores with pore diameter and specific volume of 3.19 nm and 0.78 $cm^3 \cdot g^{-1}$ respectively for **M0** and 3.51 nm and 0.74 $cm^3 \cdot g^{-1}$ for **N0** (calculated by the BJH model on the adsorption branch of the isotherm). The application of the BET model to calcined materials gave a total specific surface value of 979.6 $m^2 \cdot g^{-1}$ and 843.9 $m^2 \cdot g^{-1}$ for **M0** and **N0**,

respectively. In contrast, N_2 adsorption–desorption isotherms of functionalised solids showed nearly flat curves when compared with un-functionalised starting materials and an appreciable reduction of porosity, due to the grafting of **Glu-N**, was observed. A specific surface area of 509.6 and 220.1 $m^2 \cdot g^{-1}$ and pore volumes of 0.34 and 0.24 $cm^3 \cdot g^{-1}$ were calculated for **M1** and **N1**, respectively. Table 5.3-1 lists BET specific surface values and pore volumes calculated from the N_2 adsorption-desorption isotherms.

Thermogravimetric analyses (TGA), zeta potential and size distribution studies were also performed. TGA curves of **M1** and **N1** showed a weight loss at 100-600 °C due to the organic matter combustion that corresponded to the anchored starch derivative (see Supplementary material, Appendix 5.3-Figure S2). From TGA analyses organic matter contents of 0.10 and 0.13 g per g SiO_2 for solids **M1** and **N1**, respectively, were calculated.

As particles were administered to worms in a buffered aqueous dispersion (M9 buffer for *C. elegans*, *vide infra*), zeta potential (ζ) and particle distribution sizes were determined in M9 buffer (see Table 5.3-1). **M0** and **N0** had a negative zeta potential due to the presence of anionic silanol groups on their surface. Upon functionalisation, the surface potential changed from negative to positive, which was ascribed to the effective grafting of starch derivative **Glu-N** onto the surface of both materials.

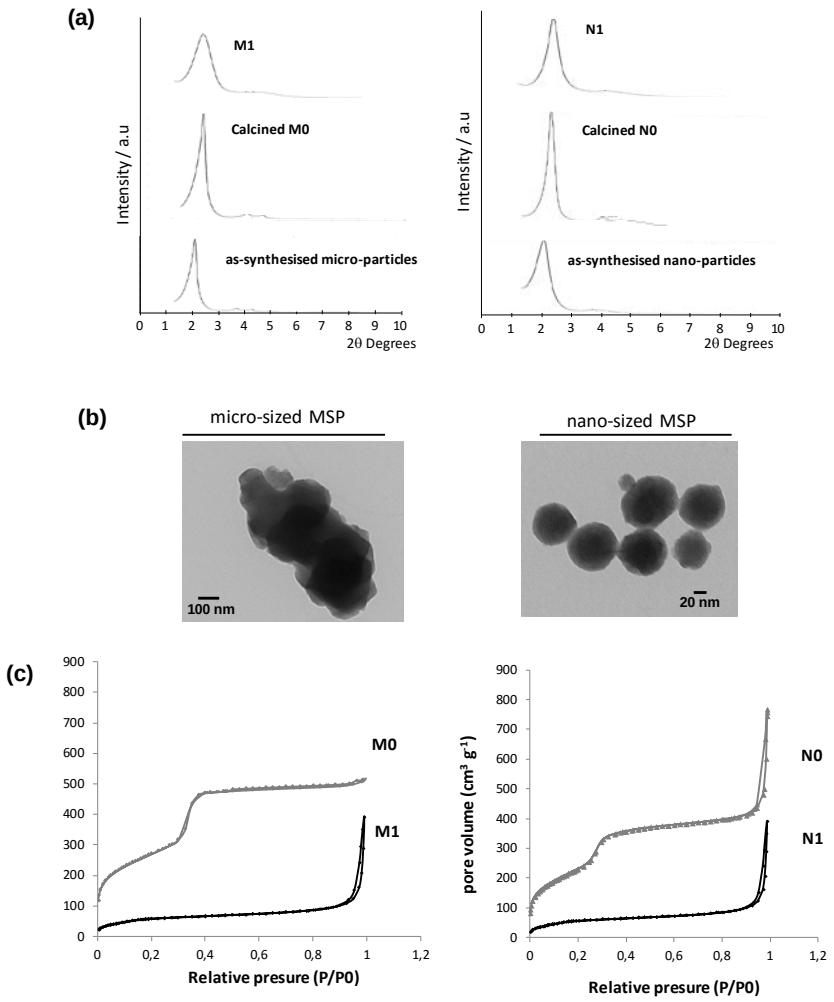

Figure 5.3-1. Materials characterisation (a) Powder X-ray patterns (b) TEM images of micro-sized particles, M0 and nano-sized particles, N0 and (c) Nitrogen adsorption-desorption isotherms: Calcined material M0 [●], and Solid M1 [■]. Calcined material N0 [▲], and solid N1 [◆].

Dynamic light scattering (DLS) studies gave a mean size of 1930 µm for **M0** and of 1114 µm for **M1**, whereas mean sizes of 338 and 141 nm were found for **N0** and **N1**, respectively (see Table 5.3-1 and Appendix 5.3-Figure S3). When

comparing size distribution and single-particle size, as determined by TEM (Table 5.3-1), mean particle size increased in the M9 buffer most likely as a result of partial particle aggregation, which agreed with previous studies (Pérez-Esteve et al., 2014).

Table 5.3-1. Characteristics of synthesised materials

	S_{BET} (m^2g^{-1})	pore volume (cm^3g^{-1})	Single-particle size (nm)*	Mean size (nm)§	Z potential (ζ) (mV)
M0	979.619^a	0.784^b	1566 ± 42^c	1930 ± 284 ^{d}	-18.60 ± 0.89 ^{e}
M1	509.591^a	0.343^b	1189 ± 81^c	1114 ± 133 ^{d}	11.06 ± 0.40 ^{e}
N0	843.899^f	0.741^g	97 ± 13	338 ± 11.82 ^{h}	-15.35 ± 2.14^i
N1	220.089^f	0.247^g	90 ± 13	141 ± 5.89 ^{h}	9.06 ± 0.28 ^{i}

*Single-particle size determined by TEM. § Mean size determined by Light Diffraction (dispersed in M9-buffer). The same letters indicate singnificant differences between group memberships ($p < 0.05$).

As stated above, bare **M0** and **N0**, MSP, were both labelled with rhodamine B isothiocyanate (RITC) using post-synthesis grafting procedure to obtain **M0-rhd** and **N0-rhd**, respectively (Xu et al., 2014). A thermogravimetric evaluation indicated a rhodamine content of 4.8 % and 5.2 % in **M0-Rhd** and **N0-Rhd**, respectively.

Validation of oral intake of MSPs by C. elegans

Recent evaluations made on *C. elegans* have confirmed the ability of nematodes to directly ingest inorganic nanomaterials (Leung et al., 2008; Cha et al., 2012; Wang et al., 2009; Gonzalez-Moragues et al., 2015). In order to validate the ability of nematodes to ingest the the different size of MSPs sythetized, a

monitoring study of the administered particles **M0-rhd** and **N0-rhd** was performed by means fluorescent microscopy.

Once particle suspension is seeded on plates, it was hypothesised that particles become available and can be swallowed by nematodes. After 5 days of **M0-rhd** and **N0-rhd** administration, nematodes were prepared for fluorescent microscopy and the oral intake of particles was monitored. Results showed that both **M0-rhd** and **N0-rhd** were ingested by nematodes and both particles were clearly located along the gastrointestinal tract (GIT) (Figure 5.3-2a and b). Both micro and nano-sized particles were located mainly in the lumen and pharynx. In addition, an uptake-gradient with a major concentration in the anterior intestine region was noticed, in agreement with results obtained in previous studies for other inorganic nanoparticles (Pluskota et al., 2009; Scharf et al., 2013).

In order to evaluate the permanence of particles in the GIT and the ability of nematodes to excrete the ingested particles, 5-day old nematodes fed with **M0-rhd** and **N0-rhd** were divided into two groups. Group one (1) was prepared for fluorescence analyses as described above.To purge particles from nematodes, group two (2) was collected with M9-buffer and transferred to NGM plates without MSPs for2 days,after the two days, nematodes from group two (2) were prepared for fluorescent microscopy. Results strongly indicated the ability of *C. elegans* to ingest and excrete MSPs (Figure 5.3-2c and d). This was specially

remarkable in nematodes fed with **N0-rhd** (Figure 5.3-2d), as nano-sized MSPs showed a higher trend to remain in the GIT (especially in the pharynx) when compared with micro-sized MSPs.

Although resolution and sensitivity of microscope limit the possibility of identifying endocytosis of particles, the lack of fluorescence outside the GIT of worms from group (2) suggested neither translocation nor accumulation of MSPs in secondary organs.

Finally, the progeny of nematodes fed with **M0-rhd** and **N0-rhd** was studied and no fluorescence was detected (Appendix 5.3-Figure S4), suggesting that there was not translocation of MSPs to the germ line.

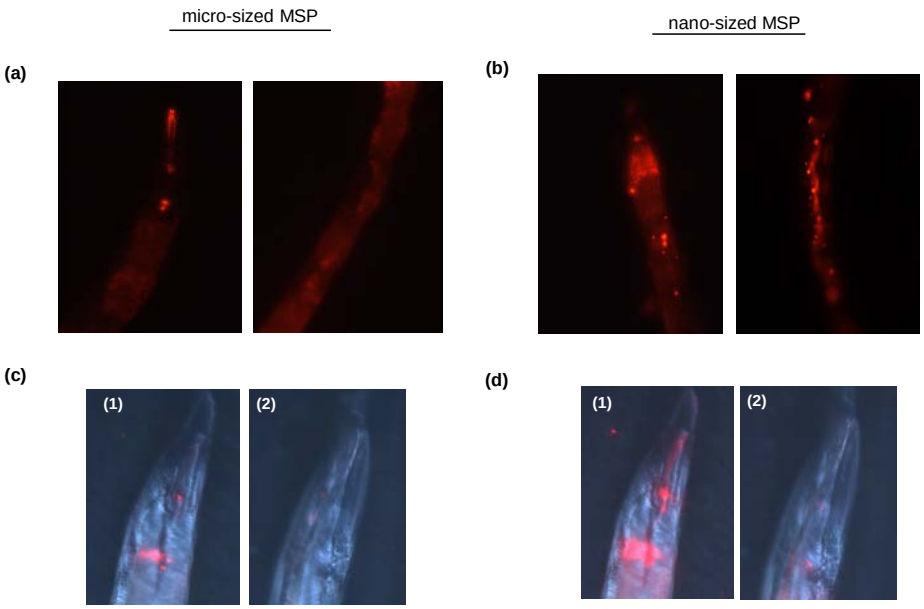

Figure 5.3-2. Particles monitored by fluorescence microscopy. (a) Micro-sized, MSP were effectively ingested by *C. elegans*, as well as (b) nano-sized, N0-rhd. No translocation

was confirmed by a lower fluorescence intensity between the worms of group (1) and group (2) for the worms fed with MSP (c) micro-sized, M0-rhd and (d) nano-sized, N0-rhd.

Influence of MSP size in C. elegans toxicity

The effect of **M0** and **N0 MSPs** on *C. elegans* lifespan was then analyzed. By using the above mentioned procedure to seed MSPs on agar plates, nematodes were fed throughout their life expectancy with three doses (0.5, 5 and 50 µg ml^{-1}) of **M0** and **N0**. In parallel, nematodes fed only on bacterial food were evaluated as the control population. Survival curves andmean lifespan (defined as the time when 50 % of worms were dead) were obtained.

Results showed that both control population and nematodes fed with **M0** displayed a similar lifespan at the three doses assayed (Figure 5.3-3A and Appendix 5.3 Figure S5). Thus, mean lifespan of **M0**-fed nematodes was similar than control fed nematodes, obtaining very similar survival curves. Only slight reduction of viability was observed with the higher dose (50 µg/mL), probable due to a reduction of confort of nematodes by the high density of microparticles in the agar.

In contrast, mean lifespan was significantly reduced at the three **N0** doses compared to the control population (p-values: 0.001; 0.007 and 0.002, for 0.5; 5.0; and 50 µg·ml^{-1}, respectively) (Figure 5.3-3A) . Moreover, survival curves showed a shortened lifespan for worms fed with **N0** at the three doses assayed

(Figure 5.3-3B, and Appendix 5.3-Figure 6S). These results clearly indicated that bare nano-sized MSPs are harmful for *C. elegans,* because a significant reduction in nematode survival was observed.

In order to further analyze the impact of feeding nano and micro-sized MSPs by nematodes, the movement capacity of *C. elegans* exposed to MSPs was evaluated. It has been previsouly reported that a declining of body movement is a change associated with premature aging (Pluskota et al., 2009; Scharf et al., 2013), Therefore, movement capacity (quantified as the total right bends per minute) of 2-day adult worms (Figure 5.3-3C) and 9-day adults (Figure 5.3-3D) was evaluated in *C. elegans* fed with 0.5, 5 and 50 μg ml^{-1} of **M0** and **N0** respectively, and compared with the control population.

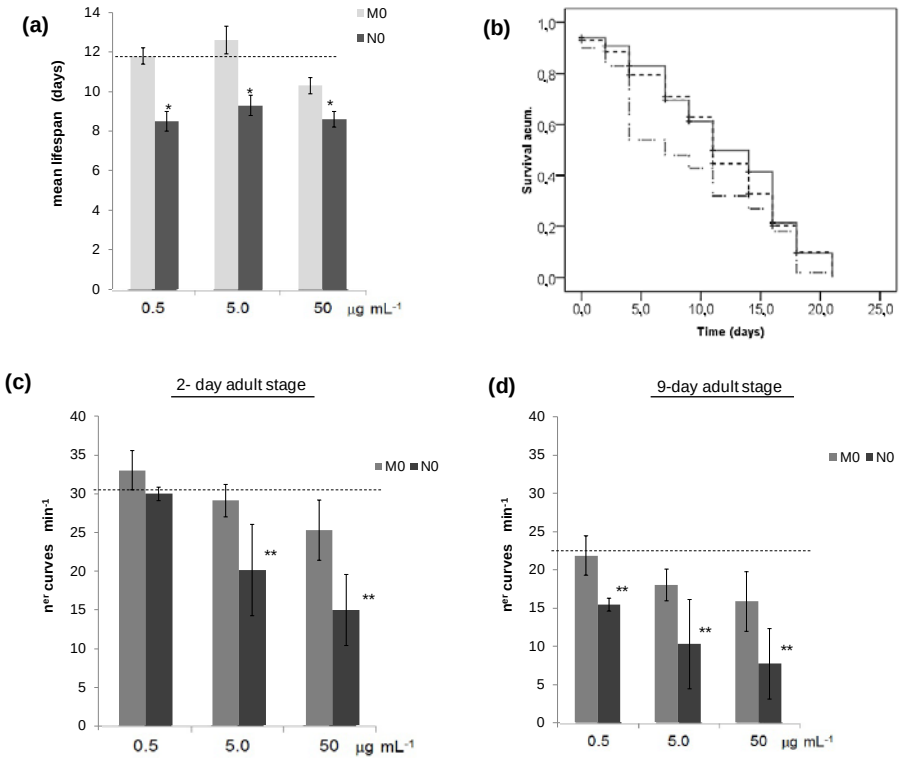

Figure 5.3-3. Evaluation of *C. elegans* behaviour after micro and nano-sized MSP were oral administered. (a) Mean lifespan of three MSP doses, X-axis: 0.5 µg·ml-1 5 µg·ml-1 and 50 µg·ml-1, showed a significant reduction due to nano-sized MSP. Dotted line represents the control population, grey Bars the M0 and darker bars the N0. (b) Lifespan of the nematodes fed with the same concentration, 0.5 µg·ml-1 of M0 and N0, showed a significantly reduced whole life cycle in the nematodes fed with N0 and not with M0 (Lifespan with other doses in Supporting material, Appendix 5-3 Figure S5-S6).

The dotted line represents the control population, the solid line denotes M0 and the dotted line (-- ·· --) indicates N0. Movement capacity analysed as a mean speed (n^{er} curves per min) of the worms administered the three M0 and N0 doses was evaluated in the (c) 2-day adult stage and (d) the 9-day adult stage. the dotted line (---) represent the control population, grey bars denote M0, and darker bars represent N0 (lifespan and movement evaluations were made in triplicate).

Significant differences as $p < 0.01$: *Mean lifespan data of the worms fed with **N0** compared to the control population gave the following p-values: 0.001; 0.007 and 0.002, for 0.5; 5.0; and 50 µg·ml-1, respectively (means and standard deviations, n = 300). **Movement capacity of the worms fed with **N0** compared to the control population resulted in p-value: 0.04 and 0.08 for the 5 and 50 µg·ml-1concentrations, respectively. P-values for 9-day adults: 0.05, 0.01 and 0.002 for 0.5; 5.0; and 50 µg·ml-1, respectively (means and standard deviations, n=210)·

In 2-day adult, the movement capacity of nematodes fed with low **M0** doses did not differ from that of the control population (Figure 5.3-3C). A slightly reduced movement was noticed in worms fed with 50 µg ml^{-1} of **M0,** but this was not statistically significant. In contrast, the effect of **N0** on depletion of movement was already evident and was significant in a dose-response manner (p-value: 0.04 and 0.08 for the 5 and 50 µg·ml^{-1}, respectively) (Figure 5.3-3C).

On the assumption that as worms aged, their motility begins to progressively slowdown, the movement of 9-day adults was quantified. The movement capacity of nematodes fed with **M0** showed similar number of curves per minute compared to the control population (Figure 5.3-3D). However, a significant reduction in movement capacity was also clearly evident in nematodes fed with **N0** (p-values for 9-day adults: 0.05, 0.01 and 0.002 for 0.5; 5.0; and 50 µg·ml^{-1}, respectively). The changes noted in nematodes' movement capacity feedingh **N0** suggested that bare mesoporous silica nano-sized particles have a toxic-impact on *C. elegans.* This clearly contrast with micro-sized MSPs, which have no significant effect on nematodes' movement or mean lifespan.

Effect of surface functionalisation on MSPs toxicity

The hypothesis of improving biocompatibility of inorganic nanomaterials through surface functionalisation was considered in this section (Wu et al., 2011; Caballero-Díaz et al., 2013; Santos et al., 2010; Bimbo et al., 2010). Evidence from

studies in cells has revealed that surface modification by anchoring organic groups in silica-based particles may modulate toxicity and may mitigate undesirable biological effects (Lankoff et al., 2013). Thus, in this context, evaluation of *C. elegans* fed with **M1** and **N1** in terms of lifespan and movement capacity was studied.

Lifespan evaluation showed no appreciable viability reduction in worms fed with **M1** compared with the control population and no significant differences between **M0** and **M1** were evidenced (Figure 5.3-4A). However, remarkable differences were found between nematodes fed with **N0** and **N1** (p-value: 0.017), see Figure 5.3-4B. As state above, mean lifespan of nematodes fed with **N0** significantly reduced compared to the control population, whereas mean lifespan of *C. elegans* fed with **N1** considerably increased when compared with **N0** (Appendix 5.3-Table S1) and was similar to that of the control population. This indicates a remarkable positive effect by coating nano-sized MSPs with the starch derivative.

Regarding movement capacity in *C. elegans*, no significant differences were found between nematodes fed with **M0** and **M1** (Figure 5.3-4C), whereas a significant increase in mobility was determined in **N1**-fed nematodes compared with **N0**-fed ones (see Figure 5.3-4D). This observation was specifically significant in 2-day adult nematodes fed with 0.5, 5 and 50 μg ml^{-1} of **N1** (p-value: 0.002) and

also in 9-day adult nematodes fed with 0.5 and 5 μg ml^{-1} (p-value: 0.015). In contrast, the 9-day adult nematodes fed with 50 μg ml^{-1}**N0** or **N1** displayed a similar movement capacity, which suggests that the positive starch functionalisation effect observed in young adult nematodes became less effective as they aged specially when using large concentration of the nanoparticles.

The above lifespan and movement capacity data are well correlated. Results demonstrated that toxicity of mesoporous silica particles is related to particle size and doses, and may be reduced by surface functionalisation. Regarding *C. elegans*' body movement, some authors have pointed out that depletion in movement is associated with reduced motor function, muscle structure and cellular deterioration (Garigan et al., 2002; Herndon et al., 2002).

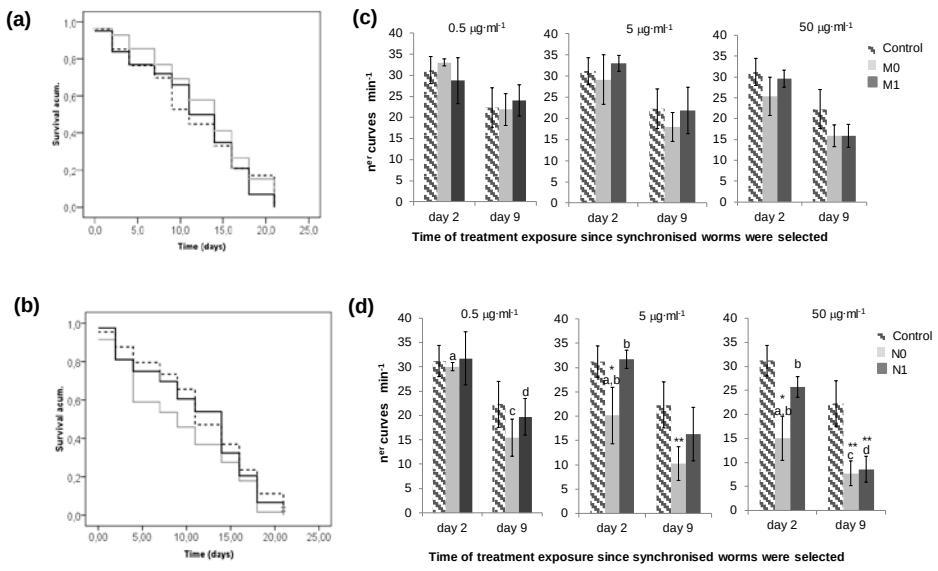

Figure 5.3-4. Influence of surface functionalisation of MSPs on *C. elegans* toxicity. (a) Lifespan assays were carried out with 5 µg mL^{-1} of particles M0 and M1, and (b) N0 and N1 (Lifespan other concentrations, see Appendix 5-3 Figure S7-S8). **Dotted line represents the control population, the grey line indicates bare particles (M0 and N0) and the black line denotes functionalised particles M1 and N1. Movement capacity analysed as the mean speed (n^{er} curves/min) of the worms fed with different concentrations of (c) M0 and M1 and (d) N0 and N1. Striped bars represent the control population; light grey bars indicate bare particles and dark grey bars show functionalised particles.**
Significant differences as $p < 0.01$ compared to the control population: the evaluation on day 2 showed differences *between **N0** and the control population. a Differences between **N0** administered at three doses, with a p-value: 0.025 and b differences between: **N0-N1**, with a p-value: 0.017. The evaluation on day 9 showed differences **between **N0** and the control population, c differences between **N0** administered at three doses, with a p-value: 0.002, and d between **N1** concentrations with p-value: 0.015 (means and standard deviations, n=210).

Therefore, it could be hypothesised that functionalisation with starch modifies the way nano-sized particles interact and influence functions in nematodes resulting in less toxicity. The functionalisation of the mesoporous silica nanoparticles with (**Glu-N**) (when compared to bare nanoparticles) improve biocompatibility and induces a recovery of lifespan and movement capacity of *C. elegans*.

Taking into account that nano-size particles can produce toxicity in *C. elegans*, we further studied other health-related variables, such resistance to oxidative stress and offspring. In *C. elegans*, a positive connection between lifespan and stress-resistance has been demonstrated for a variety of studies (Amrit et al., 2010; Grompone et al., 2012).

Therefore, in this section, changes in sensitivity to oxidative stress of *C. elegans* fed with the mesoporous silica particles was studied. The percentage of

nematodes survival after H_2O_2-induced oxidative stress was determined in a population fed with bare and functionalised nano- (**N0** and **N1**) particles. The control population was seeded on NGM plates with only bacterial food. The positive population was placed on NGM plates with antioxidant ascorbic acid (10 μg mL^{-1}) added along with bacterial food. According with previous results, *C. elegans* fed with **N1** showed better resistance to oxidative stress than those fed with **N0** (p-value: 0.009 and 0.029 to 0.5 and 5 μg·ml^{-1}, respectively), see Figure 5.3-5a.

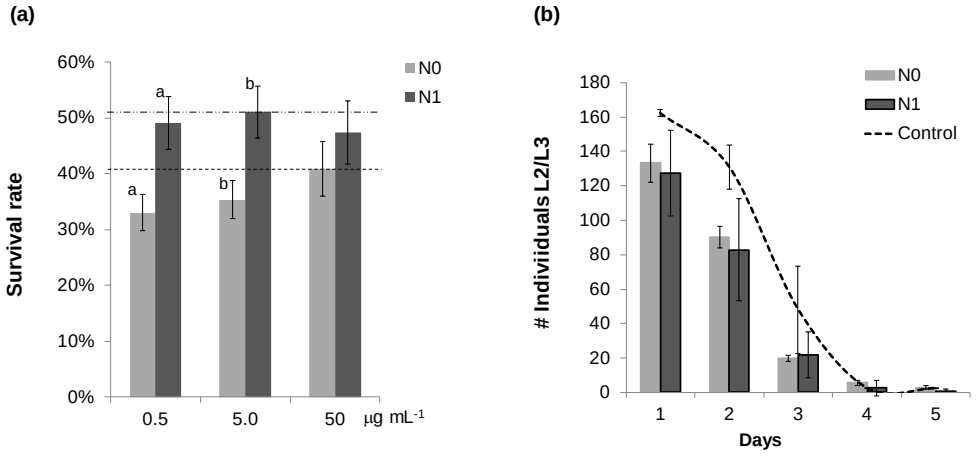

Figure 5.3-5. a) Resistance to oxidative stress in the worms fed with MSP. Three doses were evaluated (X axis) 0.5; 5 and 50 μg·ml^{-1}. Grey bars correspond to N0 and darker bars to N1. B) Progeny distribution showed a decrease on day 2 for the worms fed with MSP (5 μg·ml^{-1}): grey bars refer to the offspring of the worms fed with N0, darker bars indicate the worms fed with N1 and the dotted line denotes the control population

The dotted line (- -) represents the survival rate for the control population; the dotted line (-- ·· --) is the survival rate of the vitamin C-treated worms. Three independent experiments with 5 NGM plates and 15 individuals per plate were tested per treatment.

Significant differences between uncoated and coated particles, (grey and dark bars) with $p < 0.01$: a for concentrations 0.5 $\mu g \cdot ml^{-1}$ (p-value: 0.009), and b 5 $\mu g \cdot ml^{-1}$ (p-value: 0.029) (means and standard deviations, n=210)

Apart from reduction on resistance to oxidative stress, previous studies on *C. elegans* have shown that particles smaller than 50 nm, directly affect ovoposition due to translocation of the nanoparticles from primary organs, such as epithelial cells of the intestine, to secondary organs that belong to the reproductive tract. It was mainly found for amorphous (non-porous) silica particles, particles accumulate around nematodes and block certain organs, such as the vulva, which induce egg hatching in the parent's body (Pluskota et al., 2009). Although the present study evaluated mesoporous-silica and relatively larger particles (nano-sized MSPs are in a size range of 80-100 nm), and no accumulation of the MSPs in the vulva and in the germ line (*vide ante*) was observed, an additional progeny analysis was performed on worms fed with bare and functionalised nano-sized MSPs.

Laid eggs and the subsequent progeny of worms fed with three different doses of N0 and N1 particles were measured. Progeny distribution of worms fed with doses of 5 $\mu g \cdot ml^{-1}$ is shown in Figure 5.3-5b (to see the effect of additional dose see Appendix 5.3-Figure S9).

Progeny evaluation indicated that *C. elegans* (control population) laid the most eggs on adult day 1 and that the offspring rate was depleted in adult worm

day 2 and 3 (Figure 5.3-5b). Results suggest that nanoparticles generate acute stress on fertility because ovoposition was significantly affected from day 1 to adult day 2. In particular, nematodes fed with **N0** showed an oviposition rate significantly lowered on adult day 2 compared to the control population (p-value: 0.01). In contrast, nematodes fed with **N1** showed a minor depletion, which was not significant compared with control population (p-value: 0.6). These indicates that functionalised particlesexhibited a slightly improvingin the reproductive status of nematodes.

Since there was no reason to associate progeny depletion to only accumulation in the vulva, we suggested that the functions associated with fertility could be more sensitive to external stress due to the exposition to nano-size MSPs. It could somehow be related to the depletion of the healthspan variables, which agrees according with previous reports, where nervous parameters were related with movement and egg-laying phenotypes (Scharf et al., 2013). In any case, the heatlhspan evaluation performed in *C. elegans* offers an interesting methodology for evaluating the influence of the surface modification of MSPs on nanotoxicity. Nonetheless, more extensive studies into phenotype expressions and stress biomarkerswould be of interest and will be carried out in due course.

Conclusions

Here we show the feasibility of using *C. elegans* as *in vivo* model to evaluate the toxicity of MSPs. The intake of micro and nano-sized MSPs has been demostrated, being the gastrointestinal tract and the pharinx the main body regions for its accumulation. Evaluation of lifespan and other age-related parameters in nematodes exposed to micro and nanoparticels has allowed to demostrate the safety of micro-sized MSPs. Moreover, toxicity of nano-sized MSPs has been evidenciated through the decrease of lifespan, a reduction of movement, a depletion of the reproductive status and an increase in the sensitivity to oxidative stress. Furthermore, the starch-functionalized mesoporous silica nanoparticles (**N1**) have no significant effect in lifespan and healthspan of *C. elegans*. These results strongly suggested that surface functionalisation of MSPs is a suitable strategy to reduce toxicity and enhance biocompatibility of the smallest particles.

Acknowledgments

The authors wish to express their gratitude to the Spanish Government (MINECO Projects AGL2012-39597-C02-01, AGL2012-39597-C02-02, AGL2015-70235-C2-1, MAT2012-38429-C04-01 and MAT2015-64139-C4-1), the Generalitat Valencia (Project PROMETEOII/2014/047) and Colombian Administrative Department of Science, Technology and Research. We would also like to thank the Institut de Ciència dels Materials (ICMUV), the Microscopy Service of the

Universitat Politècnica de València and the microscopy service of IATA for technical support. We thank Roquette for the Glucidex samples.

References

Agostini A, Sancenón F, Martínez-Máñez R, Marcos MD, Soto J, Amorós P. 2012. A photoactivated molecular gate. Chem. Eur. J.; 18:12218–12221.

Amrit, F., May, R., 2010. Younger for longer: insulin signalling, immunity and ageing. Curr Aging Sci 3, 166–76.

Angelos S, Johansson E, Stoddart JF, Zink JI. 2007. Mesostructured Silica Supports for Functional Materials and Molecular Machines. Adv. Func. Mater.;17:2261-2271

Angelos S, Khashab NM, Yang YW, Trabolsi A, Khatib HA, Stoddart JF, Zink JI. 2009. pH clock-operated mechanized nanoparticles. J. Am. Chem. Soc.; 131:12912–12914.

Arbor, A., Witzmann, F.A., 2013. Nanoparticle toxicity by the gastrointestinal route: evidence and knowledge gaps. doi:10.1504/IJBNN.2013.054515.Nanoparticle

Aznar E, Oroval M, Pascual Ll, Murguía JR, Martínez-Máñez R, Sancenón F. 2016. Gated Materials for On-Command Release of Guest Molecules. Chem. Rev.; 116:561-718.

Bernardos, A., Mondragon, L., Aznar, E., Marcos, M.D., Martínez-Manez, R., Sancenón, F., Soto, J., Barat, J.M., Perez-Paya, E., Guillem, C., Amoros, P., 2010. Enzyme-responsive intracellular controlled release using nanometric silica mesoporous supports capped with "saccharides." ACS Nano 4, 6353–6368.

Bimbo, L.M., Sarparanta, M., Santos, H.A., Airaksinen, A.J., Mäkilä, E., Laaksonen, T., Peltonen, L., Lehto, V.P., Hirvonen, J., Salonen, J., 2010. Biocompatibility of thermally hydrocarbonized porous silicon nanoparticles and their biodistribution in rats. ACS Nano 4, 3023–3032.

Brunauer P.H. Teller, E., S.E., 1938. Adsorption of gases in multimolecular layers. J. Am. Chem. Soc. 60, 309–319.

Caballero-Díaz, E., Pfeiffer, C., Kastl, L., Rivera-Gil, P., Simonet, B., Valcárcel, M., Jiménez-Lamana, J., Laborda, F., Parak, W.J., 2013. The Toxicity of Silver Nanoparticles Depends on Their Uptake by Cells and Thus on Their Surface Chemistry. Part. Part. Syst. Charact. 30, 1079–1085.

Cabrera, S., El Haskouri, J., Guillem, C., Latorre, J., Beltrán, A., Beltrán, D., Marcos, M.D., Amorós, P., 2000. Generalised syntheses of ordered mesoporous oxides: the atrane route. Solid State Sci. 2, 405–420.

Cha, Y.J., Lee, J., Choi, S.S., 2012. Apoptosis-mediated *in vivo* toxicity of hydroxylated fullerene nanoparticles in soil nematode *Caenorhabditis elegans*. Chemosphere 87, 49–54.

Coll, C., Bernardos, A., Martínez-Manez, R., Sancenón, F., 2013. Gated silica mesoporous supports for controlled release and signaling applications. Acc Chem Res 46, 339–349.

Consortium, C. elegans S., 1998. Genome sequence of the nematode *C. elegans*: a platform for investigating biology. Science (80-.). 282, 2012–8.

Fu Q, Rao VR, Ista LK, Wu Y, Andrzejewski BP, Sklar LA, Ward TL, López GP. 2003. Control of molecular transport through stimuli-responsive ordered mesoporous materials. Adv. Mater.; 15:1262–1266.

Garing, D., Hsum AL., Frase, A., Kamath, R., Ahringer, J., Kenyon, C., 2002. Genetic analysis

of tissue aging in *Cenorhabditis elegans*: a role for heat- shock factor and bacterial proliferation. Genetics 161, 1101.2.

Glenn, C.F., Chow, D.K., David, L., Cooke, C. a, Gami, M.S., Iser, W.B., Hanselman, K.B., Goldberg, I.G., Wolkow, C. a, 2004. Behavioral deficits during early stages of aging in *Caenorhabditis elegans* result from locomotory deficits possibly linked to muscle frailty. J. Gerontol. A. Biol. Sci. Med. Sci. 59, 1251–1260. doi:59/12/1251 [pii]

Gonzalez-Moragas, L., Roig, A., Laromaine, A., 2015. *C. elegans* as a tool for *in vivo* nanoparticle assessment. Adv. Colloid Interface Sci. 219, 10–26.

Grompone G, Martorell P, Llopis S, González N, Genovés S, Mulet AP, Fernández-Calero T, Tiscornia I, Bollati-Fogolín M, Chambaud I, Foligné B, Montserrat A, Ramón D. Anti-inflammatory Lactobacillus rhamnosus CNCM I-3690 strain protects against oxidative stress and increases lifespan in Caenorhabditis elegans. PLoS One 2012;7:e52493

Herndon, L., Schmeissner, P., Dudaronek, J., Brown, P., Listner, K., Sakano, Y., Paupard, M., Hall, D., Driscoll, M., 2002. Stochastic and genetic factors influence tissue-specific decline in agening *C. elegans.* Nature 419, 808–14.

Kickelbick G. 2004. Hybrid inorganic-organic mesoporous materials. Angew. Chem. Int. Ed.; 43:3102-3104.

Leung, M.C.K., Williams, P.L., Benedetto, A., Au, C., Helmcke, K.J., Aschner, M., Meyer, J.N., 2008. *Caenorhabditis elegans*: An emerging model in biomedical and environmental toxicology. Toxicol. Sci. 106, 5–28. doi:10.1093/toxsci/kfn121

Ma, H., Bertsch, P.M., Glenn, T.C., Kabengi, N.J., Williams, P.L., 2009. Toxicity of manufactured zinc oxide nanoparticles in the nematode *Caenorhabditis elegans*. Env. Toxicol Chem 28, 1324–1330. doi:10.1897/08-262.1

Mal NK, Fujiwara M, Tanaka Y, Taguchi T, Matsukata M. 2003. Photoswitched storage and release of guest molecules in the pore void of coumarin-modified MCM-41. Chem. Mater.; 15:3385-3394

Mo R, Jiang T, Di J, Tai W and Gu Z. 2014. Emerging Micro- and nanotechnology based synthetic apporaches for insulin delivery. Chem. Soc. Rev; 43:3595–629

Pérez-Esteve, É., Oliver, L., García, L., Nieuwland, M., Jongh, H.H.J. De, Martínez-Máñez, R., Barat, J.M., 2014. Incorporation of Mesoporous Silica Particles in Gelatine Gels : Effect of Particle Type and Surface Modification on Physical Properties. Langmuir 30, 6970–6979.

Pluskota, A., Horzowski, E., Bossinger, O., von Mikecz, A., 2009. In *Caenorhabditis elegans* nanoparticle-bio-interactions become transparent: silica-nanoparticles induce reproductive senescence. PLoS One 4, e6622.

Roh, J.Y., Park, Y.K., Park, K., Choi, J., 2010. Ecotoxicological investigation of CeO_2 and TiO_2 nanoparticles on the soil nematode Caenorhabditis elegans using gene expression, growth, fertility, and survival as endpoints. Environ. Toxicol. Pharmacol. 29, 167–172.

Salonen J, Lehto V-P. 2008. Fabrication and chemical surface modification of mesoporous silicon for biomedical applications. Chem. Eng. J.; 137:162–172.

Sancenón F, Pascual Ll, Oroval M, Aznar E, Martínez-Máñez R. 2015. Gated Silica Mesoporous Materials in Sensing Applications. ChemOpen; 4:418-437.

Santos, H. a, Riikonen, J., Salonen, J., Mäkilä, E., Heikkilä, T., Laaksonen, T., Peltonen, L., Lehto, V.-P., Hirvonen, J., 2010. *In vitro* cytotoxicity of porous silicon microparticles: effect of the particle concentration, surface chemistry and size. Acta Biomater. 6, 2721–31. doi:10.1016/j.actbio.2009.12.043

Schafer, W., 2005. Egg-laying. WormBook 1–7. doi:10.1895/wormbook.1.38.1

Scharf, A., Piechulek, A., von Mikecz, A., 2013. Effect of nanoparticles on the biochemical and behavioral aging phenotype of the nematode *Caenorhabditis elegan*s. ACS Nano 7, 10695–10703.

Schlossbauer A, Kecht J, Bein T. 2009. Biotin-Avidin as a protease-responsive cap system for controlled guest release from colloidal mesoporous silica. Angew. Chem. Int. Ed.; 48:3092–3095.

Soler-Illia G-JAA, Azzaroni O. 2011. Multifunctional hybrids by combining ordered mesoporous materials and macromolecular building blocks. Chem. Soc. Rev.; 40:1107-1150.

Souris, J.S., Lee, C.H., Cheng, S.H., Chen, C.T., Yang, C.S., Ho, J.A.A., Mou, C.Y., Lo, L.W., 2010. Surface charge-mediated rapid hepatobiliary excretion of mesoporous silica nanoparticles. Biomaterials 31, 5564–5574.

Stein A. 2013. Advances in Microporouss and Mesoporous Solids- Highlights of Recent Progess.Adv. Mater, 2003;15:763-775.

Sun, L., Li, Y., Liu, X., Jin, M., Zhang, L., Du, Z., Guo, C., Huang, P., Sun, Z., 2011. Cytotoxicity and mitochondrial damage caused by silica nanoparticles. Toxicol. In Vitro 25, 1619–29. doi:10.1016/j.tiv.2011.06.012

Valtchev V, Tosheva L. 2013. Porous Nanosized Particles: Preparation, Properties, and Applications. Chem. Rev.; 113:6734-6760.

Vinu A, Hossain KZ, Ariga K. 2005. Recent Advances in Functionalization of Mesoporous Silica. J. Nanosci. Nanotechnol.; 5:347–371.

Wang, H., Wick, R.L., Xing, B., 2009. Toxicity of nanoparticulate and bulk ZnO, Al_2O_3 and TiO_2 to the nematode *Caenorhabditis elegans*. Environ. Pollut. 157, 1171–1177.

Wight AP, Davis ME. 2002. Design and Preparation of Organic-Inorganic Hybrid Catalysts. Chem. Rev.; 102:3589-3614

Wu, E.C., Andrew, J.S., Buyanin, A., Kinsella, J.M., Sailor, M.J., 2011. Suitability of porous silicon microparticles for the long-term delivery of redox-active therapeutics. Chem. Commun. (Camb). 47, 5699–5701.

Xu, C., Niu, Y., Popat, A., Jambhrunkar, S., Karmakar, S., Yu, C., 2014. Rod-like mesoporous silica nanoparticles with rough surfaces for enhanced cellular delivery. J. Mater. Chem. B 2, 253–256.

6 GENERAL DISCUSSION

In order to evaluate the mesoporous silica particles (MSPs) as supports for encapsulation of bioactive components. The present PhD thesis has encapsulated essential oil components (EOCs) in nano and micro sized MSPs.

To offer a better understanding of methodology and relevant findings; and according to the main objectives, results were divided into two sections: *Section I* deals with three different scenarios, where release of essential oils components (EOCs) encapsulated in mesoporous silica particles (MSPs) was evaluated. *Section II* addresses the toxicological *in vitro* and *in vivo* impact of MSPs.

Mesoporous silica-based particles are interesting supports for controlled delivery materials design. On the other hand, EOCs have shown bioactive properties asociated with gastrointestinal health, which can be valuable in future food or drug applications. Bearing in mind these facts, encapsulation may improve the biological stability of bioactive components while protects against adverse conditions. In addition, a controlled relase system can modulate the bioaccessibility of target components. In that sense, oral delivery results an interesting uptake route for functional products. However, the directly ingestion of inorganic materials, like MSPs, is still viewed as challenging.

Among the bioactive properties related to EOCs, the anticancer effect on colon cell lines was the focus of the first study. **Article 1** evaluates the viability

decrease of colon cells incubated with EOCs. Six-EOCs were selected: allyl thiocyanate, diallyl disulphide, eugenol, thymol, cinnamaldehyde and carvacrol. Activity of free and encapsulated EOCs was assessed on cancer and normal (no cancer) colon cells, and two main results were obtained: (i) A sustained anticancer effect along time, confirms the stability improvement of EOCs when encapsulated. (ii) The amount of encapsulated EOCs for viability decreasing of colon cancer cells is lower than required for non-cancer cells. This suggests a selectively effect of encapsulated EOCs.

Once the EOCs encapsulation and delivery was confirmed, the hypothesis to encapsulation may control the release of volatiles components and mask the unpleasant odours, was addressed. In a second scenary, diallyl disulphide, main responsible of unpleasant odour in garlic, was selected and encapsulated in micro sized MSPs. **Article 2** includes qualitative and quantitative assays to identify the diallyl disulphide release. Findings show that encapsulation is not enough to mask the unpleasant odours. For efficiently odour masking it is needed to coat the MSPs' surface. In particular, a previously described polysaccharide (hydrolysed starch, Glucidex 47) was grafted on MSPs surface. The dense monolayer of sugar molecules shapes an anchoring system, which deals with enzymatic stmuli. It means that release of encapsulated diallyl disulphide is only due to amylases

presence. Thus, starch-functionalised MSPs not only mask the unpleasant garlic-related odour, but also, control the masking effect with an enzymatic manner.

The final scene for EOCs' evaluation includes a hybrid support design for encapsulation and controlled release of diallyl disulphide-associated components. **Article 3** combines a composite material with "gate-like" structures based on MSPs. Micro-sized MSPs with two different anchoring systems were entangled on polyamidic nanofibers. Main results point that: (i) The hybrid composites show a sustained delivery in function of pH changes and enzymatic stimuli. (ii) The MSPs are effectively immobilised in nanofibers, even after release tests.

Section II evaluates mesoporous silica particles' toxicity, and the hypothesis of toxic decrease after surface functionalisation was considered. Two approaches were addressed: an *in vitro* study of viability of colon cells incubated with MSPs, and an *in vivo* evaluation through *C. elegans* model.

Article 4 evaluated cell viability, in relation to three MSPs features: doses, size and starch capped system. Results show that significant decrease of cell viability is obtained with smaller particles, higer doses, and bare particles. In function of the threshold dose of MSPs stablished on cell viability assays, the doses range of micro and nano sized MSPs was fixed for *in vivo* model. **Article 5**, analyses the lifespan and healthspan of *C. elegans* fed for 21 days with MSPs. Results confirm

two interesting facts: (i) There is a size-influence on MSPs toxicity risks, which are mainly associated to decrease of mean lifespan and damage in aging behaviour. (ii) Nematodes population fed with functionalised particles showed a health recovering in relation to population fed with smaller and bare particles.

Toxicity study of MSPs requires a whole particles characterization as well as is important identify possible uptake routes to define the assessments to apply. Thus, despite unknowledge MSPs heatlh effects, the findings of *Section II* suggest that certain particles are well tolerated by both cells and superior animals. Therefore, it is hard to draw conclusive conclusions about the biocompatibility and toxicity of MSPs as a unique concept. In any case, the use of biocompatible organic molecules to functionalise the MSPs' surface appears as a good strategy to minimize associated-risks while improves the controlled delivery of encapsulated components.

In this way, throughout both sections, the findings of all the studies carried out to asses the general objective of this thesis have been sequentially and relatedly discussed.

7 CONCLUSIONS AND PERSPECTIVES

Conclusions

- Mesoporous silica particles (MSPs) are suitable supports to encapsulated and control the release of essential oil components (EOCs).

- The *in vitro* effect of EOCs against colon cancer cells was confirmed. In addition, the encapsulation of EOCs enhace their anticancer effect due to a sustained effect along the time and a yield improvement.

- Encapsulated EOCs showed a selectively effect on cancer cells, while a mild effect was evidenced on normal colon cells.

- A masking encapsulation system for garlic-related odour was described. Major bioactive component in garlic (diallyl disulphide, **DA**) was encapsulated in mesoporous silica supports, and the surface functionalisation allows the masking of unpleasant odours while control the delivery in function of an enzyme stimuli.

- A new composite material based on the incorporation of two gated silica mesoporous hybrid solids on a electrospun polyamidic nanofiber have been prepared and their controlled release behaviour was confirmed.

- Composites development including gate-like systems based on silica are interesting way to prepare smart fabrics showing “zero” release that can be opened at will using appropriate stimuli.

- The effect of size, doses and surface functionalisation of mesoporous silica particles was evaluated to determine a low toxicity system.

- Depletion of cell viability not only depends of size and surface characteristics but also it strongly depends on synthesis process to obtain MSPs.

- The *in vivo* studies confirm that MSPs are effectively ingested by a multicellular model.

- The oral administration of MSPs to *C. elegans* strongly suggest that surface functionalisation (especially for nanoparticles) is a suitable strategy to reduce toxicity and enhance biocompatibility.

- The encapsulation approach evaluated in this thesis offers new opportunities for the development of functional products. And also motivate the future design of new hybrid supports for oral delivery applications with low and zero-risk for health.

Future Perspectives

- These results can be extrapolated to the encapsulation and protection of other bioactive components of nutritional and industrial interest.
- *In vivo* evaluations need to be assessed to evaluate the EOCs anticancer effect.
- The nanotoxicological evaluation of bare and functionalised MSPs need to be studied in murine models, to identify the acute and chronic toxicity.
- The future developments related with on-command delivery of natural-derived anticancer agents and their application on *in vivo* models should include omics techniques to understand the associated mechanisms.

8 APPENDICES

Appendix I. Scientific comunications

Papers published

Carolina Acosta, Edgar Pérez-Esteve, Carlos A. Fuenmayor, Simona Benedetti, Maria Stella Cosio, Juan Soto, Félix Sancenón, Saverio Mannino, José Barat, María D. Marcos, and Rámon Martínez-Máñez. Polymer Composites Containing Gated Mesoporous Materials for On-Command Controlled Release. *ACS Applied Materials & Interfaces*. **2014** 6 (9), 6453-646

Pérez-Esteve, É., Fuentes, A., Coll, **C., Acosta,** C., Bernardos, A., Amorós, P., Marcos, M.D., Sancenón, F., Martínez-Máñez, R., & Barat, J.M. (2014) Modulation of folic acid bioaccesibility by encapsulation in pH-responsive gated mesoporous silica particles. Microporous & Mesoporous Materials, 15, 124-132.

Oral communications

"X International workshop on sensors and molecular recognition". Nanotoxicology Evaluation of Functionalized and Non-functionalized Mesoporous Silica Particles on *Caenorhabditis elegans* **C. Acosta,** P. Martorell, S. Genovés, D.Ramon, J. M. Barat, R. Martínez-Máñez. Valencia, Spain, Julio **2016**

"6th International Conference on Nanotechnology: Fundamentals and Applications". Validation of *Caenorhabditis elegans* as an *in vivo* model for nanotoxicological studies of mesoporous silica particles. **C. Acosta**, J. M. Barat, R. Martínez-Máñez, M. Orzaez, P. Martorell, S. Llopis, N. Gonzalez, S. Genovés, D. Ramón. Barcelona, Spain, July **2015**

"VIII Congreso CYTA/CESIA" Surface Functionalization of silica nanoparticles to reduce toxicity of nanomaterials for food applications. **C. Acosta**, J. M. Barat, R. Martínez-Máñez, S. Llopis, N. Gonzàlez, D. Ramón,S. Genovés, P. Martorell., Badajoz, Spain, Abril **2015**.

Poster presentation

"X International workshop on sensors and molecular recognition". Activity Of Essential Oil Components Against Colon Cancer Is Enhanced Through Encasulation Into Mesoporous Silica Particles. **Carolina Acosta**, Andrea Bernardos, Miroslava Císarová, Pavel Kloucek, José Manuel Barat, Ramón Martínez-Mañéz. Valencia, Spain, Julio **2016.**

"IX International workshop on sensors and molecular recognition". Toxicity evaluation of functionalized mesoporous silica nanoparticles in *C. elegans* as *in vivo* model. **C. Acosta**, C. Coll, P. Martorell, D.l Ramon, J. M. Barat, R. Martínez-Máñez. Valencia, Spain, Julio **2015**

III Congreso Internacional de Calidad y Seguridad Alimentaria ACOFESAL 2015 (ISBN 978-84-606-8827-3) Evaluation of bioactive garlic compounds entrapped into a gated mesoporous silica system. **Acosta, Carolina**.; Martínez-Máñez, Ramón; Barat Baviera, José Manuel. Orzáez, Mar. Valencia, Spain, Junio **2015**

"VIII Congreso CYTA/CESIA". Hybrid nanocomposites for encapsulation and controlled release of antioxidant phenolic compounds. C. Fuenmayor, **C. Acosta**, E. Pérez-Esteve, F. Sancenón, P. Hernández-Muñoz, R. Gavara, J. M. Barat, M. D. Marcos, R. Martínez-Máñez. Badajoz, Spain, Abril **2015**

" VI Workshop on sensors and molecular recognition". Electrochemical monitoring of garlic compounds released from masoporous silica microparticles, coated by polyamine and immobilized into nylon nanofibers **Carolina Acosta**, Simona Benedetti, Edgar Péreza, José Barat, Ramón Martinez, Saverio Mannino. Valencia, España **2012**

Appendix 4.3: A study of capped mesoporous silica supports as masking garlic odour systems

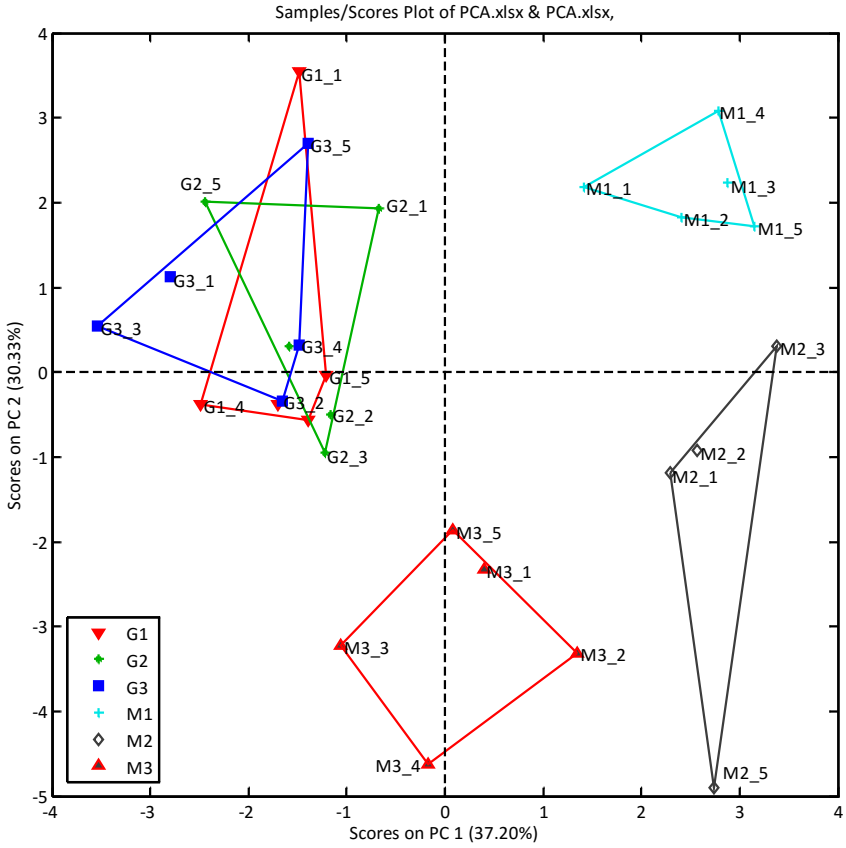

Figure S1. Principal Component Analysis with two principal components

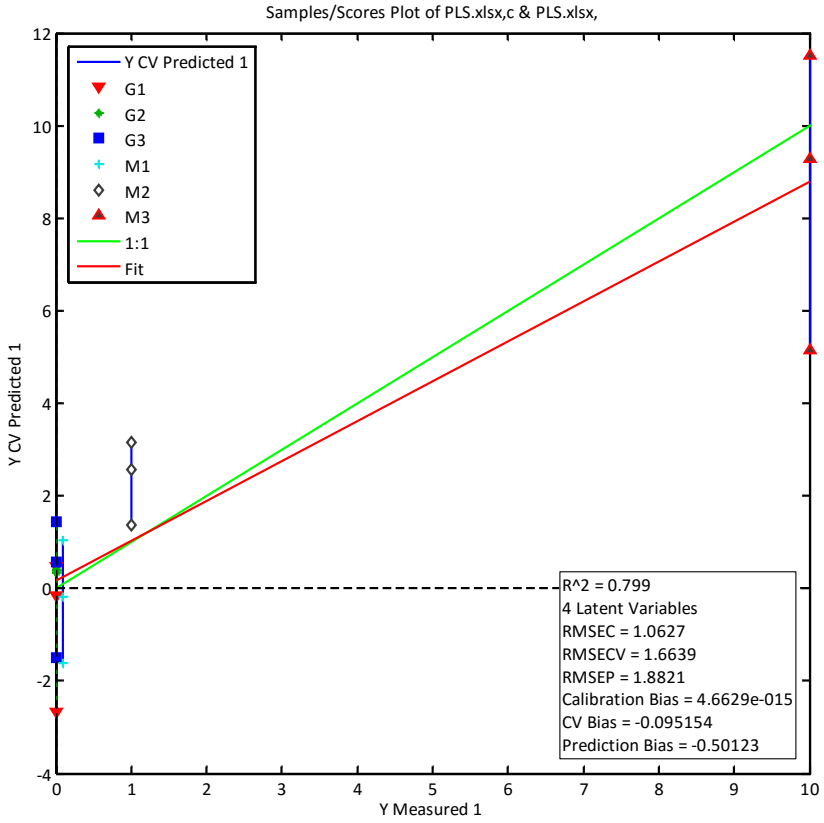

Figure S2: Partial Least Square analysis

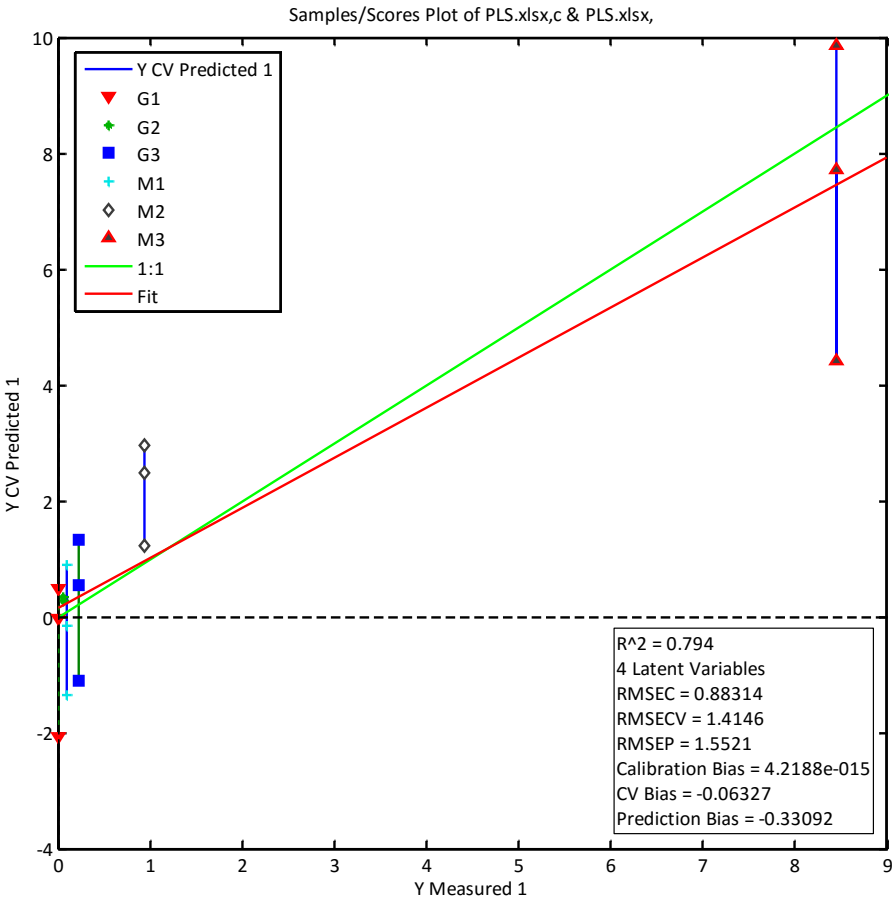

Figure S3 Partial Least Square analysis with release data

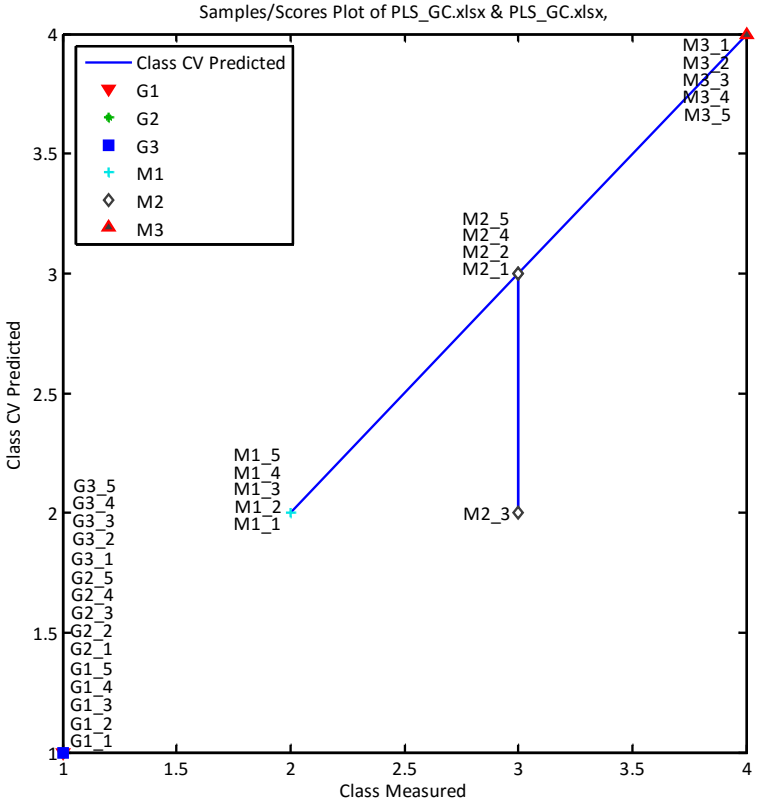

Figure S4. Support Vector Machine, SVMDA

Appendix 4.4: Polymer composites containing gated mesoporous materials for on-command controlled release

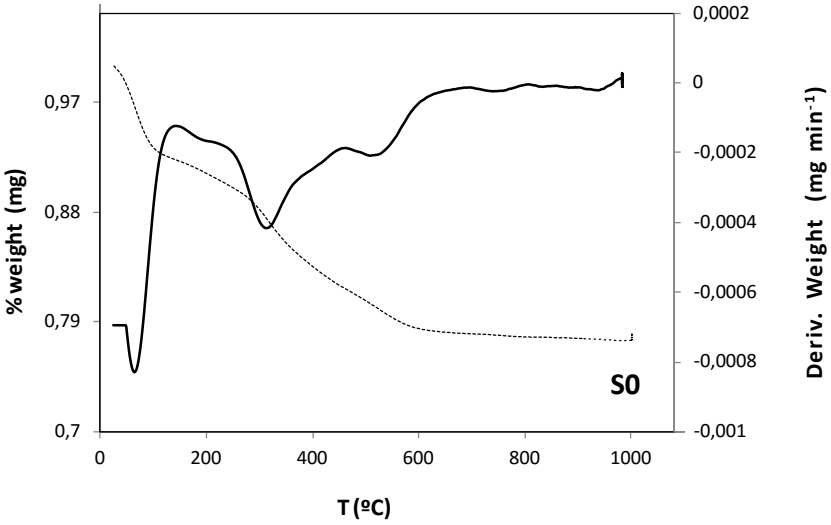

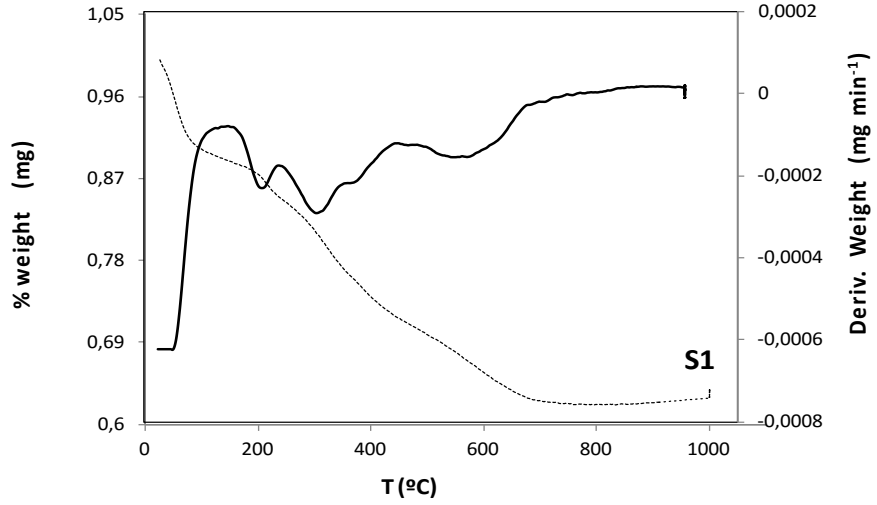

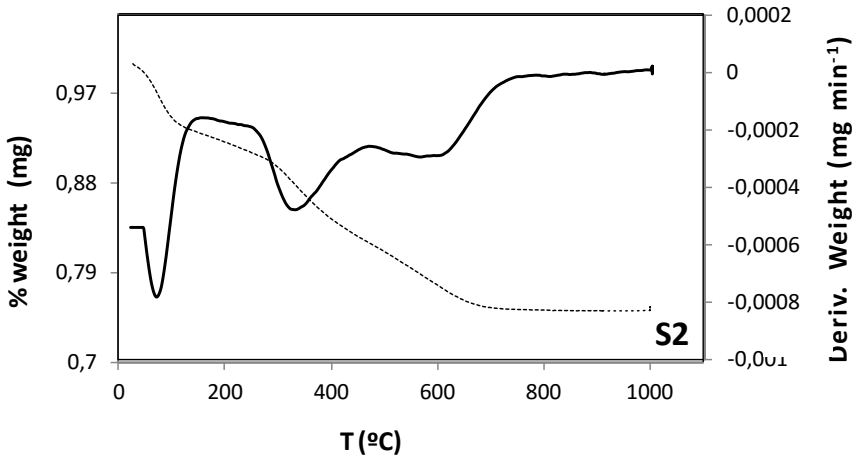

Figure S1. TGA Analyses for solids **a)** Mesoporous microparticle MCM-41 loaded with garlic extract, (**P0)**, **b)** Particle loaded and functionalized with **N3**-gate (**P1**) and **c)** Particle loaded and functionalized with **G47**-gate (**P2**). Curve of weight loss (**- - -**) and 1st derivative of the weight loss curve (**▬**)

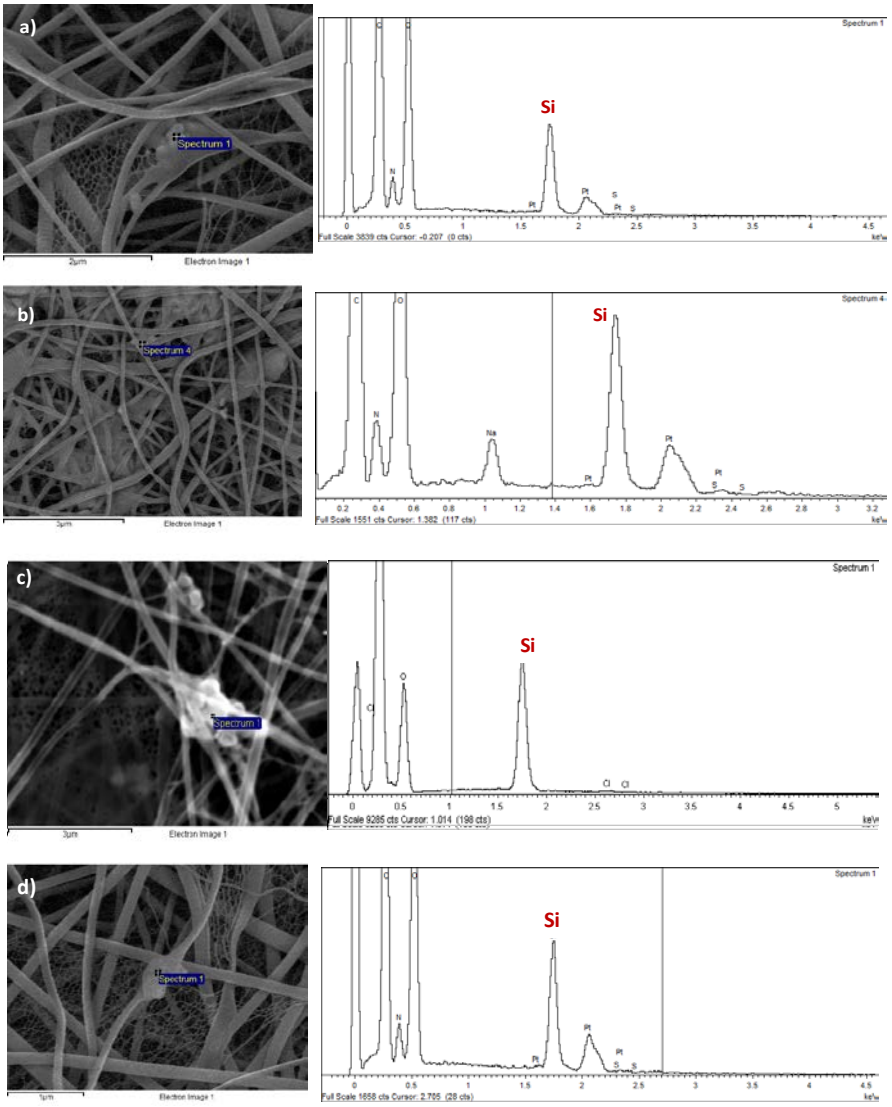

Figure S2. Representative EDX spectra **a)** Composites **M1** with microparticles entangled before release procedure and **(b)** Composites **M1** after release procedure. **c)** Composites **M2** with microparticles entangled before release procedure and **d)** Composites **M2** after release procedure analysed by FE-SEM[2]

[2] EDX analyses were carried out by FE-SEM ULTRA 55-44-22 evaluated by secondary (SE2) and backscattered electrons (AsB) detectors. In specific case of M2 before release procedure (Figure S2 a. EDX assay were done by Field Emission Scanning Electron Microscope JEOL JSM6300, were samples were sputter coated with graphite.)

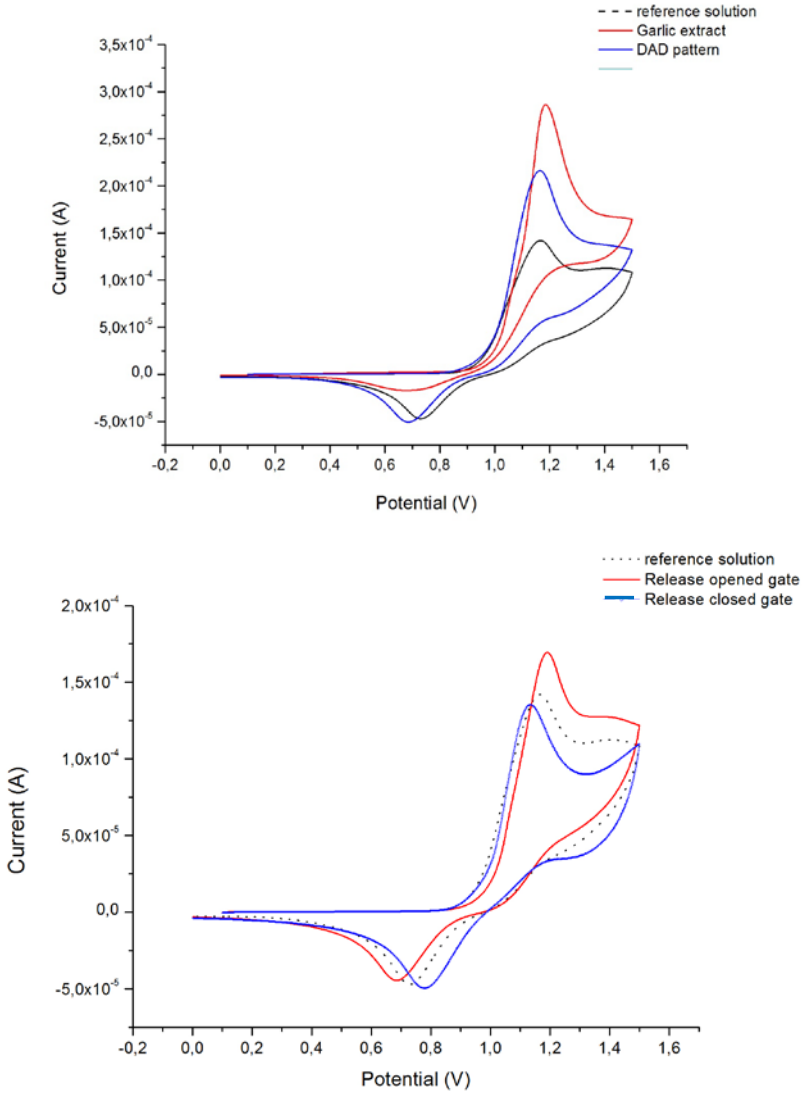

Figure S3. a) Voltammetric evaluations of garlic extract and diallyl disulfide (DAD) pattern **b)** Brief sampling of voltammetric evaluations of release studies

Appendix 5.3: A *C. elegans in vivo* nanotoxicology evaluation of bare and functionalised micro and nano mesoporous silica particles

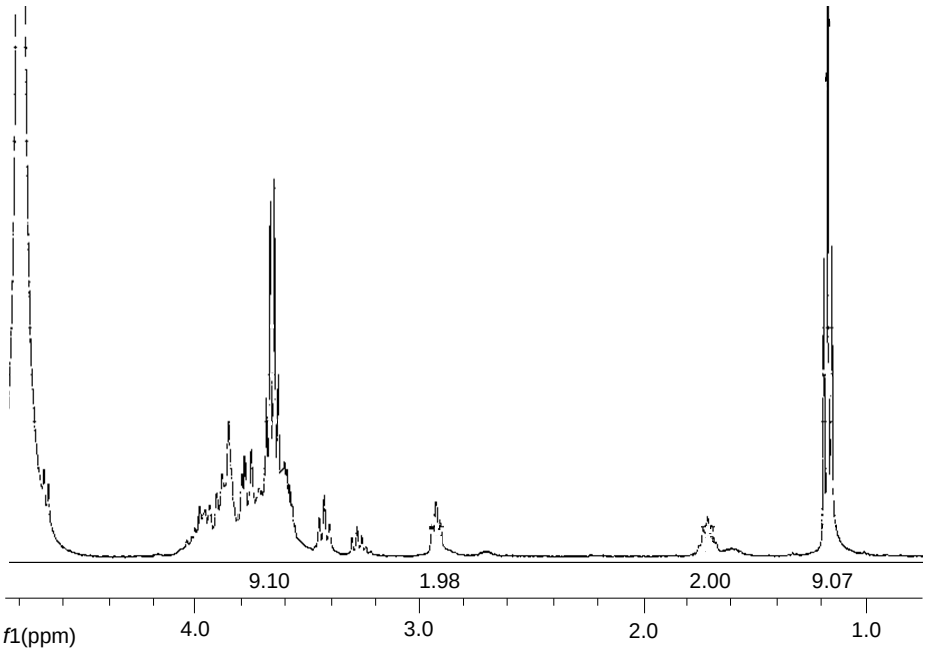

Figure S1. ^{1}H-NMR spectrum of **Glu-N.** Starch derivative was obtained after starch reaction with amino group from hemiacetal hydroxyl of APTES, which is compatible with the shift from 2.4 ppm to 2.8 ppm. Signal at 2.4 ppm appears to APTES methylene which is bonded to amino group.

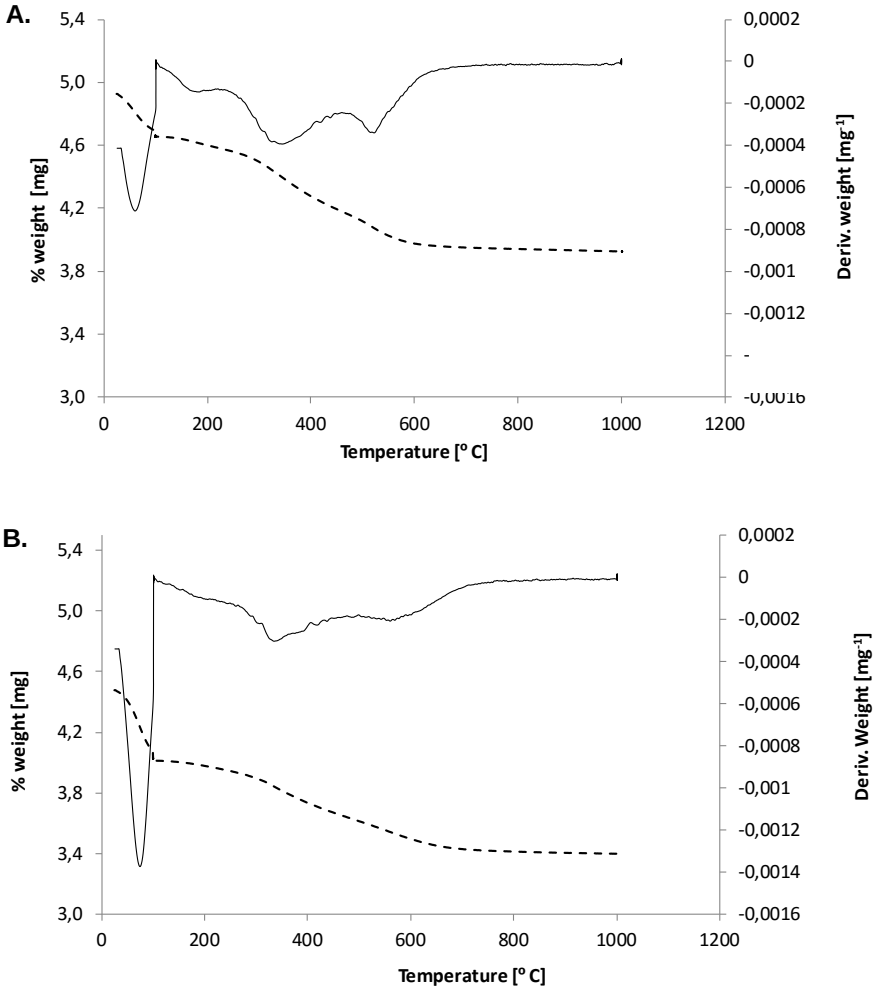

Figure S2. TGA Analyses for MSPs **A.** Functionalised micro-sized particles, **M1** and **B.** Functionalisednano-sized particles **N1.** Curveofweight loss (- - -) and 1st derivative of the weight loss curve (--)

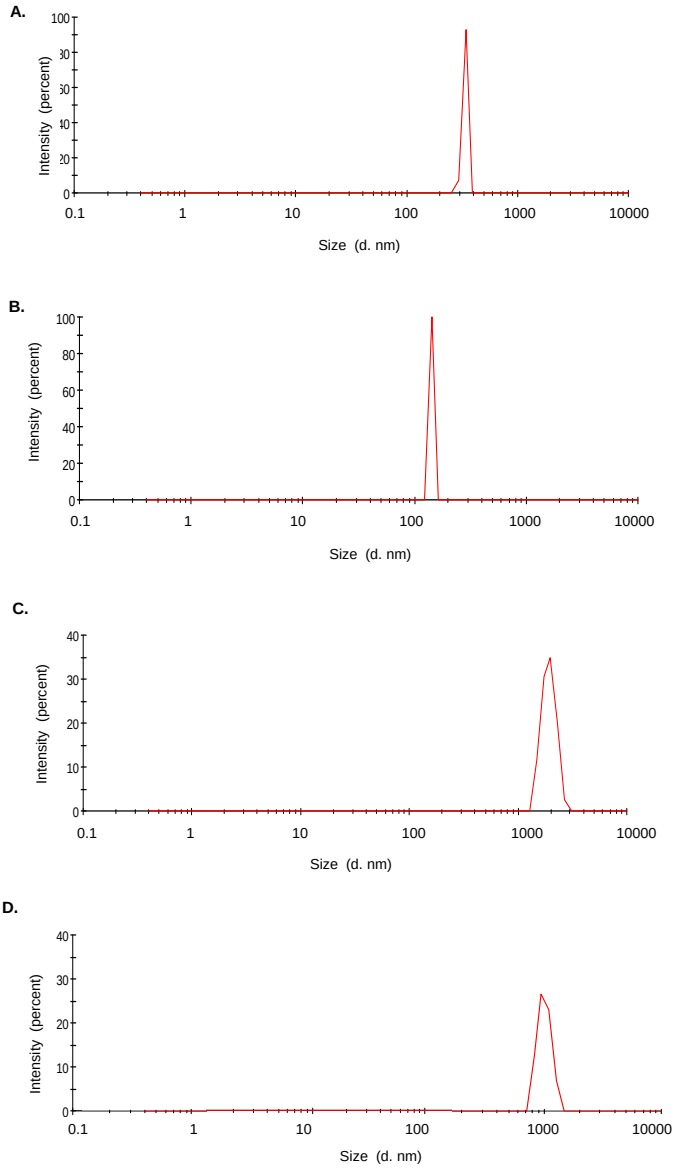

Figure S3. Size distribution by Intensity, Determined by dynamic light scattering, DLS**,** to: **A. N0, B. N1, C. M0 and D. M1**

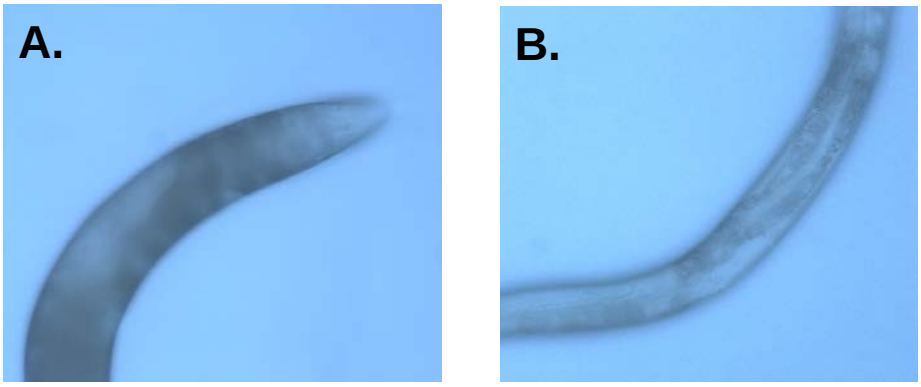

Figure S4. There was no evidence of significant red signal in progeny of worms from group (2) fed with**A**.Worms fed with**M0-rhd,** a representative image of pharynxregion and **B.** worms fed **N0-rhd**, a representative image of intestine.

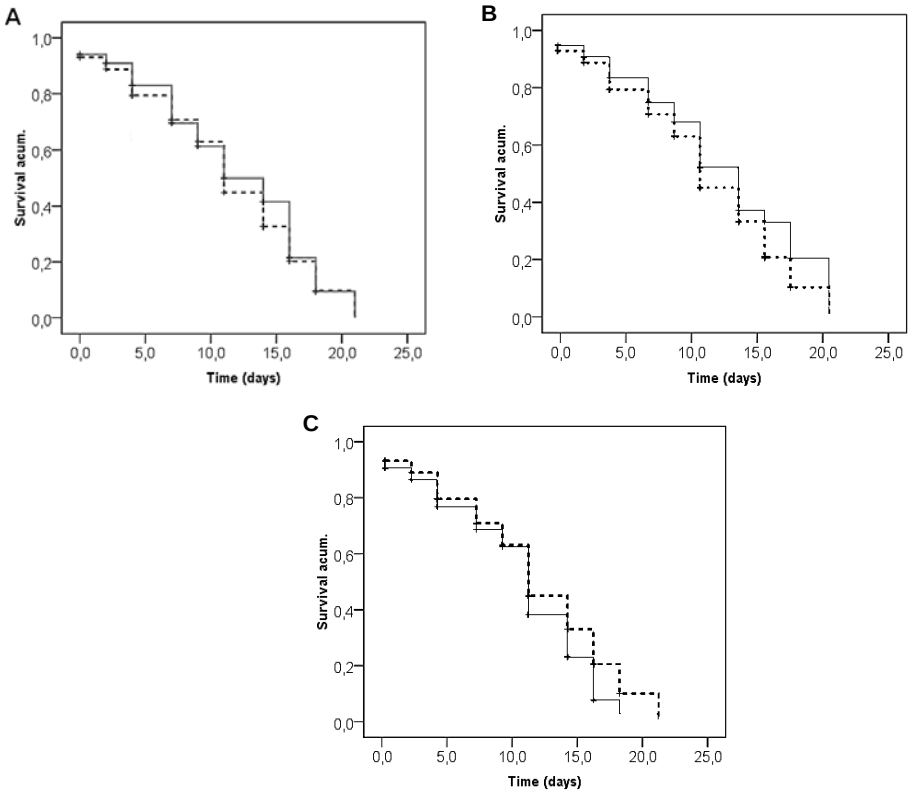

Figure S5. Lifespan of *C. elegans* oral administered with MSPs, doses evaluation: **A.** 0.5 µg·ml^{-1} **B.** 5 µg·ml^{-1} and **C.** 50 µg·ml^{-1}. Dotted line: NG curve (control response) and line in black worms fed with bare micro-sized particles **M0.**

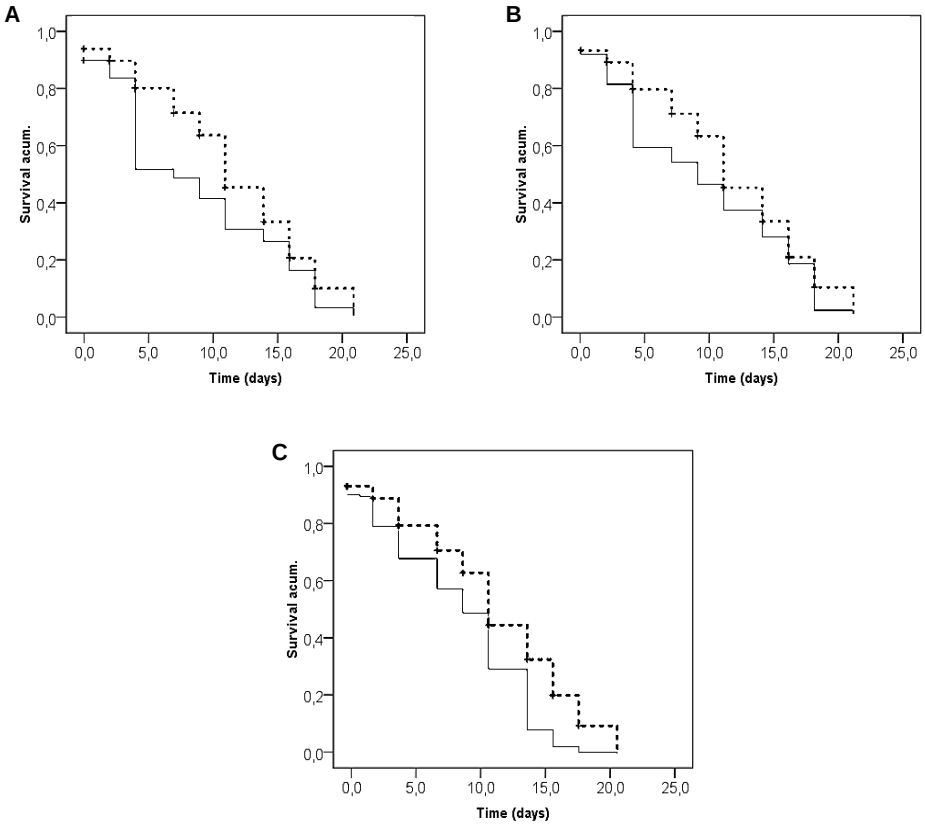

Figure S6. Lifespan of *C. elegans* oral administered with MSPs, doses evaluation: **A.** 0.5 µg·ml^{-1} **B.** 5 µg·ml^{-1} and **C.** 50 µg·ml^{-1}. Dotted line: NG curve (control response) and line in black worms fed with bare nano-sized particles **N0.**

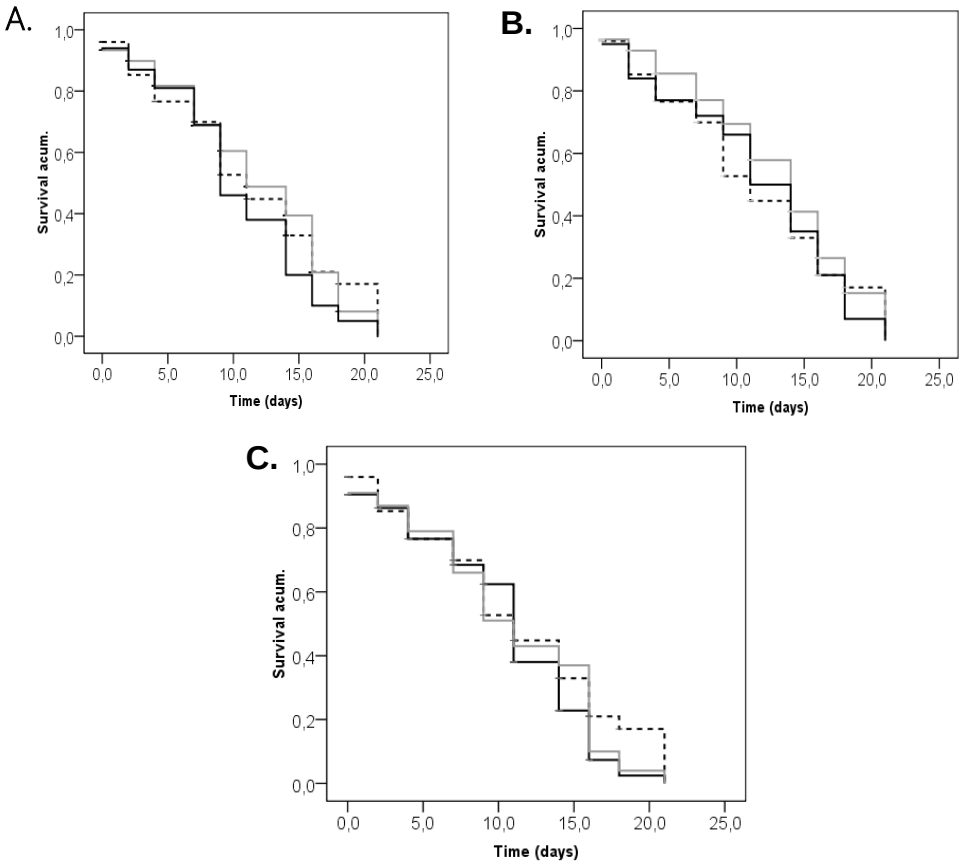

Figure S7. Lifespan of *C. elegans* oral administered with MSPs, doses evaluation: **A.** 0.5 µg·ml^{-1} **B.** 5 µg·ml^{-1} and **C.** 50 µg·ml^{-1}. Dotted line: NG curve (control response) Grey line: particles without functionalisation (**M0**) and black line: Functionalised particles (**M1**)

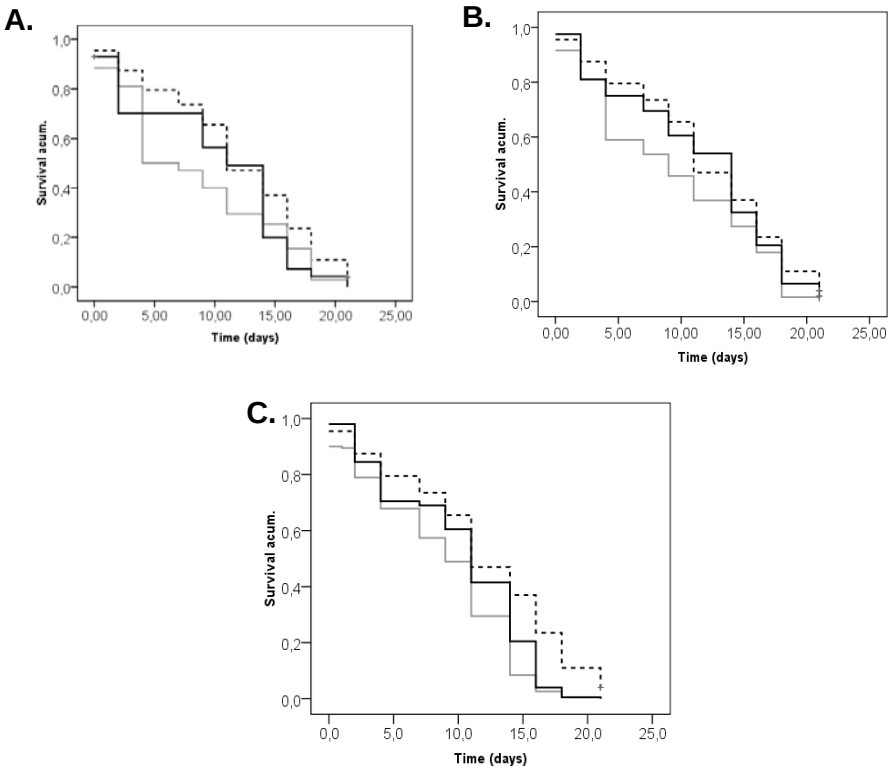

Figure S8. Lifespan of *C. elegans* oral administered with MSPs, doses evaluation: A. 0.5 µg·ml^{-1}B. 5 µg·ml^{-1} and C. 50 µg·ml^{-1}. Dotted line: NG curve (control response) Grey line: particles without functionalisation (N0) and black line: Functionalised particles (N1)

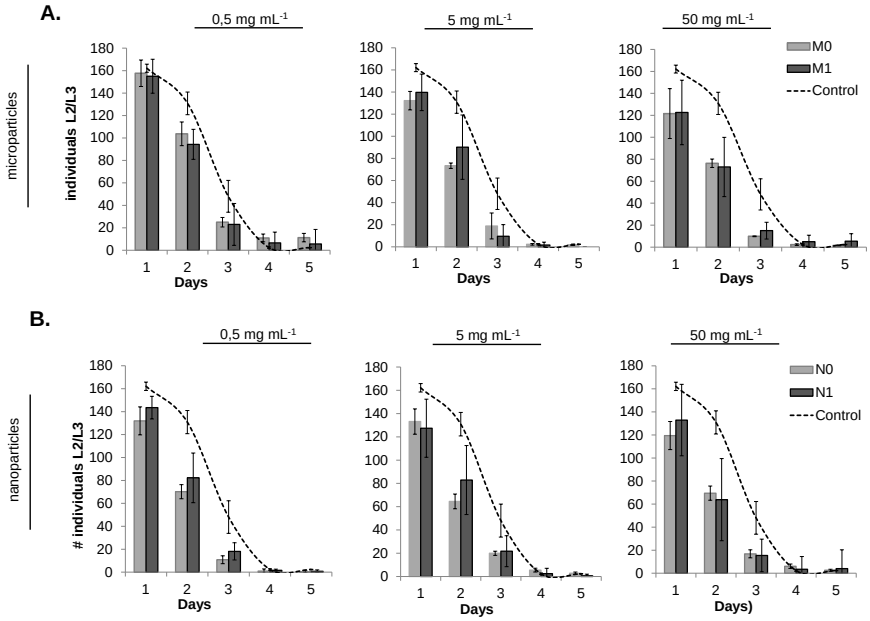

Figure S9. Progeny distribution for the worms fed with**A.** Micro-sized particles, at three doses (0.5, 5 and 50µg·ml^{-1}), and **B.** For the worms fed with Nano-sized particles. Grey bars refer to the offspring of the worms fed with bare particles, darker bars indicate the worms fed withfunctionalised particles and the dotted line denotes the control population.

Table S1. Mean lifespan of the worms fed with different MSPs concentrations

	0.5 µg mL^{-1}	**5 µg mL^{-1}**	**50 µg mL^{-1}**
M0	11.8 ± 0.4	12.6 ± 0.7	10.3 ± 0.4
M1	10.2 ± 0.6	11.5 ± 0.6	10.6 ± 0.6
N0	8.5 ± 0.5 $^{*.a}$	9.3 ± 0.5 $^{*.a}$	8.6 ± 0.4 $^{*.a}$
N1	10.0 ± 0.6 ^{a}	11.3 ± 0.4 ^{a}	10.1 ± 0.4 ^{a}

*Significant differences related to the mean lifespan of the control population ($p<0.01$) (means and standard deviations, n=300) ^{a} Significant difference between N0 and N1 at the same concentration had p-values: 0.001; 0.003 and 0.001for 0.5; 5.0; and 50 µg·ml-1, respectively.